NTNU – Trondheim
Norwegian University of
Science and Technology

Effect of marine environment on the tribology performance of materials used in lubricated rotating parts of offshore wind turbines

Toril Nyhus

Chemical Engineering and Biotechnology
Submission date: July 2012
Supervisor: Kjell Wiik, IMTE
Co-supervisor: Nuria Espallargas, IPM

Norwegian University of Science and Technology
Department of Materials Science and Engineering

Preface

I would like to thank my supervisors, professor Kjell Wiik and associate professor Nuria Espallargas, for guidance and support throughout the work.

PhD-student Fahmi Mubarok also deserves a thank for all help and motivation this semester. Good luck with the rest of your PhD.

My friends here in Trondheim also deserve some glory: Thank you for all the support this last year. I am going to miss our lunch- and coffee breaks. And to my friends and family back home all I can say is; I am finally coming home.

This Master Thesis was written at the Department of Material Science and Engineering (IMT) at the Norwegian University of Science and Technology (NTNU) during 20 weeks spring 2012. The work completes the course TMT4900 'Materials Chemistry and Energy Technology, Master thesis'. The work was done in cooperation with the Department of Engineering Design and Material (IPM).

I hereby declare that the work has been performed according to the regulations at NTNU.

Trondheim, Juli 3, 2012

Toril Nyhus

Abstract

The use of offshore wind turbines as a source of renewable energy is promising. However, many challenges have to be solved before they will be cost effective. The operation time, without any maintenance required, is desired to be as long as possible, because downtime and maintenance costs are high. Thus it is important that the rotating parts in the turbine have a long operational time.

The harsh marine environment, combined with the desire for elongated operating times and little or no maintenance, give rise to many tribological challenges. It is important that the chosen materials and lubricants can withstand the marine environment, and the high loads.

The effect of marine environment on lubricating properties of lubricants is not well understood. The objective of this thesis has been to investigate this effect. Two lubricants that are commonly used as gear lubricants in onshore wind turbines were tested in this work; polyalphaolefin and polyalkylene glycol. They were both contaminated with different amounts of artificial seawater in order to investigate the effect on the lubricating properties. The lubricants were tested in a rotating ball-on-disc tribometer, with self-mated stainless steel, and self-mated silicon carbide. Stainless steel was selected as it is commonly used in gear bearings, whereas silicon carbide was chosen due to its promising excellent properties.

The results obtained from this work show that PAO has a very low saturation limit for water, and an emulsion will be formed even at low contamination levels. This made the lubricant unstable, and the measured COF were unstable. It was found that the amount of two-body abrasive wear increased as a function of seawater content. The PAG lubricant managed to dissolve much larger quantities of seawater that PAO. But even though the system was one-phased, the results for COF were unstable. Wear induced pitting was found for both clean and contaminated lubricant. It is believed that it is caused by the additive package of the lubricant.

For dry tribological testing COF was found to be mush less for self-mated silicon carbide than for self-mated stainless steel. This is as expected, since silicon carbide has shown outstanding tribological properties in previous work.

For self-mated silicon carbide testing only abrasive wear could be found for both dry contact, and lubricated. The results from PAO contaminated with seawater, showed a clear increase in COF as a function of seawater content. Further, the COF all stabilized after the running-in period. PAG showed no such trend with increasing amounts of seawater, but the standard deviation of the measurements increased.

Sammendrag

Bruk av offshore vindmøller som fornybar energi er lovende. Men mange utfordringer må løses teknologien kan bli kostnadseffektivt. Det er ønskelig at driftstiden til en vindmølle, uten at vedlikehold må utføres, er så lang som mulig, fordi det er høye kostnder relatert til vedlikehold og tiden en vindmølle er ute av drift. Derfor er det viktig at roterende deler i vindmøllen er svært driftssikre.

Det marine miljøet i kombinasjon med ønsket om lang driftstid, og minst mulig vedlikehold, gi opphav til mange tribologiske utfordringer. Det er viktig at de valgte materialene og smøremidlene tåler det marine miljøet, og de høye belastningene.

Effekten av marint miljø på smøreegenskapene til smøreoljer, er ikke godt forstått. Målet med denne masteroppgaven har vært å undersøke denne effekten. To smøremidler som ofte brukes som onshore vindturbiner, ble testet i dette arbeidet; polyalfaolefin (PAO) og polyalkylene glykol (PAG). De ble begge tilsatt små mengder kunstig sjøvann for å undersøke effekten på smøreegenskapene. Oljene ble testet i en roterende ball-on-disc tribometer, med selv-paret rustfritt stål, og selv-paret silisiumkarbid. Rustfritt stål ble valgt da det ofte er brukt i maskinkomponenter, mens silisiumkarbid ble valgt på grunn av sine gode, lovende egenskaper.

Resultatene fra dette arbeidet viser at PAO har en svært lav løselighet for vann, og en emulsjon vil bli dannet selv ved små mengder sjøvann. Dette gjorde oljen ustabil, og den målte friksjonskoeffisienten var ustabil. Det ble funnet at mengden abrasiv slitasje økte med mengde sjøvann i oljen. PAG kunne løse mye større mengder sjøvann enn PAO. Systemet var da enfaset, men resultatene for friksjonskoeffisienten var likevel ustabil. Det ble funnet gropdannelse (pitting) for både ren PAG og Pag med sjøvann. Det ble funnet at gropdannelsen skyltes slitasjen, og den var dermed ikke korrosjons-indusert.

For tribological testing av selv-paret silisiumkarbid uten smøremiddel, ble det funnet at friksjonskoeffisienten var lavere enn for rustfritt stål. Dette var som forventet, ettersom silisiumkarbid har vist fremragende tribologiske egenskaper.

For selv-paret testing av silisiumkarbid ble det kun funnet abrasiv slitasje, for både tørr kontakt og med olje.

Table of contents

1 Introduction

In the late-1800s, wind turbines were used to make electrical energy out of wind. During the first half of the 1900s the wind turbines improved, and after the oil crisis in 1973 the wind industry was encouraged to develop even further. The wind turbines that are present today have developed drastically in complexity, size and power capacity, compared to the first turbines. But still, the wind power industry is improving, and it is one of the fastest growing energy resources. A probable reason for this is that it is an environmentally friendly source of renewable energy. [1] [2]

The power output, P, from a wind turbine can be calculated from

$$P = \frac{1}{2} C_P \rho A U^3 \tag{1}$$

where C_P is the power coefficient, which denotes the fraction of wind power that can be converted into usable mechanical work; ρ is the density of air; A is the rotor sweeping area; and U is the wind speed.

In order to increase the turbine power output, one can either design a turbine with longer rotors so that the rotor sweeping area increases, or one can place the turbine at a location with higher wind speed [1]. Thus, by placing the wind turbines offshore, where the wind speed is normally higher than onshore, the power output will increase. Also, constrictions due to visual appearance are less of an issue offshore than onshore. For countries with area constrictions, like Denmark, Holland and Germany, placing the wind turbines offshore obviously has a major advantage. [2]

One of the typical drawbacks with offshore wind turbines is the cost. Both the construction, operational and maintenance cost are higher for offshore wind turbines than onshore. This is primarily because they are more difficult to access. [1] [2]

The harsh marine environment, combined with the desire for elongated operating times and little or no maintenance throughout this period, give rise to many tribological challenges. It is important that the chosen materials and lubricants can withstand the marine environment. Further, the alternating wind speed, and direction, gives rise to rapidly changing loads for the gearbox. In order to prevent failure, the proper lubricant has to be selected. Other devices may also be necessary to minimize wear and prolonging lifetime, e.g: filtration and cooling systems. [2]

The effect of the marine environment on the lubricating properties of the lubricant is not well understood. This problem has been the objective for this master thesis. Two lubricants that are commonly used as gear lubricants in onshore wind turbines have been investigated. Experimental testing was performed with both stainless steel and silicon carbide.

2 Theory

The first parts of this section describe basic theory regarding tribology and degradation mechanisms. Further, there will be given an introduction to lubricants, and the two specific lubricants utilized in this work will be described. Also relevant lubrication mechanisms will be explained. Some effect of water on lubricants will be presented. Then, relevant properties of the materials used in this work are given. Relevant previous work will be implemented in the whole section.

2.1 Tribology

Tribology is a relative new field of science, and it is defined as "*The science and technology of interacting surfaces in relative motion and of related subjects and practices*" [3]. A British committee defined the word "tribology" in 1966, and it originates from the Greek word "tribo" which means to rub. [3]

When two surfaces slide against each other, they will resist the sliding motion. This resistance will result in friction, which is a result of topography, adhesion, surface films and material properties. The friction will cause wear and energy dissipation. This is a enormous problem because wear causes loss of material and mechanical performance. In order to manage friction and wear, one should optimize the operating environment, material, lubricant and coating selection, surface treatments and surface finishing relative to each other. [4, 5]

2.1.1 Surface roughness

A perfectly flat surface is one that is completely planar, and only has two dimensions. However, a real surface will never be perfect. It will always consist of different surface features, like surface roughness and flaws. Flaws are unwanted imperfections in the surface, like scratches. Roughness is surface irregularities, which consist of hills (local maxima, referred to as asperities) and valleys (local minima) with varying amplitude and spacing. The roughness of a surface can be characterized in many different ways, but the most common is the roughness average R_a given by

$$R_a = \frac{1}{L}\int_0^L |z|\,dx \tag{2}$$

where z is the height profile measured relative to a reference line, and L is the sampling length of the profile in x direction, as indicated in Figure 2.1. [4]

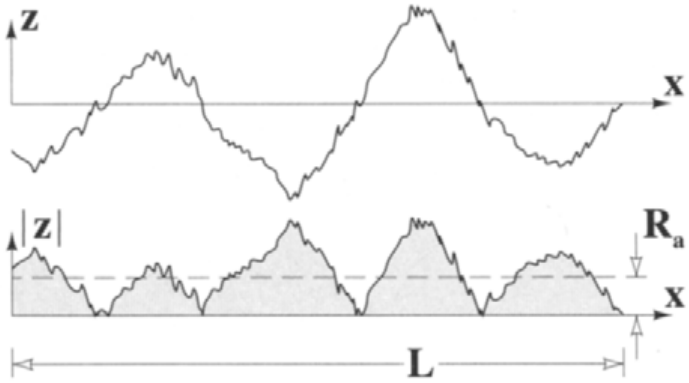

Figure 2.1: Measurement of roughness average [4]

As can be seen from equation (2), R_a represents the average roughness over the sampling length. This equation averages out the effect of irregularities, like scratches, and the effect on R_a is small. Thus, two different surfaces with the same R_a-value can be significantly different, as the R_a -value does not provide any information about shape or size of the asperities. However, this parameter contains information about the relative deviation from the reference line in vertical direction, thus it is useful when comparing surfaces that are prepared in the similar methods. [4] [6]

2.1.2 Contact between surfaces

When two surfaces are in contact, real contact area is much less that nominal contact area. This is because no real surface is perfect, as stated above. Thus, contact is only achieved between the asperities on the two bodies. Hence, real contact area is the sum of many small micro-contacts. As contact pressure is load divided by contact area, real pressure in these contacts are extremely high, as illustrated in Figure 2.2.

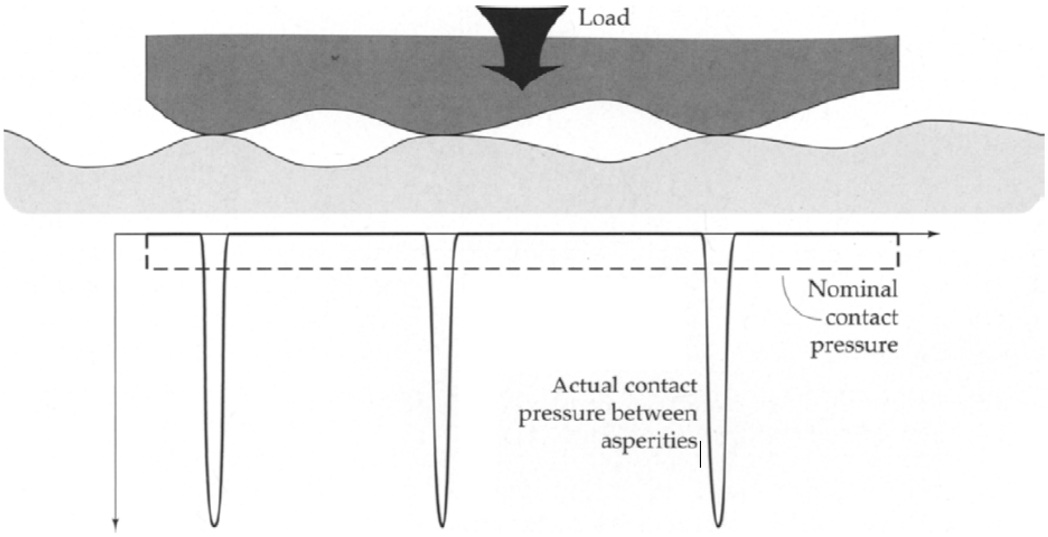

Figure 2.2: Contact stresses between the asperities [4]

Many micro-contacts are entirely elastic. However, if pressure in the contacts exceeds the elastic limit of the material, plastic deformation will occur. Following, the real contact area will increase until the pressure in the contacts is equal to the elastic limit. [4] [7]

2.1.3 Friction and wear

Friction can be defined as "dissipation of energy between sliding bodies", where heat development is an inevitable result. Since contact is only achieved between the asperities, friction in these areas will be very large. Hence, the temperature in these areas can also get very high, and the material properties might alter. Chemical reactions can also become accelerated, due to this high temperature. [4] [7]

The coefficient of friction *COF* is defined as the ratio between frictional force F and nominal force W applied on the surface:

$$\mu = \frac{F}{W} \tag{3}$$

The coefficient obviously is much less for lubricated contacts than for dry. Further, it depends on mechanical properties, chemical properties, like humidity, oxide films and additives, and on material properties, such as hardness, ductility and microstructure. Usually it is desired to have friction as low as possible, in order to minimise the wear in the system. However it is important to remember that this is not always the case. As with car breaks, high friction and low wear is desired. [4] [7]

Metal surfaces that are in contact with the atmosphere will adsorb gas molecules, so that an oxide film will forme on the surface. This film will prevent metal-to-metal contacts, which will reduce the friction coefficient and the amount of wear. [7]

Almost any interaction between two surfaces will cause wear. Some of the most typical wear mechanisms are adhesive wear, abrasive wear, corrosion and surface fatigue.They are all defined as two-body wear mechanisms. That is, they take place at the interface between two interacting surfaces. If the wear is caused by free hard particles between the two bodies, the wear is said to be three-body wear, but here this wear mechanism is classified as a special case of two-body wear [5] . These wear mechanisms will be described further in the next section.

2.2 Degradation mechanisms

2.2.1 Running-in wear

When two bodies are brought into contact and sliding starts, it usually takes some time before the friction stabilizes. This phase is called the running-in period. When the friction is more or less stabile, the running-in period is said to be over. In addition, the wear rate has usually stabilized by then. During this initial period it is believed that the high pressure in the asperities causes the peaks to deform so that they get rounded, and the valleys between them are filled. [5] [8]

2.2.2 Abrasive wear

Abrasive wear can be defined as the “loss of material by the passage of hard particles over a surface” [4]. That is, wear is caused by hard particles or hard asperities, as they scratch the softer surface when they pass over it. This wear mechanism is divided into two different modes; two-body and three-body abrasive wear. Two-body abrasion is caused by hard asperities on one of the surfaces. They can either be a part of the surface, and thus be of the same material, or they can be grits of a hard material embedded in the surface. Three-body abrasion is the case when free hard grits are trapped between the two surfaces. The visual appearance of a worn surface will be different for the two wear modes. Two-body wear will give a series of scratches at the worn surface, whereas three-body wear will give a more random topography. [4]

Removal of material can be performed by one or several of the mechanisms illustrated in Figure 2.3; micro cutting, micro fracture, fatigue by repeated ploughing or pull-out of individual grains.

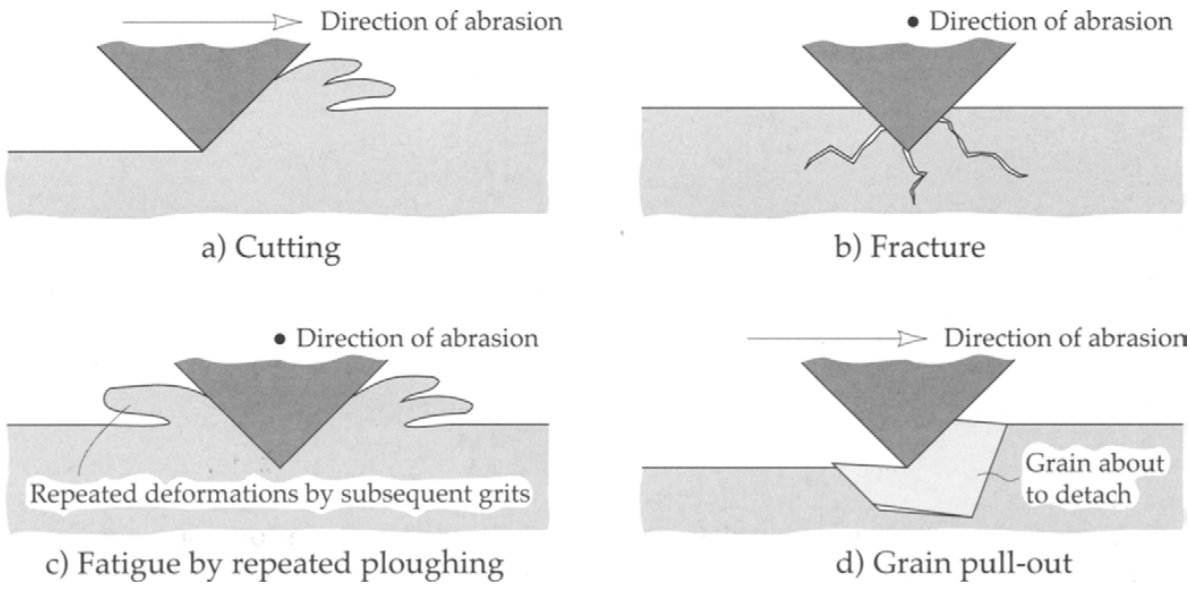

Figure 2.3: Different mechanisms of abrasive wear: a) cutting, b) fracture, c) fatigue by repeated ploughing, and c) grain pull-out [4]

2.2.3 Adhesive wear

When two materials are in contact, most solids will to some extent adhere. The wear mechanism is characterized by local micro-welding, or bonding, between contacting asperities, followed by material removal when the surfaces are pulled apart. The weaker material will be transferred onto the stronger material, as illustrated in Figure 2.4 below.

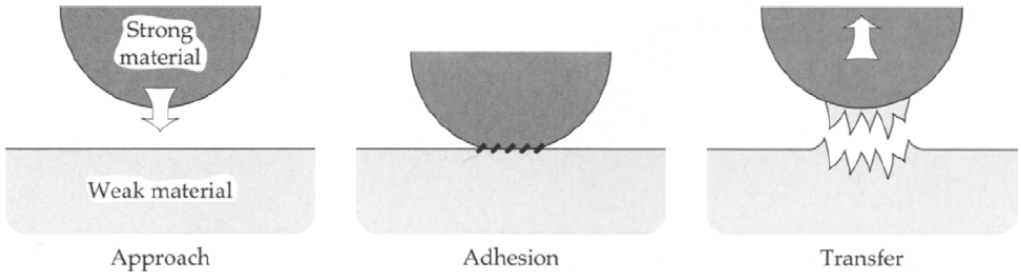

Figure 2.4: Material transfer due to adhesion [4]

The transfer of material can either be permanent or temporary. If only temporary, the transferred material will eventually break loose from the other surface, and become a free wear particle. This particle can again cause abrasive wear, as described below. Adhesive wear will typically give unstable friction coefficients and high wear rates [4]. Heat development is also typical, and the wear is often so severe that it can stop a machine [5].

2.2.4 Corrosion

General corrosion

Corrosion can be defined as the destructive attack of metal by chemical or electrochemical reactions with its environment [9]. Besides tribocorrosion, which will be described below, corrosion of metals is a result of an irreversible oxidation-reduction reaction (redox reaction). The metal is oxidized and an oxidizing agent is reduced during this reaction. The oxidizing agent depends on the environment. For wet corrosion, it is normally either solvated protons or dissolved oxygen.

The corroding metal is the anode in the redox reaction. Hence, it undergoes oxidation. For active metals this will result in material loss due to

$$M \rightarrow M^{n+} + ne^{-} \tag{0.4}$$

As the reaction denotes, the metal will be oxidized into metal ions, and material will be lost.

The oxidizing agent is the cathode in the redox reaction, and it will be reduced by the electrons from the oxidation reaction. The most common reduction reactions are reduction of water, hydrogen protons or oxygen. [7, 9]

Metals might be protected from active corrosion by formation of a passivation. This is a phenomenon where a thin, protective, oxide layer is formed on the metal surface, by the reaction

$$M + nH_2O \rightarrow MO_n + 2nH^{+} + 2ne^{-} \tag{0.5}$$

The oxide layer will act as an ionic barrier to the electrolyte, so that further corrosion is prevented. Stainless steels are protected from corrosion by these layers. It is formed by chromium and oxygen (Cr_2O_3) in air. [9]

Pitting corrosion can appear for passivated metals if the environment consists of chloride- or bromide ions. This will create pits in the metal surface. Other ions that might induce pitting corrosion on stainless steels are thiosulfate ($S_2O_3^{2-}$). [9]

Tribocorrosion

Passive metals are often preferred in engineering applications due to their passivating oxide film on the surface, which prevents corrosion. However, they may undergo tribocorrosion when the preventing oxide layer is worn off in a corrosive environment. When the oxide layer is abraded away, bare metal will be exposed to the environment. A new oxide film will be formed, but dissolution of active metal might occur before the new film is formed.

During tribocorrosion, both wear and corrosion occurs at the same time, but the total material loss is larger than the sum of these two mechanisms. In fact, they interact with each other, so that the rate of material loss is accelerated. [7] [4]

2.2.5 Fatigue wear

Fatigue is a phenomena that might occur when two solid surfaces is repeatedly sliding across each other. When two surfaces are brought together, only asperities will be in contact. There will be great local stresses at these points. When contact is repeated a large number of times, fatigue cracks will be formed. These cracks will propagate to the surface so that wear particles are formed. [3] [4]

Fatigue wear can occur even if the two surfaces are separated by a lubricating film. This is because even thought the film reduces the surface stresses, it does not eliminate them completely.

Micropitting

Micropitting, as a tribo-related failure mode, is a surface fatigue phenomenon. The pits are in the micron range, and they are caused by cracks induced by contact between asperities. The pits can can be formed rather early in the service life of a component. [5]

In a gear, it might reduce the accuracy, cause noise, and also escalate into macropitting or other failure modes. A wear particle will be formed during micropitting, and this will contaminate the lubricant. For steel it has been found that contamination of the lubricant with iron particles will accelerate wear. [10]

In lubricated contacts it has been found that pitting life is dependent of the ratio of the oil film thickness to the surface roughness. It has also been found that the chemical composition of the lubricant influences the pitting life, as well as the composition and microstructure of the metal. [3]

Lainé et al. found that the anti-wear agent secondary, C_6, zinc dialkyl-dithio-phosphate (ZDDP), will influence the formation of micropits. They also found results that suggest that the relationship between surface roughness, lubricating film thickness and micropitting wear is strongly related. [11]

2.3 Lubricants and lubrication regimes

The main purpose of lubrication is to avoid metal-to-metal contact so that frictional forces and wear is reduced. In addition, heat dissipation, removal of wear particles and contaminates from the contact can be a part of the lubrication system.

Mineral oil is one of the most commonly used lubricants today, and their low cost and availability might be a reason for this. Still mineral oil also has some disadvantages, like oxidation and viscosity loss at high temperatures, and solidification at low temperatures. Thus, synthetic lubricants for greater performance have been developed throughout the years. [4]

In this section, general theory about composition and physical properties of synthetic lubricants will be presented. Further, the two lubricants used in this work will be described. At last, different lubricating mechanisms will be presented and explained to some extent.

2.3.1 Composition

One classification of synthetic fluids is based on their chemical composition, and three basic types that are currently in use are presented in Table 2.1.

Table 2.1: Different synthetic lubricants [4]

Synthetic fluids	Composition
Hydrocarbon synthetic lubricants	
- Polyalphaolefins	C,H
- Esters	C, H, O
- Cycloaliphatic	C, H
- Polyalkylene glycols	C, H, O
Silicon analogues hydrocarbons	
- Silicones	C, H, O
- Silahydrocarbons	C, H, O, P
Organohalogenes	C, F (O, Cl)

The properties and performance of lubricating fluids can differ both between lubricants with the same composition, and between lubricants of different base oils.

Additives and additive package

A lubricant normally contains an additive package, which makes up approximately 1 to 10 weight present. The package consists of different types of additives, which are usually organic or organometallic chemicals that are added to the base oil in order to improve the properties.

Different additives are combined to give the base oil the desired properties. Some frequently used additives are:

- Anti-wear additives
- Extreme-pressure (EP) additives
- Oxidation inhibitors
- Corrosion inhibitors
- Contamination control additives
- Viscosity improvers
- Pour points depressants
- Foam inhibitors

Anti-wear additives are used to prevent metal-to-metal contact at the asperities, and thereby reducing the wear. The additives react chemically with the surface, and it is the reaction products, formed at the surface, that prevents the contact. It is mostly for mixed lubrication that the wear is reduced, but it also is for boundary conditions to some extent. [7]

The combination of different additives can improve the properties of a base oil rather drastically. This is probably why the additive package normally is a company secret.

2.3.2 Physical properties

Viscosity

Selecting the correct viscosity of a lubricant can be challenging, and it is very important for the tribological properties and lifetime of the component. If the viscosity is too low, the lubricating film will not be formed, thus the surfaces will be in contact and severe wear will occur. On the other hand, if the viscosity is too high, the viscous resistance will also be high. This will result in temperature increase, and efficiency loss due to the resistance.

The dynamic viscosity η is given by

$$\eta = \frac{\tau}{\dot{\gamma}} \tag{6}$$

where τ is the shear stress [N m^{-2} = Pa], and $\dot{\gamma}$ is the local shear strain rate [s^{-1}]. Thus, the dynamic viscosity of a fluid is a measurement of its resistance to relative shearing motion. The unit of the dynamic viscosity is Pa s or Ns m^{-2}. However, the dynamic viscosity is normally measured in centipoise (cP). This unit is adapted from the c.g.s. system, where the unit corresponding to Pa s is poise [dyne s cm^{-1}]. So, by definition

$$1\ \text{cP} = 1 \cdot 10^{-2}\ \text{poise} \equiv 1 \cdot 10^{-3}\ \text{Pa s} = 1\ \text{mPa s} \tag{7}$$

The kinematic viscosity υ is measured more often than the dynamic viscosity, as it is used for flow due to self-weight or gravity. It is defined as

$$\upsilon = \frac{\eta}{\rho} \tag{8}$$

where ρ [kg/m^3] is the density of the fluid. In the SI system the kinematic viscosity has the unit $m^2\ s^{-1}$, which corresponds to stoke [$cm^2\ s^{-2}$] in the c.g.s. system. Thus kinematic viscosity is normally given in centistokes (cS).

The viscosity of the lubricant is dependent on both the operating temperature and pressure. With increasing temperatures the viscosity can drop drastically, thus it is important to know the viscosity at the operating temperature, as it influences the lubricating film thickness. In heavily loaded contacts such as in gears, the pressure between two surfaces can get very high very quickly, so that the lubricant can act as a solid instead of a fluid. [12] [4]

Viscosity index, VI

The viscosity-temperature characteristics of oil is described by the viscosity index VI. This parameter is entirely empirical, and it compares the kinematic viscosity of a

specific lubricant to two different reference oils. The viscosity sensitivity for the two reference oils differs significantly with temperature change. The reference oils are selected so that one has a VI equal to zero, and the other equal to one hundred at 37,8°C (100°F), and they both has the same viscosity as the selected lubricant at 98,89°C (210°F), as shown in Figure 2.5.

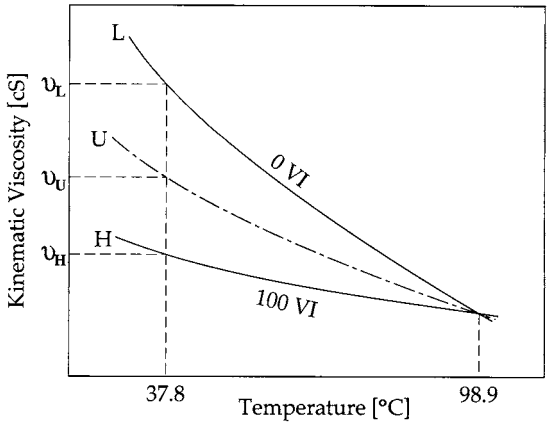

Figure 2.5: The different oils for calculating the viscosity index [4]

The viscosity index is calculated by

$$VI = \frac{L\text{-}U}{L\text{-}H} \cdot 100 \tag{9}$$

where U is the viscosity of the selected lubricant at 40°C. L and H are the viscosity of the reference oils. The values corresponding to the selected lubricant at 100°C can be found from standard tables (ASTM D2270). [4]

In Table 2.2 the low-temperature fluidity, the viscosity index and the pressure-viscosity behavior for PAO and PAG are compared with mineral oil. As it can be seen both the synthetic lubricants has better low-temperature fluidity, VI and pressure-viscosity behavior than the mineral oil. Further, the PAO lubricant has a better low-temperature fluidity than PAG, whereas the opposite is the case for the pressure-viscosity behavior.

Table 2.2: Relative comparison of viscosity properties [13]

Lubricant	**Low-temperature fluidity**	**VI**	**Pressure-viscosity**
Mineral oil (paraffinic)	Fair/good	Good	Good
PAOs	Excellent	Very good	Good
PAGs	Very good	Very good	Very good

Stability

The stability of a lubricant is an important property, as it influences its lifetime. In Table 2.3 the stability of PAO, PAG and a mineral oil is compared. The most important that can be read from this table, is that the synthetic lubricants are much more stable towards oxidation than the mineral oil.

Table 2.3: Relative evaluation of stability properties of different lubricants [13]

Lubricant	Thermal	Oxidation	Hydrolytic	Volatility
Mineral oil (paraffinic)	Good	Fair	Excellent	Poor/fair
PAOs	Very good	Very good	Excellent	Very good
PAGs	Good	Good	Good	Good

2.3.3 Polyalphaolefin (PAO)

Polyalphaolefins (PAOs) are hydrocarbon synthetic lubricants, and the commercial development of these fluids as a lubricant started in the early 1970s [13]. Today, most synthetic lubricants are based on PAO oil [10]. The intrinsic characteristics of PAOs are very desirable for a lubricant, and this is why PAOs are so popular. Some of these properties are:

- Wide operational temperature range
- Good viscometrics, that is high viscosity index (VI)
- Thermal stability
- Oxidative stability
- Hydrolytic stability
- Shear stability
- Low corrosivity
- Compatibility with mineral oils
- Compatibility with various construction materials
- Low toxicity
- They can be tailored to specific end-use application requirements

These properties make PAO based lubricants suited as lubricant in engines, compressors, gears and hydraulics. [13] [14]

One of the drawbacks with PAO is that extreme pressure and anti-wear additives have a moderate solubility in the oil. Another drawback is that the biological degradation is moderate for low viscosity grades and poor for higher viscosity grades. This makes PAO less suited as high performance gear oils and fast biodegradable oils. [13]

PAOs are produced under controlled conditions from pure alpha-olefins, which again are synthesized from ethylene, thus PAOs are true synthetics. The chain length of the olefin

precursor will have a huge impact on the properties of the final product. During the manufacturing process, one can tailor the properties, like the viscosity grade, further. This can be done by carefully selecting the reaction variables, such as temperature, time, pressure, and type and amount of catalyst. In the last step of the manufacturing process, the molecules undergo hydrogenation. This is why the final product has a high chemical resistance, and an enhanced oxidative stability. [14] [13]

2.3.4 Polyalkylene glycol (PAG)

Polyalkylene glycol (PAG) base oils are also frequently used as lubricants today. They consist of carbon, hydrogen and oxygen atoms, as shown in the structure:

$$\mathrm{RO-(CH_2-\underset{\displaystyle R'}{\underset{|}{CH}}-O)_n-R''} \tag{10}$$

where R and R'' can be H or a alkyl group, and R' can be either H, CH_3 or an alkyl group. [14]

The oxygen atoms in the structure enhance the polar nature of the lubricant. Thus the oil is insoluble in mineral or PAO based oils, and a two phase system, or gelation in severe cases, might form if they are mixed. Further, since PAGs are polar they are water soluble.

PAG lubricants are suited for, and thus also frequently used as warm gear oils, fire resistant hydraulic fluids, compressor oils, fast biodegradable lubricants and metalworking lubricants. This is due to its properties, given here:

- Extraordinary high thermal and oxidative stability
- Highest chemical stability of all lubricating oils
- Very wide service temperature range
- High VI
- Very low volatility
- Very good cold flow behaviour
- Compatible with seal materials, plastics, and paints
- Fire resistant
- High radiation stability
- Good friction behavior
- Good wear and scuffing protection
- Low surface tension; good wetting properties
- Not toxic
- Fast biodegradable

As for all lubricants, PAGs also have some disadvantages. Some of the most important drawbacks are that they have a low solubility for additives and that they show moderate viscosity-temperature behavior. Further, the base oil has a low corrosion protection. Due to these disadvantages PAG oils are not that well suited as engine oils and high performance gear and hydraulic oils.

PAGs are manufactured by polymerization of alkaline oxide monomers. The polarity, and thus also the solubility in water, can be adjusted by selecting different monomers as the precursor. This polarity will also increase the affinity of the lubricant to the metal surface. This might increase the boundary lubrication properties. [13]

2.3.5 Lubrication mechanisms

Hydrodynamic lubrication

In hydrodynamic lubrication two surfaces are fully separated by a lubricating film. Thus COF will be small, and little or no wear is experienced. In these conditions, COF is only dependent on the bulk viscosity of the lubricant. [15]

Reynolds theory explains this phenomenon through the generation of a viscous liquid film between two surfaces in relative motion. In order for this film to form between the surfaces there are two conditions that has to be fulfilled:

- the two surfaces must move relative to each other with a velocity that are high enough for the film to be generated, and,

- the surfaces must be inclined with some angle to each other so that the pressure field needed to form the lubricating film can be formed

The generated pressure in the film will separate the two surfaces, and it will also support some of the load. [4]

Elastohydrodynamic lubrication (EHL)

Elastohydrodynamic lubrication (EHL) can be defined as a special case of hydrodynamic lubrication where the two bodies in contact undergo elastic deformation. The model for EHL is based on Hertz's theory.

Hertz's model is normally used to calculate contact stress. It is based on five simplyfying assumptions. The contacting bodies must be homogenous and the yield stress cannot be exceeded. Further, the applied load must be normal to the contact tangent plane. The contact area also needs to be significantly smaller than the dimentions of the contacting bodies, and the effect of surface roughness is neglected. The final assumption is that the contacting bodies are at rest and in equilibrium [4].

An illustration of the contact between a sphere and a flat surface is given in Figure 2.6, and as it can be seen the contact area is circular.

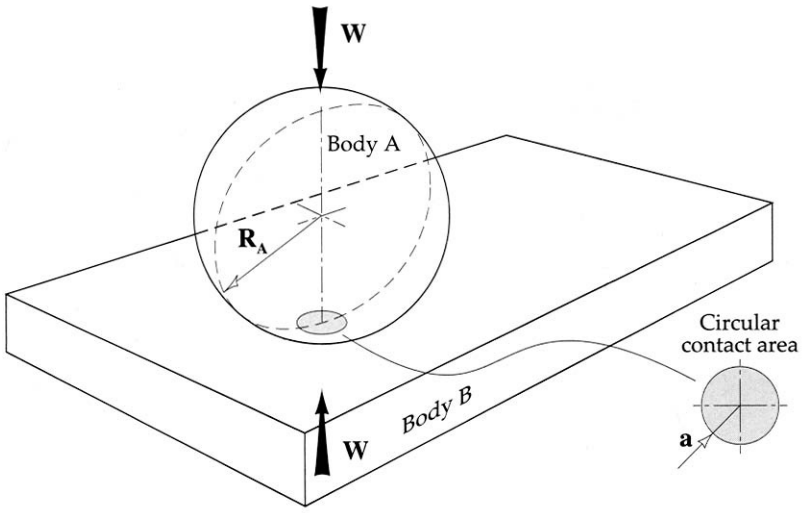

Figure 2.6: Contact between a sphere and a flat surface [4]

The contact area and stresses obtained when two elastic bodies are in contact is dependent on the contact geometry, load and material properties. In order to calculate the contact pressure between a ball and a flat surface, the following parameters have to be determined;

Reduced radius of curvature [m]:

$$\frac{1}{R'} = \frac{2}{R_A} \tag{11}$$

Reduced Young's modulus [Pa]:

$$\frac{1}{E'} = \frac{1}{2}\left[\frac{1-\upsilon_A^2}{E_A} + \frac{1-\upsilon_B^2}{E_B}\right] \tag{12}$$

Radius of contact area [m]:

$$a = \left(\frac{3WR'}{E'}\right)^{1/3} \tag{13}$$

where R_A is the radius of the ball [m] as defined in Figure 2.6, E_A and E_B are the Young's moduli of the two contacting bodies [Pa] , υ_A and υ_B are the Poisson's ratios of the two bodies, and W is the normal load [N].

Then, the maximum contact pressure [Pa] can be calculated by

$$P_{\max} = \frac{3W}{2\pi a^2} \tag{14}$$

and the average contact pressure [Pa];

$$P_{average} = \frac{W}{\pi a^2} \tag{15}$$

Equatiion (11) to (15) are taken from [4].

There are three aspects that are very important in the formation of an EHL film; the hydrodynamic film formation, change of film geometry due to elastic deformation, and viscosity and rheological changes of the lubricant due to the high pressure. [4]

Boundary and extreme pressure lubrication

The lubricating film is very thin for boundary and EP lubrication. Thus, properties of the thin film are not the same as in bulk phase [15]. Additives in the oil normally control the lubricating mechanisms.

Boundary and EP lubrication is divided into four different categories dependent on temperature and load. If both temperature and load are low, contact between the asperities can be avoided by formation of a thin layer of fluid with an anomalously high viscosity on the surfaces. This layer can be caused by alignment of linear hydrocarbons normal to the surfaces.

For situations with low temperature and high loads, friction and wear is minimized by formation of a mono-molecular layer of adsorbed surfactants on the surfaces.

At high temperature and medium load two different mechanisms to prevent wear can occur; chain matching and formation of a thick, soapy layer of amorphous material. This layer is formed when surfactants in the lubricant react chemically with the worn metal surface.

A reaction between additives and the worn surface will also happen when both temperature and load are high. The reaction product is an inorganic material that will form a sacrificial film on the worn surface. This film will prevent metallic contact, and thus also severe wear. [4]

2.4 Effect of water in synthetic lubricants

When oil is contaminated with water, the water can dissolve, form an emulsion or a free water phase. Only small amounts of water can be dissolved in oils. This is because water is a polar molecule, whereas oil is not, at least not to the same extent. This will limit the waters possibility to dissolve. Some lubricants will have increased water solubility compared to others, partly due to the chemical structure of the base oil, and partly because of polar extremities in some additives. The saturation limit of water in a specific lubricant is dependent on temperature, humidity, pressure, additive package and properties of the base oil. The equilibrium concentration of some oils as a function of temperature is given in Figure 2.7. [16] [17]

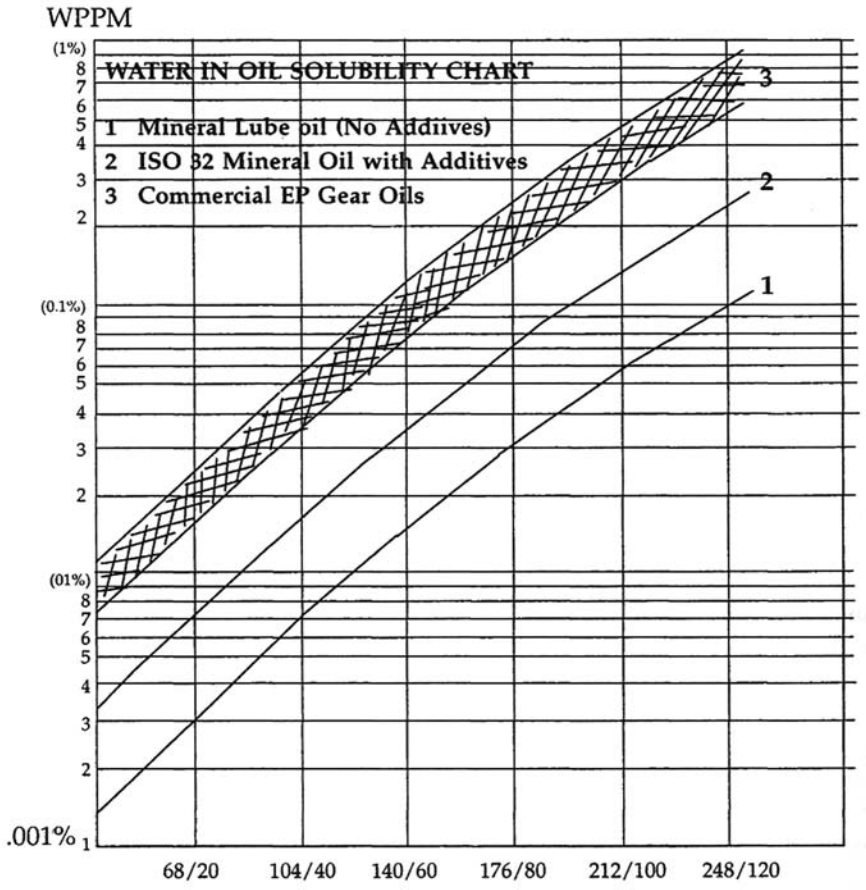

Figure 2.7: Solubility of water in some oils as a function of temperature (F/°C) [16]

If the water content in a oil exceeds the saturation limit, the system will no longer consist of only one phase, and a secondary phase of water will be formed. The two phases can either form an emulsion, or the water can settle as a free phase.

If an emulsion is formed, the water will cause a visible cloud or haze in the oil. Water-in-oil (W/O) emulsions are rather stable, and the two phases do not separate by gravity. Thus, emulsified water appears to behave like dissolved water. However, the effect on viscosity is higher for emulsions than for dissolved water. [17, 18]

Compared to clean oil, emulsions have much lower carrying capacities. This might increase the wear rate [4].

Hamaguchi et al. found that for rolling contacts lubricated with W/O-emusions, EHL film thickness is almost independent of water concentration and particle size distributions. This is an interesting result, since viscosity of emulsions is clearly dependent upon these two variables. Thus they concluded that EHL properties of W/O-emulsions are mostly determined by EHL properties for pure oils. [19]

Benner et al. also studied the effect of water content in a W/O-emulsion on film thickness. Like Hamaguchi et al., they found that the film thickness did not change with

increasing water content. They suggested that this was because the water was expelled from the emulsion before the lubricant entered the contact zone. Further, they also suggested that the water flows around the contact area. Thus it does not influence the film thickness. [20]

Water as a separate phase in oil will reduce the lubricating properties. This is due to the negative effect on viscosity, and the poor load capacity of water. Water droplets in the contact area between two surfaces, will not be able to withstand the high pressure. Thus they will collapse. This will create micro-jets that will induce micro-pitting. [21]

The corrosive and oxidative properties of synthetic lubricants will be influenced by water contamination [4]. Oil degradation, which will change its properties, can be catalyzed by water. This will normally produce resins, sludge and varnish, which are dissolved in the hot oil. These can then deposit on colder machine elements, and clogging might occur [21].

Sludge and resins consist of acids and polymerized compounds among other. If acids are formed due to oil degradation, excessive wear can occur due to surface corrosion in tribological systems.

Hydrolytic stability is the ability for a oil to withstand degradation when it is contaminated with water. Studies performed by Beran showed that PAOs has a higher hydrolytic stability than PAGs. In general, they found that hydrocarbon base oils had excellent hydrolytic stability. This is because the molecules are resistant to hydrolytic decomposition. However, they found that stability was reduced by impurities containing sulphur or acidic compounds. Also, some additives reduced the stability. [22]

2.5 Material selection

Materials used for engineering components must be able to withstand the applied load, without undergoing dimensional or material changes that can lead to failure, during the designed lifetime.

Young's modulus E and Poisson's ratio ν describes the elastic strains of a material, thus they describe the materials recoverability for a given geometry and applied load. When the load increases, the material will first deform elastically and then plastically. This transition is defined by a materials yield stress, and it is extremely dependent of small changes in material composition, mechanical or heat treatment, etc. The hardness of a material is an important property in a tribological manner, as it is used as a measure of the strength of a material. [12]

2.5.1 Stainless steel, AISI 440C

Stainless steels (SS) are in general highly resistant to corrosion in many different environments. In air this resistance is due to the formation of an non-porous oxide layer of chromium oxide that adhere well to the surface. This layer prevents further corrosion of the base material. In order for this protecting layer to form, the chromium content has

to be at least 11 wt%. Alloying elements like nickel and molybdenum can increase the corrosion resistance further [9] [5] . [23]

Stainless steels are divided into three classes based on their microstructure austenitic, ferritic and martensitic. Austenitic and feritic SS's are not heat treatable, and they are hardened and strengthened by cold work. Martensitic SS's however, are heat treated in order to form the martensitic structure. [23]

The composition of AISI 440C, which is a martensitic stainless steel, is given in Table 2.4. This grade has one of the highest hardnesses for hardenable stainless steels. [24]

Table 2.4: Chemical composition of AISI 440C [24]

Element	Content, %
Carbon	1.1
Chromium	17
Iron	Balance
Manganese	≤1
Molybdenum	≤ 0,75
Silicon	≤ 1

2.5.2 Silicon carbide, SiC

Silicon carbide is a promising material for bearings and gears. This due to its outstanding properties such as increased hardness, great corrosive and wear resistance, high temperature strength retention and its low friction coefficient for sliding in aqueous media [25] [26].

Silicon carbide is a ceramic material, thus it is an inorganic and non-metallic material. A general property of ceramics is that they are brittle. At room temperature ceramics will rarely undergo severe plastic deformation when a tensile load is applied. Instead, brittle fracture will occur. In addition, ceramics are relatively stiff and strong, in comparison to those of metals, but they are typically much harder. Compared to many other ceramics, SiC's have a lower density. These are some of the reasons why it is such a promising material. [23] [24]

In general, silicon carbides have a low wear rate, and the main deteriorating mechanisms are microfracture and oxidation [27]. In theory, it is chemically inert, but some tribo-chemical reactions in air and water have been reported. [28]

Zum Gahr et al. found that COF for self-mated SiC contacts depends on the initial surface roughness, as it influences the running-in period. They also found that the running-in period, and thus also the COF, is dependent on the humidity of air. The COF and the running-in period for contacts in humid air were lower than in vacuum. This is due to tribochemical smoothening of surface roughness. [25]

Sliding in water will induce tribochemical reactions, which will generate tribochemical wear and hydrodynamic lubrication by having very smooth wear surfaces in nano-meter scale [29]. For-self mated contact with boundary lubrication in water, it has also been found that the surfaces undergo tribochemical polishing [25]

Chen et al. reported that self-mated SiC show very low COF (10^{-3}) by running-in in water starting with high COF(around 0,7) [30].

Friction properties during running-in in water were investigated by Andersson, and it was found that tribochemical reactions caused strong "running-in" wear of silicon-based ceramics. Futher, it was found that the reaction products were dissolved in the water. Thus, no wear debris was found in the water [31].

According to Ericson et al., the main wear mechanisms for SiC are plastical deformation, subsurface microcrack formation, microfracture and micr-abrasion of the surface, along with chemical reactions [27]. Ericson et al. also found that reaction bonded SiSiC surfaces were less affected than pure SiC (>99%). He stated that this was due to the free silicon in the SiSiC that could easily react to form SiO_2, which are relatively soft and ductile. Thus, this layer protected the underlaying surface material against stress peaks. [27]

2.6 Tribological testing

Tribological testing is beneficial to predict the behavior of machine components in varying operating conditions, i.e. load, temperature, etc. Further, both dry and lubricated contacts can be tested, and the lifetime of a specific system can be approximated. [5]

A challenge with triological testing and wear studies is reproducibility. The mechanical and operational variables must be well controlled in order to achieve accurate results. Also environmental parameters, like humidity and temperature, should be controlled. [7]

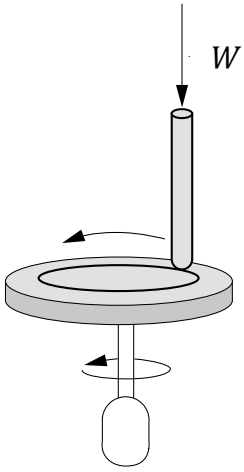

Figure 2.8: Pin-on-disk [7]

A typical pin-on-disc tribometer used for tribological testing, is illustrated in Figure 2.8. Many other tribometer configurations also exist, but this is probably one of the most frequently used within tribology. In this equipment a ball or pin is pressed down on a rotating disc with a constant normal force *W.* This will create a wear track on the disc. Measurement of normal force and angular momentum during the sliding, will give the friction coefficient. [12] [7]

3 Experimental

3.1 The test materials

Two different materials were tested in this work; stainless steel (grade AISI 440C) and silicon carbide (reaction bonded SiSiC). As described in Section 2.6 the tribological testing requires a sample disc and a counter ball. In this work it was desired to perform self-mated tribo-measurements. That means that both the disc and the counter ball are made out of the same material. Thus, both the disc samples and the balls were ordered in stainless steel and silicon carbide. The properties of these materials were described in section 2.5.

Due to the advantageous properties of silicon carbide, described in section 2.5, it is believed that a top coating of SiC on stainless steel will increase the lifetime of mechanical components. However, a method for applying this coating on top of the base material had not been determined when this project was started. Thus tribological testing of SiC as a coating on SS could not be tested. Instead the tribological properties of bulk SiC were tested in this work.

The stainless steel samples were very rough when delivered, and they had to be ground before polishing. Struers Waterproof Silicon Carbide paper FEPA p #80, 120, 220, 500, 800, 1200 and 2400 where used. The grinding was performed manually with a JeanWirtz Pheonix 2000 grinding machine. Water was used during the grinding as a coolant and lubricant. After grinding, the samples were polished at a Knut Rotor-2 polishing machine. DP-Lubricant Blue was used for cooling and lubrication. Struers DP Spray P containing 3 µm and 1µm diamond particles, were used as polishing material. The samples were cleaned with water and ethanol between the different steps. This procedure made mirror like sample surfaces.

The stainless steel samples were delivered as 2.5x5 cm bars, and they were too large to fit into the pin-on-disc apparatus. Therefor they were cut in half. Water-cooling was used during the cutting to avoid heating of the material.

The silicon carbide samples were grinded and polished on the automatic Struers LaboPol-2. They were first grinded with Struers MD Piano 1200 and MD Fuga diamond grinding pads. DP-Lubricant Blue was used for cooling and lubrication. Then the samples were polished with Struers DP Spray P 1µm diamond particles.

3.2 The lubricants

Two different lubricants were tested in this work; polyalphaolefin (PAO) and polyalkylene glycol (PAG). The chemical, physical and lubricating properties of these lubricants were described in section 2.3.3 and 2.3.4. They were selected, because they are frequently used as gear lubricants in onshore wind turbines. Both the PAO and PAG lubricant were delivered by Klübersynth, and their company names are GEM 4-320N and GH 6-320 respectively.

One of the objectives for this work was to investigate the lubricating properties of the oils when they were contaminated by marine atmosphere. This was done by contaminating the oils with small amounts of seawater. It was found that many synthetic lubricants have a saturation limit of 500ppm water, so this was set as the maximum contamination level.

In Table 3.1 the volume of seawater added to 100 ml lubricant in order to get the desired concentration, is given. An example of the calculations is given in Appendix A.

Table 3.1: Calculated seawater content

Lubricant (100 ml)	**Seawater content** (ppm)	**Mass** (g)	**Volume** (µl)
PAO	100	0,085	85
	300	0,255	255
	500	0,425	425
PAG	300	0,3201	320
	500	0,5335	534

A volumetric flask was used to measure 100 ml of the lubricant. When the oil was pored into the flask, a lot of air got into the oil. In order to get the correct volume, these bubbles had to be removed. This was done by waiting until the bubbles had removed themselves. The correct amount of seawater was measured with an automatic micropipette, and added to the lubricant. Then the flask was turned up and down until the water was dissolved or evenly distributed. The oil mixture was always prepared the day before running the tests, except for the degradation test.

3.3 Experimental procedure for the tribological tests

A rotating ball-on-disc apparatus, was used to perform the tribological tests. The tribometer is described in more detail in Section 2.6. Before the tribological testing started the samples were polished and the lubricants were prepared, as described above.

The experimental conditions are listed in Table 3.2. All the experiments were performed at room temperature.

Table 3.2: Experimental conditions

Experimental parameters	
Applied load	4 N
Linear speed	10 cm/s
Acquisition rate	1 Hz
Distance	500 m

The sample was mounted in a Teflon holder as shown in the left image in Figure 3.1. The ball was mounted in the ball-holder, so that sliding was restricted, and then in was fastened in the arm so that the ball was in contact with the sample surface, as shown in the middle and right image respectively.

Figure 3.1: Images of the sample mounted in the Teflon holder (left), the ball and the ball-holder (middle), and the ball in contact with the disc

The arm holding the ball-holder had to be leveled before starting the test, so that the load was properly distributed in the contact between the ball and the disc. This was done by fixating the ball-holder to its arm when the leveler showed no tilting angle, as shown in Figure 3.2.

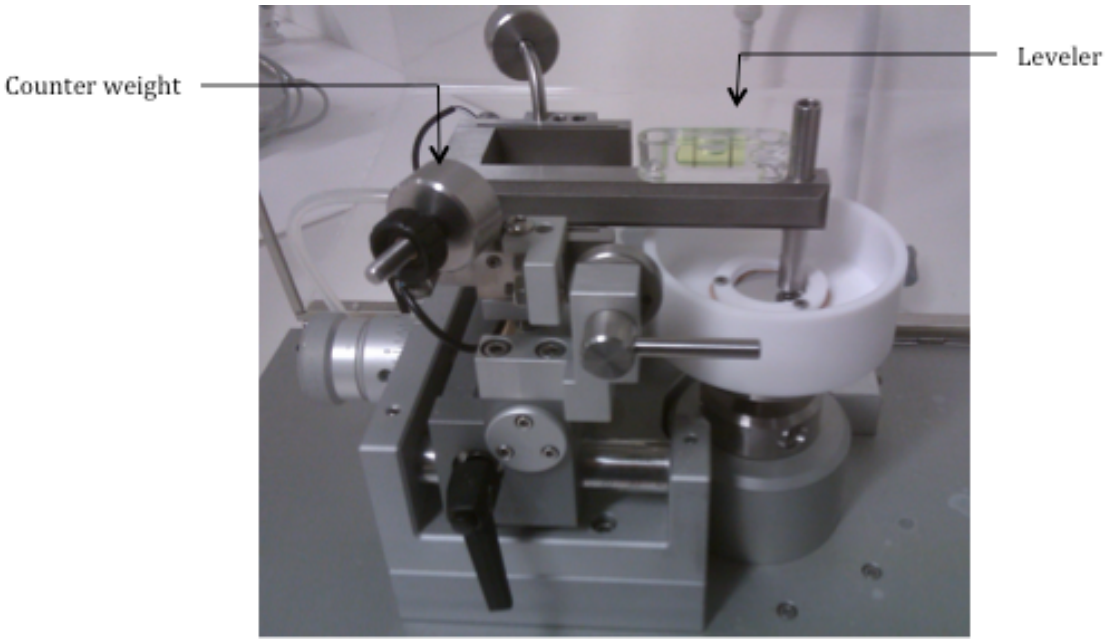

Figure 3.2: The leveler and the counter weight

Further, the initial load before putting on the desired weight shall be zero, so that the applied load is the same as the normal load in the contact. This was performed by

adjusting the counter weight, showed in Figure 3.2, until the ball was barely in contact with the surface.

Figure 3.3: Pin-on-disk apparatus ready to use

The desired test load was put on top of the arm holding the ball-holder, as shown in Figure 3.3. The load is centred around the contact point between the ball and the disc, so that the applied load is the actual load in the contact.

The right image in Figure 3.3 show how the teflon holder with lubricant. Approximately 40 ml lubricant was used for all the tests.

The tests were executed with test conditions as in Table 3.2. After the tests the samples were cleaned with water, soap and ethanol in order to get them clean.

3.3.1 Lubricant degradation test

It was desired to measure the effect of water on the oil properties as a function of time after mixing. This was done by preparing 250 ml of polyalphaolefin with 300 ppm seawater. Tribological testing with self-mated stainless steel was performed right after the mixing, and after 2, 5 and 8 days.

3.3.2 Pitting tests

Two different tests were performed to investigate pitting on the stainless steel samples lubricated with PAG. The two tests were;a non-tribological test, and tribological testing with an additive-free PAG oil.

The non-tribological test was performed by immersing a polished stainless steel sample in PAG lubricant (with the additive package). The sample was left in the oil for approximately 24 hours.

For the tribological test, a PAG lubricant without an additive package was chosen. Unfortunately, this lubricant had a viscosity of 200, but this was the only additive-free PAG available at the time. The test conditions for the tribological test were the same as for the other tests described above.

Both the samples were investigated in the SEM after the testing, in order to determine if any pitting had occurred.

3.4 Analysing methods

3.4.1 SEM

Only the disc samples, and not the balls, were investigated in the SEM. The stainless steel samples has a good conductivity, thus the preparation is simple. Both the sample and the sample holder need to be cleaned properly before putting it in the SEM, and gloves were used during the preparation. The sample was cleaned with water and ethanol. Because there was almost no wear on the lubricated samples, the wear track had to be indicated with a waterproof pen so that the track could be found more easily.

The samples were attached to the sample holder with carbon tape. The height of the sample and the sample holder was measured before installing it in the SEM. This was to avoid crashing the sample in the detector inside the chamber.

The wear track on the sample surface was studied in a Hitachi 3400N LVSEM. Secondary electrons were used for imaging at an accelerating voltage of 20 or 15 kV. The other parameters (probe current etc.) were set to obtain the best possible image. The main focus of using the SEM was to investigate the different types of wear, and to find traces of corrosion in the wear track.

3.4.2 Weight loss

The volume loss of the stainless steel samples was approximated by measuring the width of the wear track. The width was measured at several points around the wear track, and an average of these values were used to calculate the volume loss. These mesurements were performed by PhD student Fahmi Murbarok, and they are based on ASTM G99.

4 Results and discussion

4.1 Dry contact

Dry contact tribological testing of self-mated stainless steel and silicon carbide were performed as described in section 3.3. Results from the tests and SEM images for all the repetitions can be found in Appendix B.

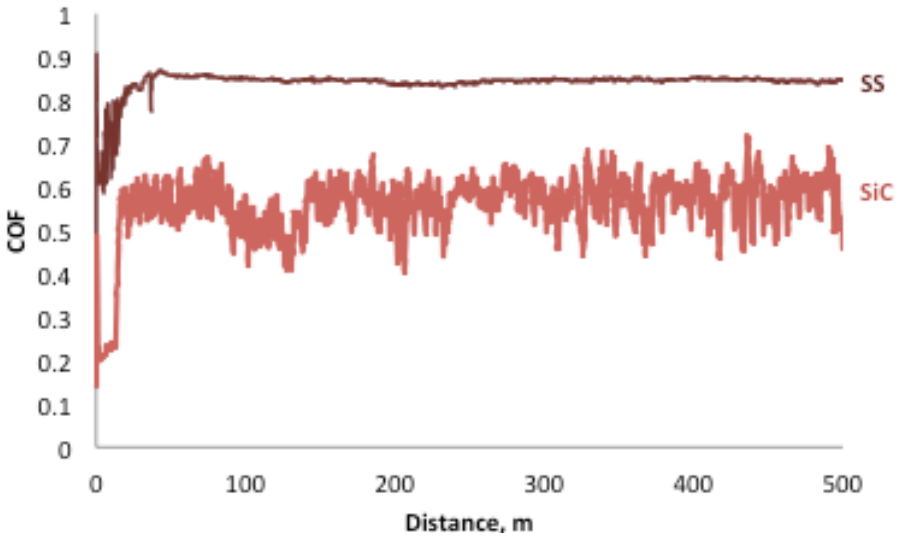

Figure 4.1: Comparison of COF for dry contact, for the stainless steel and silicon carbide samples

In Figure 4.1 the coefficient of friction as a function of test distance, is given for stainless steel and silicon carbide. For the stainless steel sample the friction coefficient is stable and approximately 0.85 after the running-in period. For the silicon carbide however, the friction coefficient is much less stable. The mean value after the running-in period is around 0.58, but it varies between 0.45 and 0.7. The friction coefficient for stainless steel is clearly higher than for silicon carbide. This is as expected since silicon carbide has good friction and wear properties as described in section 2.5.2.

The two wear tracks were investigated in the SEM, and the resulting images are shown in Figure 4.2. The images to the left are for the stainless steel sample, and it can be seen that the wear is severe. This is evident with the high friction coefficient. Further, the images show both two-body abrasive wear and adhesive wear.

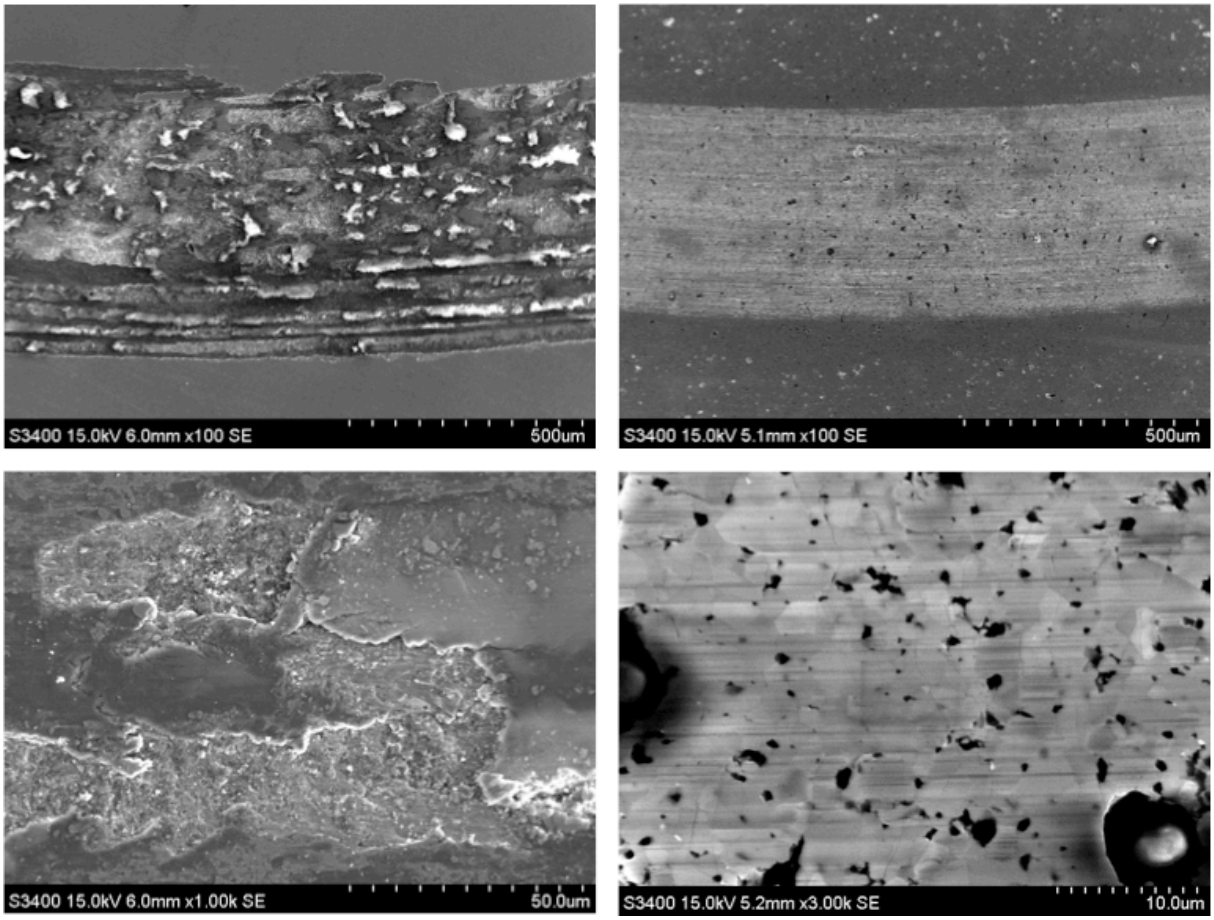

Figure 4.2: SEM images of wear track from dry contact tribological testing of self-mated stainless steel (left) and silicon carbide (right)

The two right images in Figure 4.2 are for the dry, self-mated silicon carbide testing. The black spots in the two images are pores in the polished surface, and they were made during the sintering process. Hence, they are not a wear property. The images only show two-body abrasive wear, and not adhesive wear as for the stainless steel.

The width of the two wear tracks in Figure 4.2 can be compared. It can be seen that the wear track on the stainless steel sample is wider than for the silicon carbide. This implies that there are less wear on the silicon carbide samples than on the stainless steel samples for dry contacts. This is in accordance with COF for the two tests, and with theory, as explained above.

4.2 Tribocorrosion tests in seawater

Tribological testing in pure seawater for self-mated stainless steel and silicon carbide, were performed as described in section 3.3. Plots of COF as a function of distance, and SEM images for all the repetitions, can be found in Appendix B.

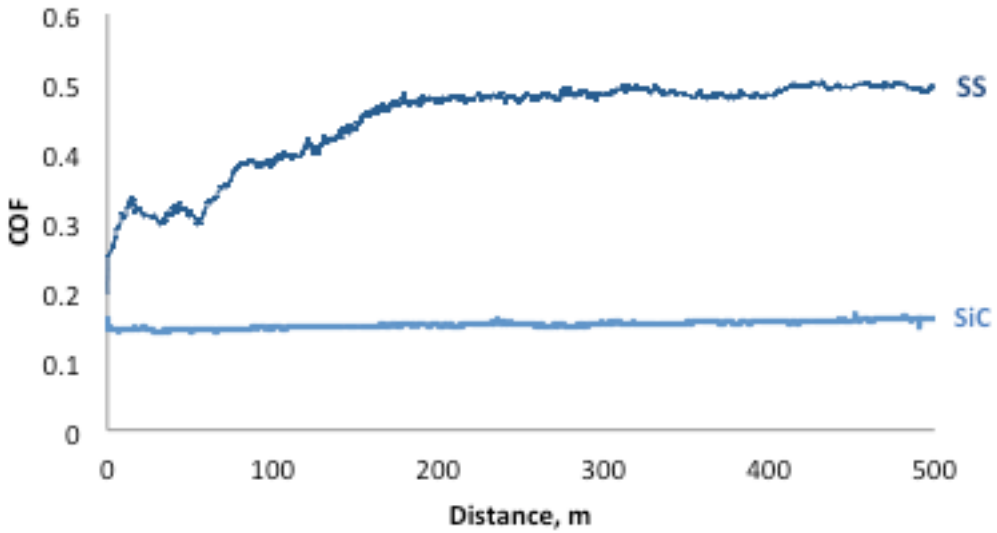

Figure 4.3: Comparison of COF for the stainless steel and silicon carbide samples in pure seawater

In Figure 4.3 COF is plotted as a function of sliding distance for SS and SiC. As it can be seen from the plot, SS has a rather long running-in period of about 200 m, before it stabilizes at approximately 0.5. This value is lower than for dry contact, where it was stable at 0.85. This is expected because the water prevents metal-to-metal contact to some extent. Thus, the friction will be reduced.

COF for silicon carbide is less in seawater than in dry contacts. This is expected from the previous work presented in section 2.5.2. However, a running-in period, before the surface is polished, was also expected. The absence of this period might be due to that the surface was polished before the test.

SEM images of the two wear tracks are shown in Figure 4.4. The images to the left are for the stainless steel sample, and they show obvious signs of tribocorrosion. Further, they show that abrasive wear has occurred, but no adhesive wear can be seen, as it could for dry contact. This implies that the seawater has prevented adhesion between the surfaces so that adhesive wear cannot occur.

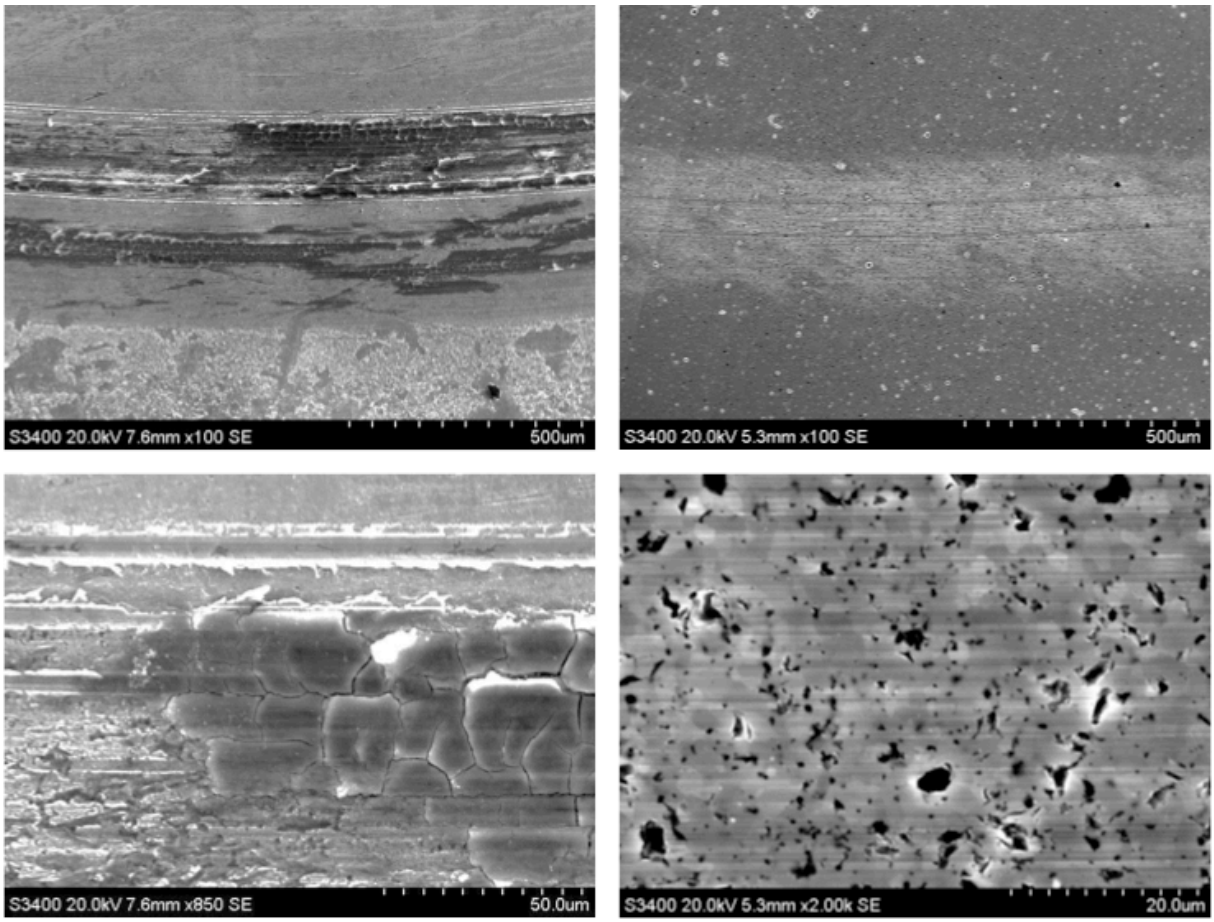

Figure 4.4: SEM images of the weartrack produced from tribological testing in pure seawater. The left images are from self-mated stainless steel, and the right images are from self-mated silicon carbide

The two images to the right in Figure 4.4, are from the silicon carbide samples. As expected, no tribocorrosion has occurred. As for the dry contact only abrasive wear can be seen.

The wear track on the stainless steel sample is wider than on the silicon carbide sample. Hence, the wear is less severe for the silicon carbide, and this comprehends with the COF values in Figure 4.3. This result is the same as for the dry contact.

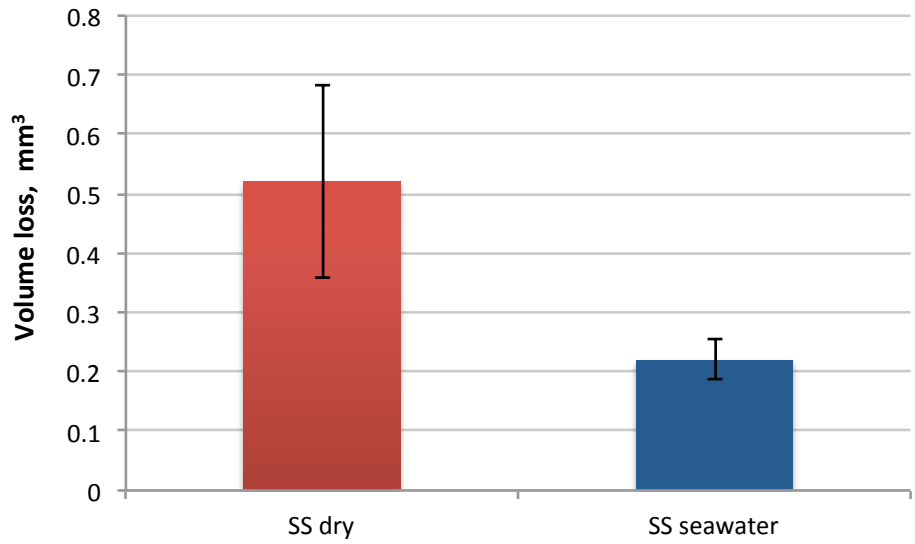

Figure 4.5: Measured volume loss for dry contact on stainless steel and with seawater

The approximated volume loss on the stainless steel samples for dry contact and with seawater, is shown in Figure 4.5. It is clear that the volume loss is much higher for dry contact that with seawater. This is not in directly compliance with the theory for tribocorrosion, which says that wear rate is accelerated. One reason for this might be that the water provides some lubricating effects, and separates the two surfaces so that metallic contact is avoided. It might also be that the wear rate in seawater would have been higher if the test distance were longer.

The volume loss for the silicon carbide samples was not investigated. This was because there was so little wear on the samples, that the measurements could not be performed accurate.

4.3 Tribological testing with clean lubricant

Tribological testing with the clean lubricants was performed as described in section 3.3, for both the materials. The results from all the repetitions are given in Appendix B, together with SEM images of the wear track. The mean values for the friction coefficients obtained from the different repetitions, are presented in Figure 4.6 with standard deviation.

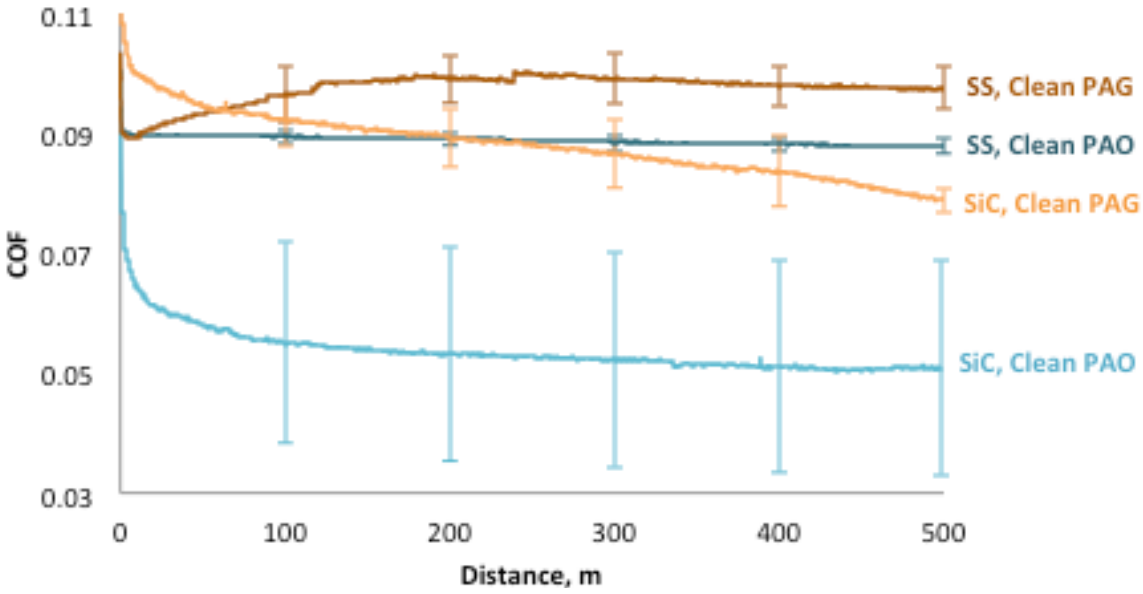

Figure 4.6: COF as a function of distance for the two materials (stainless steel (SS) and silicon carbide (SiC)) with clean PAO and clean PAG as lubricant

The coefficient of friction on stainless steel changes differently for the two lubricants, as shown in Figure 4.6. The COF for PAO is constant over the whole distance, with a value of approximately 0.09. This value is relatively low, and little wear can be expected. Also, the standard deviation is quite low, thus the lubricating properties of the oil are stable, and the different tests have been performed with high accuracy. The coefficient of friction for PAG however, is not stable throughout the whole distance. The COF is lower in the beginning and increases before it stabilizes at approximately 0.1. Compared to PAO, PAG has a higher friction coefficient, and the standard deviation is also higher.

For the silicon carbide, the COF for PAO decreases in the beginning, but after the running-in period it stabilizes at about 0.052. This is a rather low value, but unfortunately the standard deviation is quite high. As described in section 2.5.2 COF for self-mated SiC contacts depend on the surface roughness. Thus, one reason for the high deviation might be differences in the surface roughness between the samples. It might also be due to small changes in the performance of the experiments. Anyhow, more tests would have to be performed in order to minimize this deviation, and get more accurate results.

For PAG on silicon carbide, the COF is higher, and the standard deviation is much less, compared PAO. It has the same type of reduction in COF during the running-in period, but apposed to PAO it does not stabilize after this period. In stead it continues to decrease throughout the whole distance.

If the COF obtained for the two materials lubricated with PAO are compared, it can bee seen that the coefficient is less for silicon carbide. However, the standard deviation is much less for the stainless steel. For the PAG lubricant it is not as simple. In the beginning the friction coefficient is higher for silicon carbide, but after the running-in

period it is the opposite. Further, the standard deviations for the two is approximately the same.

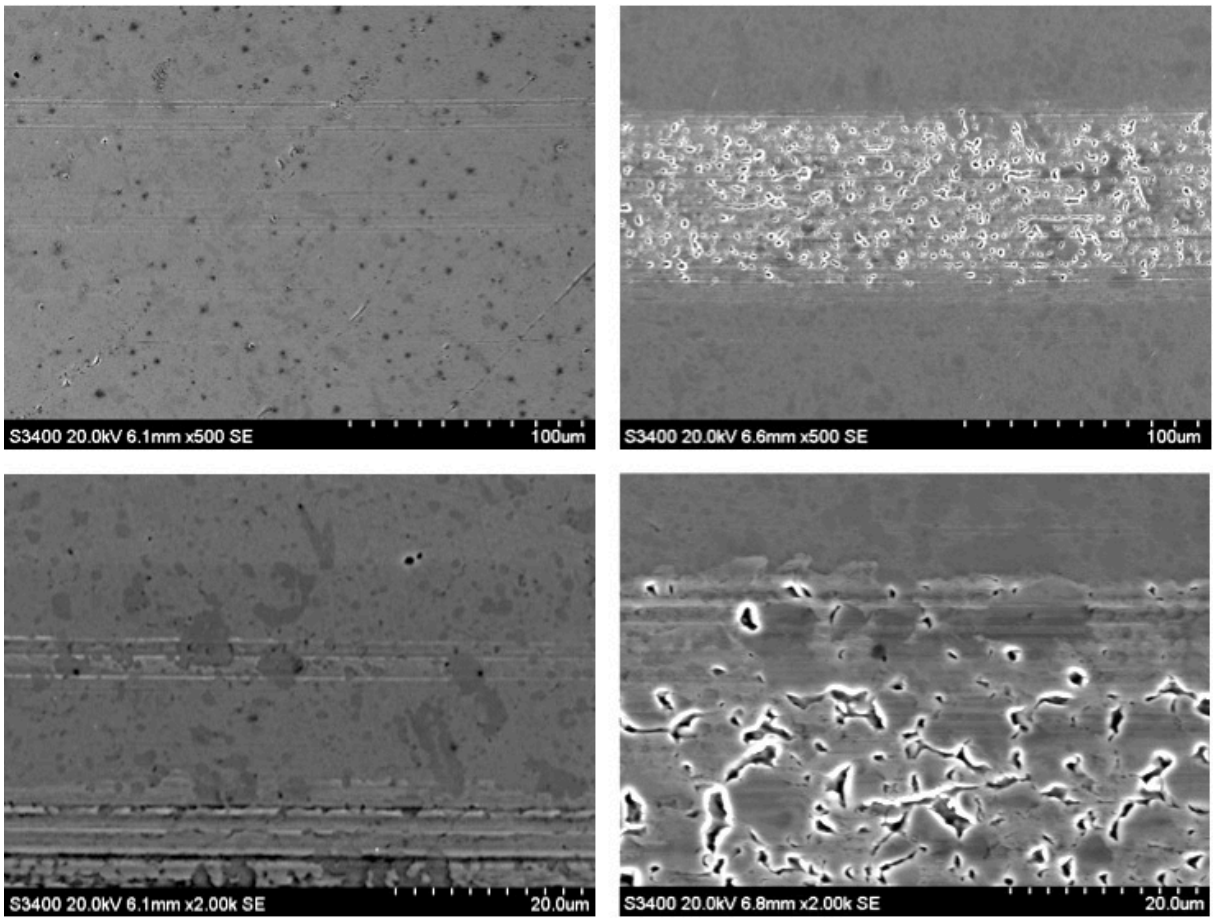

Figure 4.7: Tribological testing of stainless steel with clean PAO (left) and clean PAG (right) as the lubricant

SEM images of the wear track on stainless steel lubricated with clean PAO are show in the two images to the left in Figure 4.7. The images show signs of abrasive wear, and some plastic deformation. The two right images in the figure are for the PAG lubricated stainless steel samples. Here, severe pitting can be seen. This pitting will be described further below. In addition, both abrasive wear and plastic deformation can be seen.

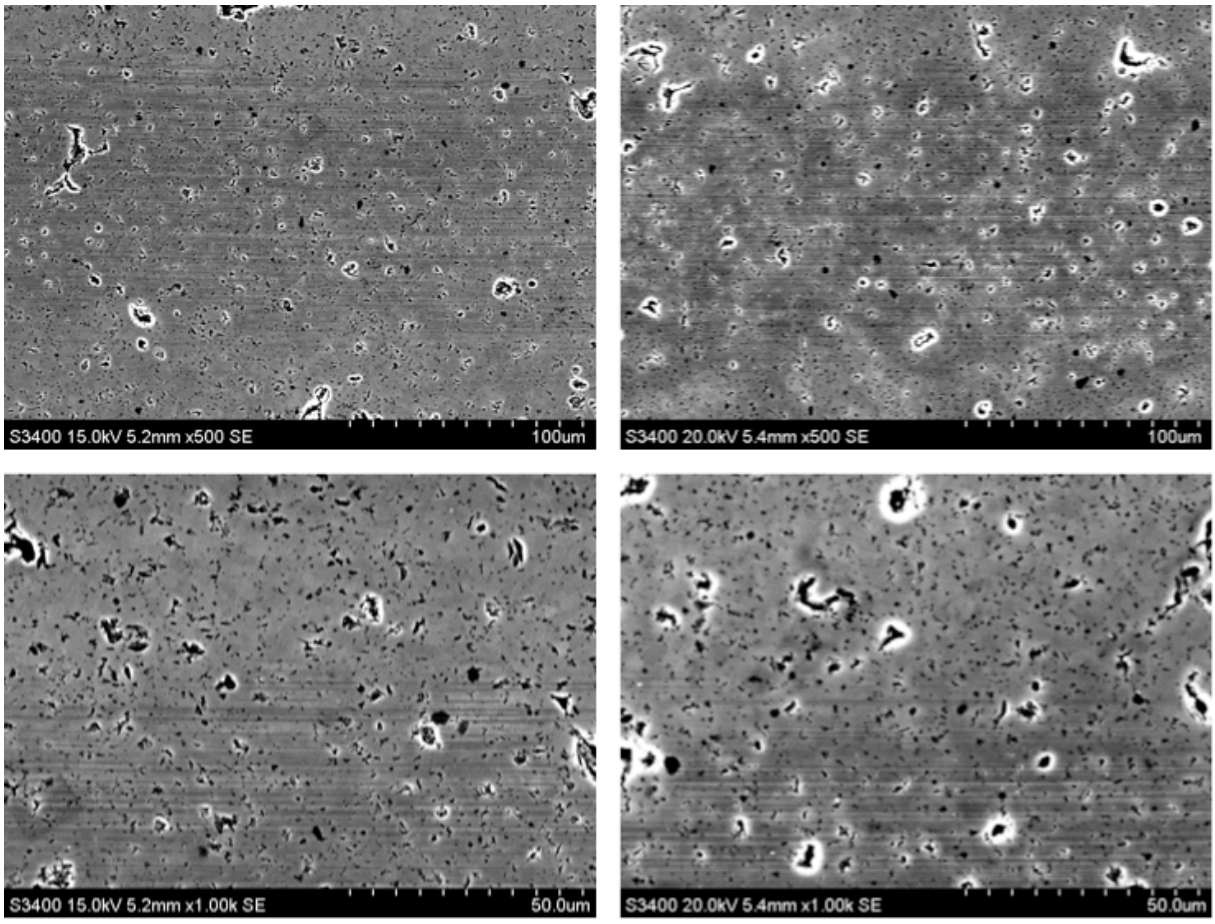

Figure 4.8: Tribological testing on silicon carbide with clean PAO (left) and clean PAG (right) as lubricant

In Figure 4.8 SEM images of the silicon carbide samples are shown. The left images are from the contact lubricated with clean PAO, and PAG is at the left. Only abrasive wear can be seen, for both the lubricants.

A expected, COF is much higher for dry contacts in stainless steel, than for those with seawater and lubricant, as shown in Figure 4.9. This is also the result for the tests with silicon carbide, as shown in Figure 4.10, but the difference between the different conditions are much less. This is expected, since silicon carbide has shown little wear and low COF in previous work, as described in section 2.5.2.

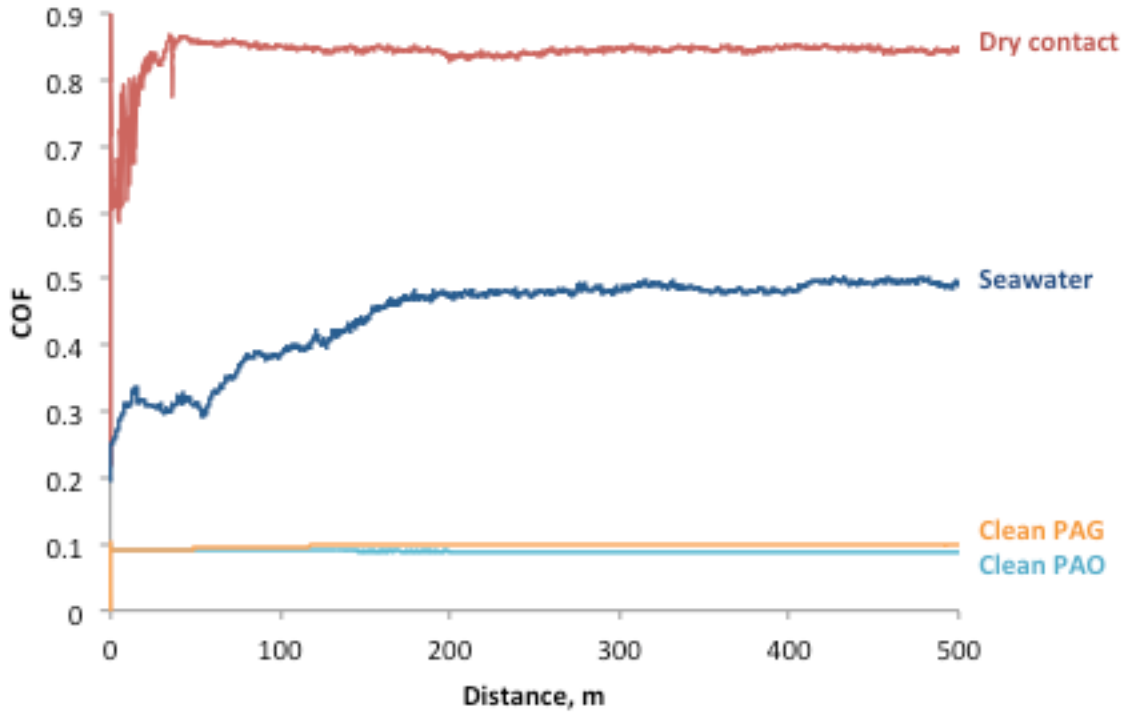

Figure 4.9: COF for dry contact on stainless steel and contact lubricated with clean seawater, clean PAO and clean PAG

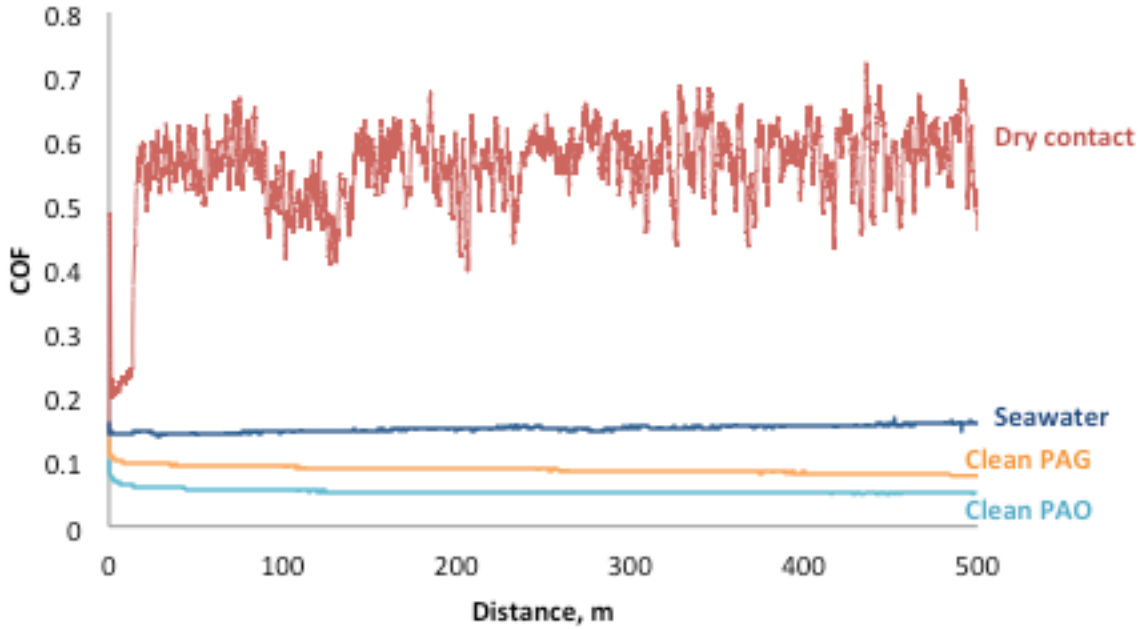

Figure 4.10: COF for dry contact on silicon carbide and contact lubricated with clean seawater, clean PAO and clean PAG

4.3.1 Pitting

For the tribological testing of stainless steel with clean PAG as the lubricant, pitting occurred, as shown in Figure 4.11 a and b. A non-tribological test was performed, as described in section 3.3, in order to determine if the pitting was corrosive or wear induced. This test did not give any pitting at all, as shown in Figure 4.11c. This indicates that the pitting is completely wear induced.

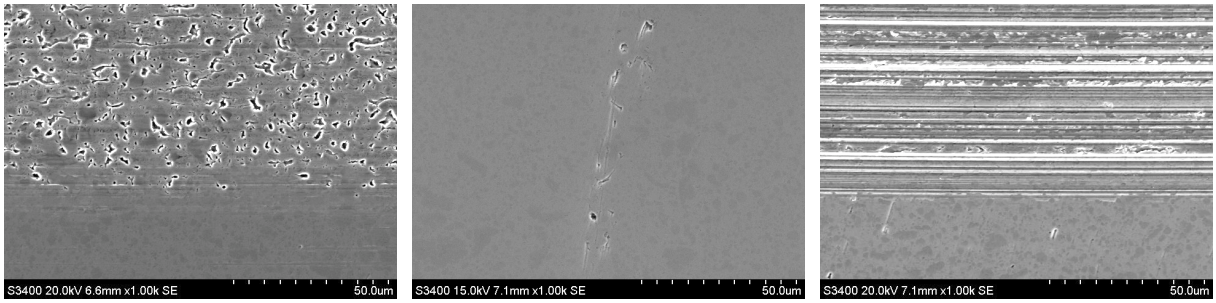

Figure 4.11: The left image show the wear track from the tribological test with clean PAG as lubricant. The image in the middle shows the surface of a polished stainless steel surface after the non-tribological immersion-test in clean PAG. To the right there is an image of the wear track produced with an additive-free PAG oil as the lubricant

Further, it was desired to determine if the pitting was a result of the additive package composition. This was investigated by performing a tribological test with an additive-free PAG oil, as described in section 3.3. A SEM image of the wear track is given in Figure 4.11d, and no pitting has occurred. Hence, the pitting is most likely a result of the additive package composition.

According to the supplier of the PAG lubricant it is supposed to have good micro-pitting resistance, as described in section 2.3. This is not in accordance with the results obtained in this work.

The supplier has not specified for what material the lubricant is micro-pitting resistance, and it is believed that the pitting is a result of this specific stainless steel (AISI 440C) in combination with the specific additive package in this lubricant. Since the composition of the additive package is a company secret, it is difficult to propose a more detailed explanation. Thus, more tests have to be performed in order to explain the pitting.

4.4 Contaminated lubricant

4.4.1 Effect on visual appearance

As described in section 2.4 an oil will remain transparent as long as the water content is below the saturation limit. If more water is added, an emulsion will form, and the oil will appear cloudy.

A photo of clean and contaminated PAO is given in Figure 4.12. As it can be seen the lubricant tappears cloudy even with as little as 100 ppm of seawater. This means that the saturation limit already has been exceeded, and two phases exists. A saturation limit below 100 ppm is very low. This is consistent with the chemical composition of the base oil that says that PAO base oil is very hydrophobic, as described in subsection 2.3.3.

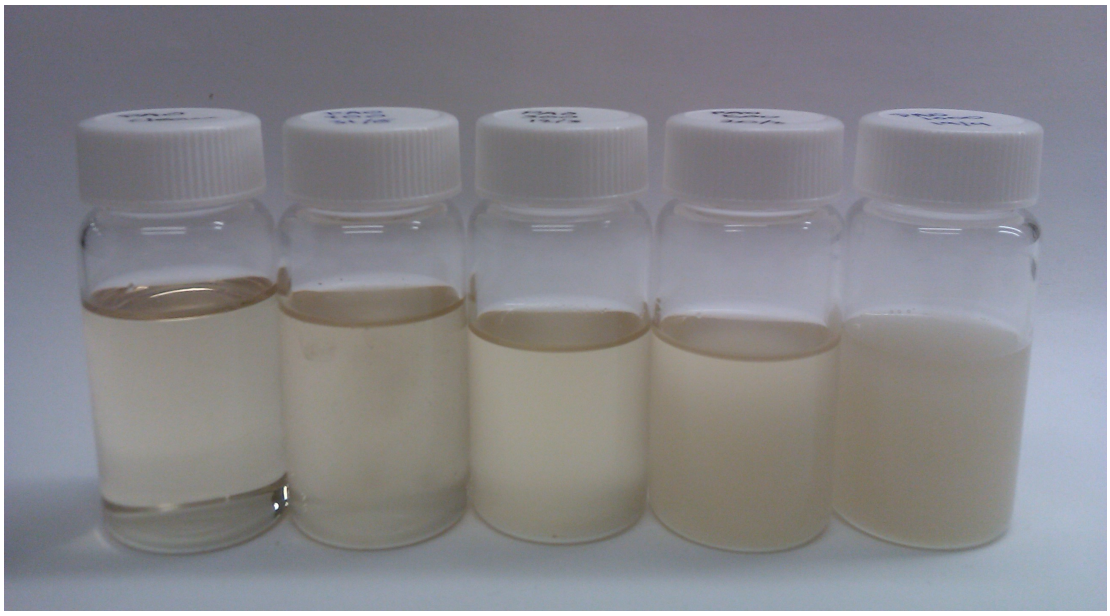

Figure 4.12: Visual appearance of polyalphaolefin with increasing amount of seawater content; 0, 100, 300, 500 and 1000 ppm from left to right

A photo of the PAG lubricant with 0, 300 and 500 ppm of seawater is shown in Figure 4.13. The lubricant does not turn cloudy when the seawater content increases, as it did for PAO. This implies that there only exists one phase, so that the water is dissolved in the lubricant. Hence, this lubricant is much more hydrophilic than PAO, and the saturation limit is much higher. This is explained by the chemical composition of the base oil, as described in subsection 2.3.4

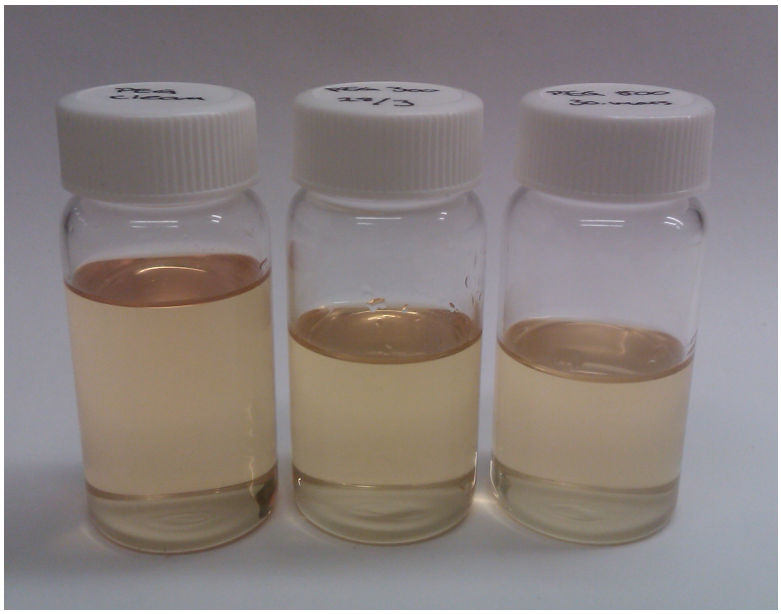

Figure 4.13: Visual appearance of polyalkylene glycol with increasing amount of seawater content; 0, 300 and 500 ppm from left to right

It should be mentioned that certain additives can influence the water solubility in the oils, as described in section 2.3.1. However, since this package is unknown, it can not be determined if this has influenced the solubility.

4.4.2 Lubricant degradation

It was performed a degradation test for PAO to look at the effect of the seawater in the oil as a function of time. The tribological test was performed with stainless steel as the test material, and with PAO contaminated with 300 ppm sweater as lubricant, as described in section 3.3.

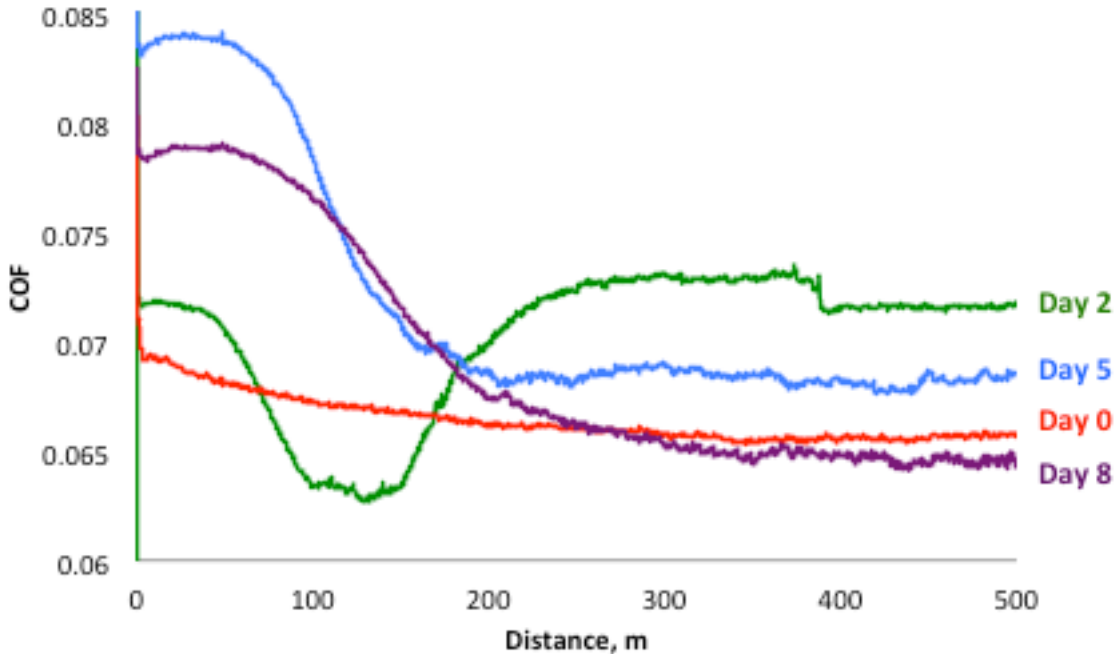

Figure 4.14: Degradation test of PAO with 300 ppm seawater, on stainless steel

The results from the degradation test is given in Figure 4.14. It can easily be seen that the COF for the tribological test changes as a function of time after mixing lubricant and seawater.

It appears that COF becomes more unstable as the time increases, but a clear trend can not be found from these results. For the experimental work in this project it was desired to have a stable COF after the running-in period, so it would be easy to compare the results. It was chosen to prepare the mixture the day before the experiments, because it was believed that this would be enough time for the seawater to effect the lubricating properties of the oil, but not so long that the COF would be unstable

4.4.3 Effect on COF

These tribological tests with contaminated lubricants were performed as described in section 3.3. An overview of all the tests are given in Table 4.1, and all the results and SEM images from all the repetitions can be found in Appendix B.

Table 4.1: Overview of performed (X), and not performed (-), tests with contaminated lubricants

	Repetition	Self-matet stainless steel	Self-mated silicon carbide
PAO 100 ppm	1	X	-
	2	X	-
PAO 300 ppm	1	X	X
	2	X	X
	3	X	-
	4	X	-
PAO 500 ppm	1	X	X
	2	X	X
	3	X	-
	4	X	-
PAO 1000 ppm	1	X	-
	2	X	-
PAG 300 ppm	1	X	X
	2	X	X
PAG 500 ppm	1	X	X
	2	X	X

Stainless steel

The mean values for the friction coefficients with standard deviation, has been calculated for the different contamination levels. The result for PAO is plotted as a function of distance in Figure 4.15 together with the values for the clean lubricant.

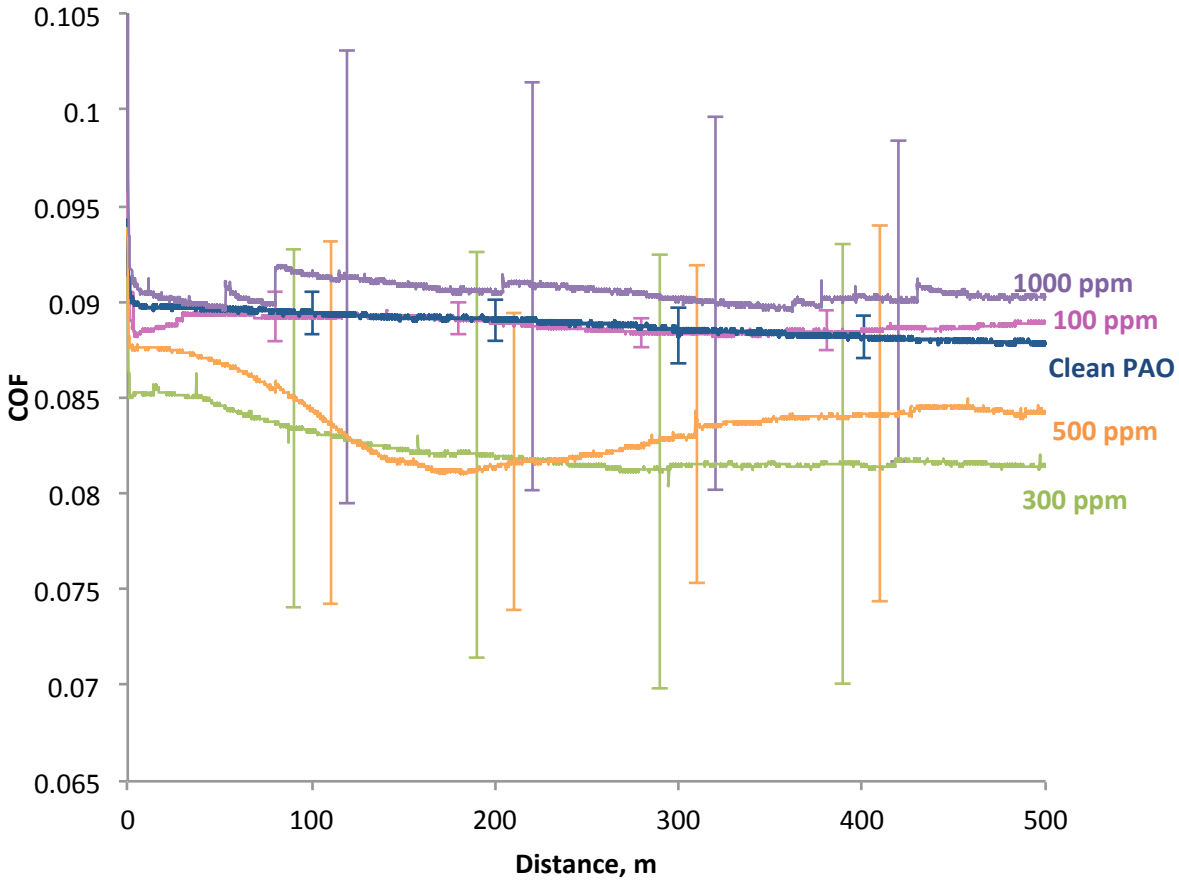

Figure 4.15: Mean values of COF calculated from the different repetitions with standard deviations, for PAG with different amounts of seawater

The lines for clean lubricant and with 100 ppm seawater is almost overlapping, and they both have low standard deviations. Both PAO with 300 and 500 ppm seawater has a lower COF, but the standard deviation is much higher. PAO with 1000 ppm seawater has the highest COF, and the standard deviation is also high. This might indicate that as the seawater increases, the COF get unstable and that the standard deviation increases.

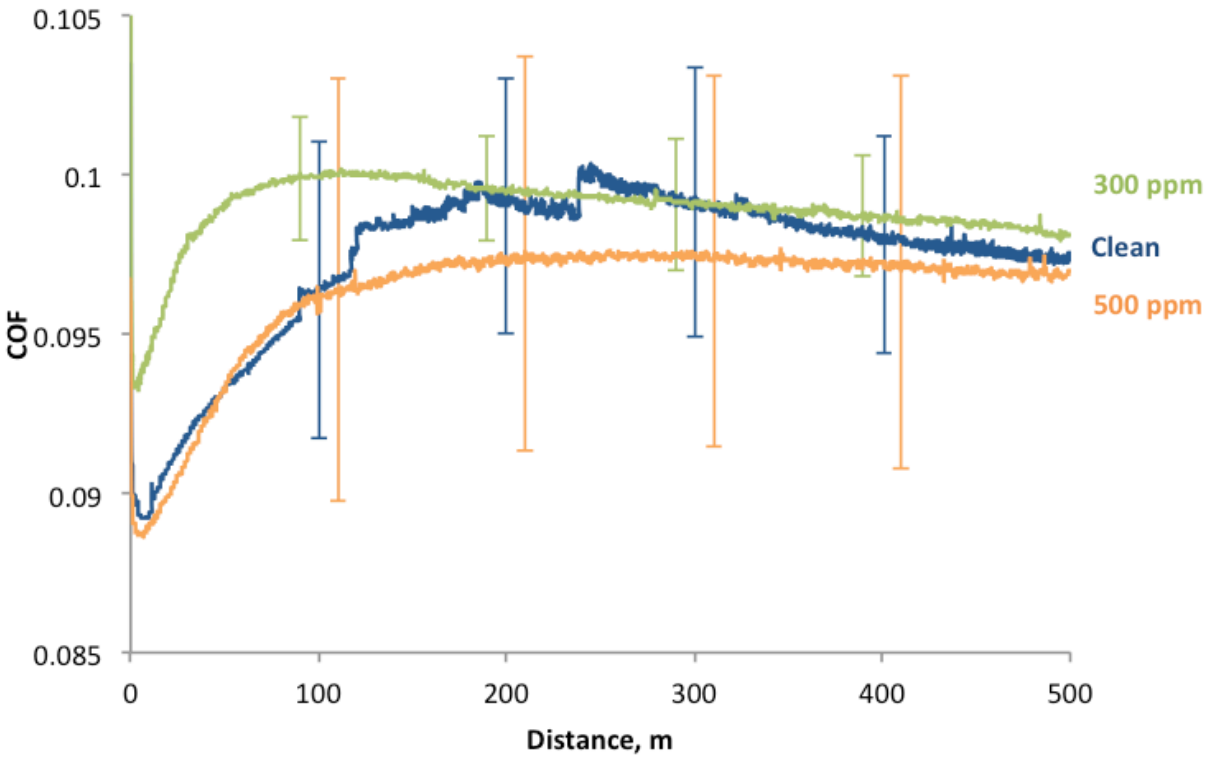

Figure 4.16: Mean values of COF calculated from the different repetitions with standard deviations, for PEG with different amounts of seawater.

A plot of the friction coefficient obtained for PAG with 0, 300 and 500 ppm seawater, is shown in Figure 4.16. As for the PAO lubricant, it is difficult to find any obvious trend among the data. The lubricant contaminated with 300 ppm seawater has a COF higher than the clean lubricant. In addition, it has a standard deviation that is narrower than for the clean lubricant. Whereas, the lubricant contaminated with 500 ppm seawater has a COF less than the clean lubricant, but the standard deviation is higher.

The mean values, and also the standard deviation, for the PAG lubricant, are only calculated from two measurements (three repetitions for the clean lubricant). Thus the mean value, and the standard deviation, is very sensitive to inconsistency in test performance and surface treatment. By performing a larger number of repetitions, this uncertainty would be reduced, and the result would be more accurate. Unfortunately, this was not done in this work.

Silicon carbide

The mean values for the COF from testing with self-mated silicon carbide lubricated with PAO are shown in Figure 4.17. As it can be seen, the clean lubricant exhibits the lowest COF. In the upper part of its standard deviation, the COF for PAO with 300 ppm sweater can be found. PAO with 500 ppm of seawater has a COF that is higher than both clean and 300 ppm lubricant. This implies that as the seawater content in the lubricant increases, the COF also increases.

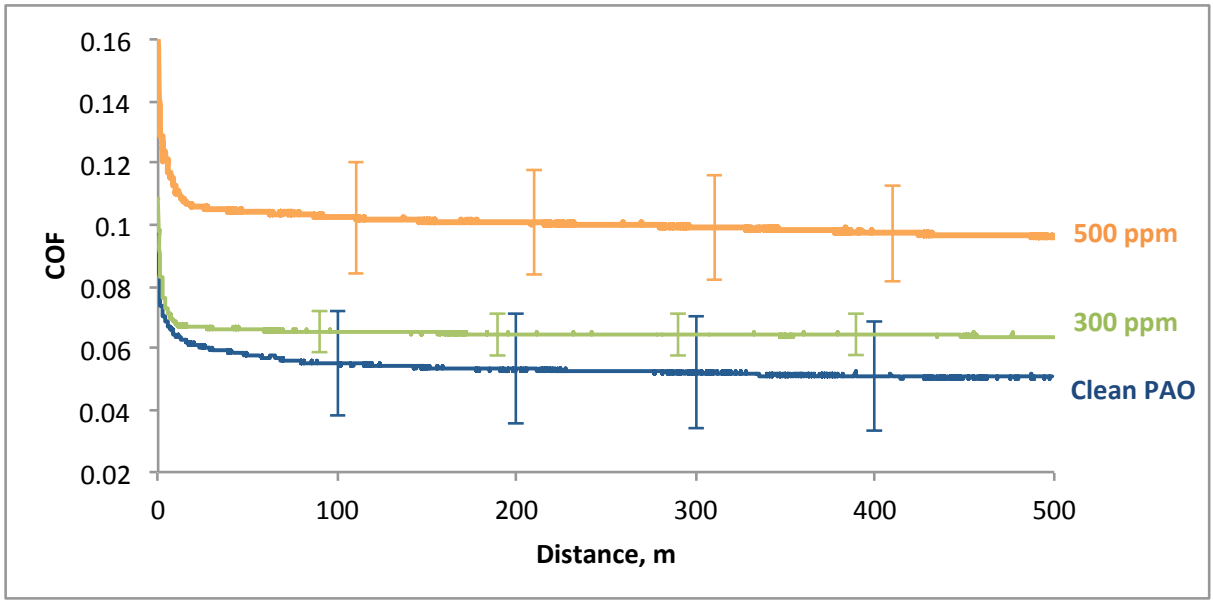

Figure 4.17: COF for self-mated SiC with PAO as lubricant with different amounts of seawater. The line for the different concentration is the mean value obtained from the different repetitions. The bars indicate the standard deviation between the repetitions

Further, it can be seen from Figure 4.17 that all the lines stabilize in the same manner after the running-in period. However, it appears that when the lubricant is contaminated with seawater, the running-in period gets shorter. It also seems that the end of the period gets more defined. That is, for the clean lubricant the transition is smooth and it is not easy to define the end of it. Whereas for the contaminated lubricants, the transition is more well defined by a sharp change in the slope of the line. As it was concluded above in subsection 4.4.1, the seawater did not dissolve inn the seawater. In stead an emulsion was formed. These results might be explained by the results obtained in previous work presented in section 2.5.2.

The results for silicon carbide with contaminated PAG are plotted in Figure 4.18. These results do not show the same trend as the PAO lubricant described above. Both the contaminated lubricants have lower COF than the clean PAG. Further, the lubricant with 300 ppm seawater has a COF that is even lower than the one with 500 ppm. From the

plot it can also be seen that as the seawater content increases, the standard deviation increases.

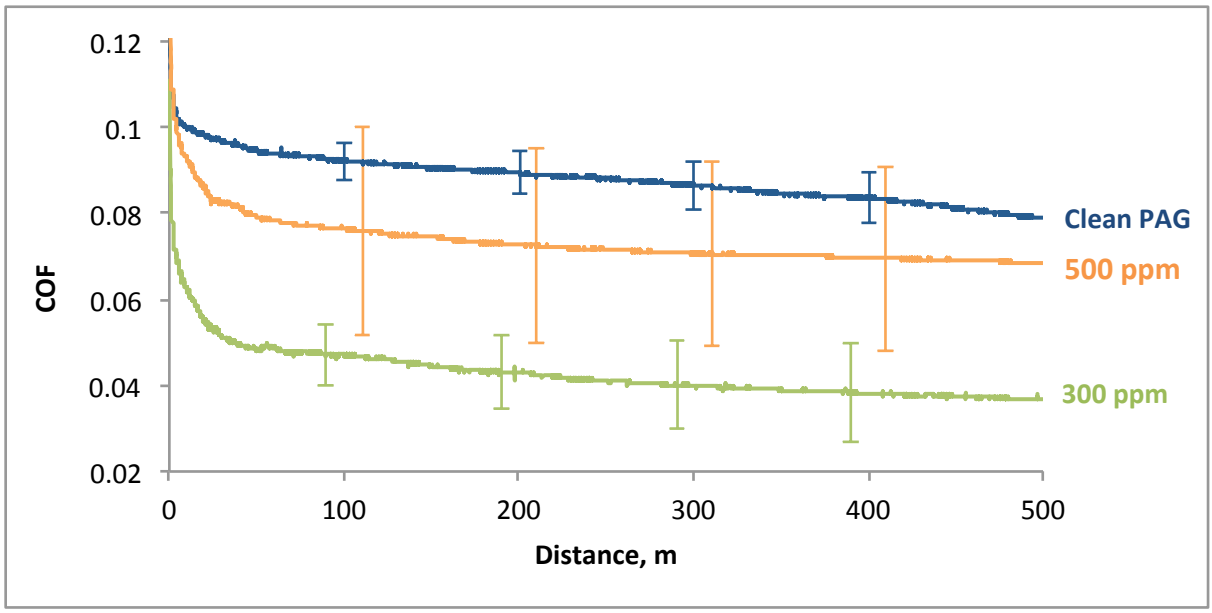

Figure 4.18: COF for self-mated SiC with PAG as lubricant with different amounts of seawater. The line for the different concentration is the mean value obtained from the different repetitions. The bars indicate the standard deviation between the repetitions

4.4.4 Effect on wear mechanism

Stainless steel

The wear mechanisms for the contacts lubricated with contaminated oils were investigated in the SEM, as described in section 3.4.1. More SEM images for the different conditins, can be found in Appendix B.

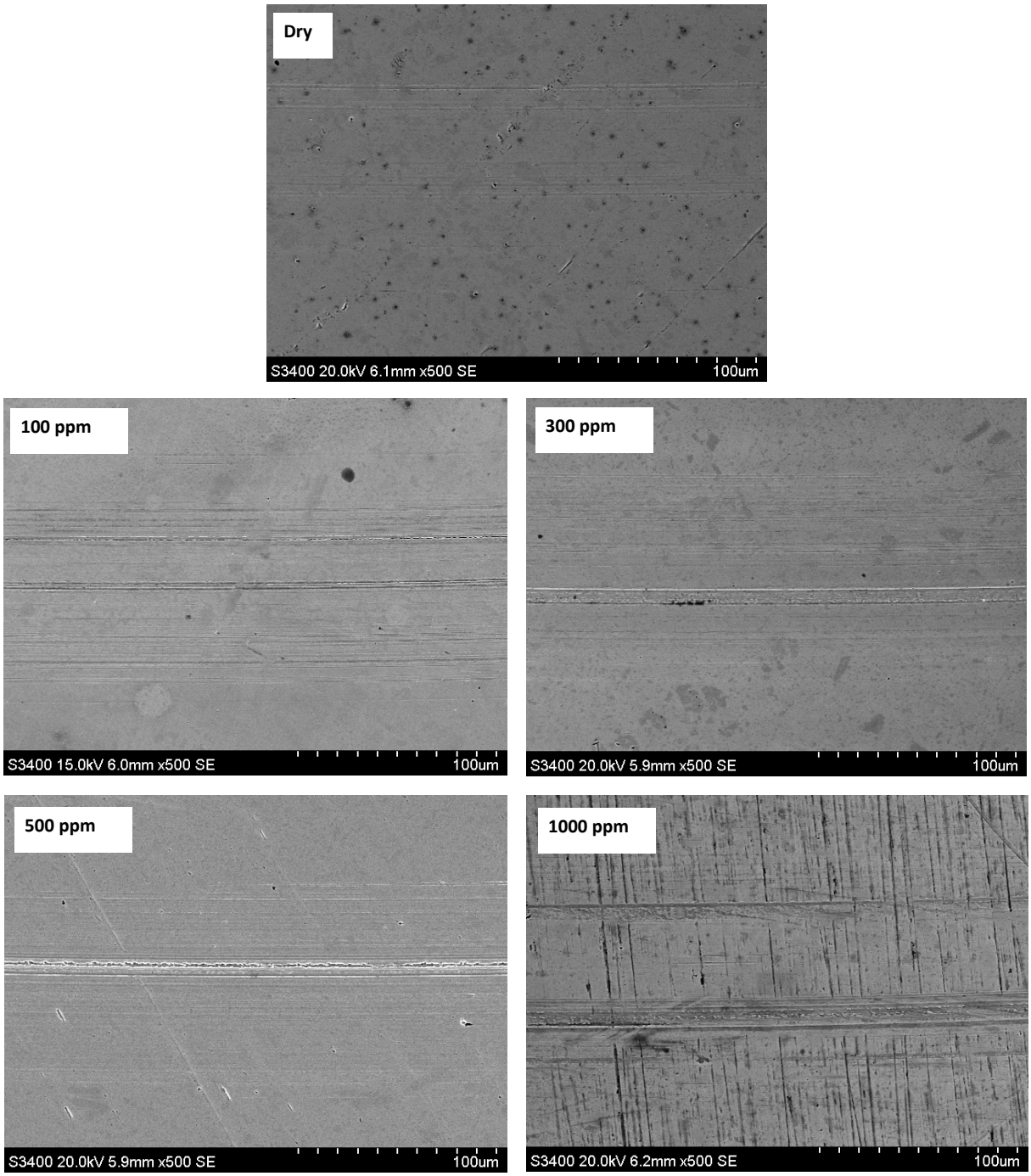

Figure 4.19: SEM images of the stainless steel samples from testing with PAO lubricant, both clean and contaminated with 100, 300, 500 and 1000 ppm seawater.

In Figure 4.19 some of the wear tracks on stainless steel from testing with PAO, both clean and lubricated, are shown. It can be seen that with increasing seawater content, the amount of abrasive wear also increases. This might be due to tribocorrosive behaviour, as described in section 2.2.4.

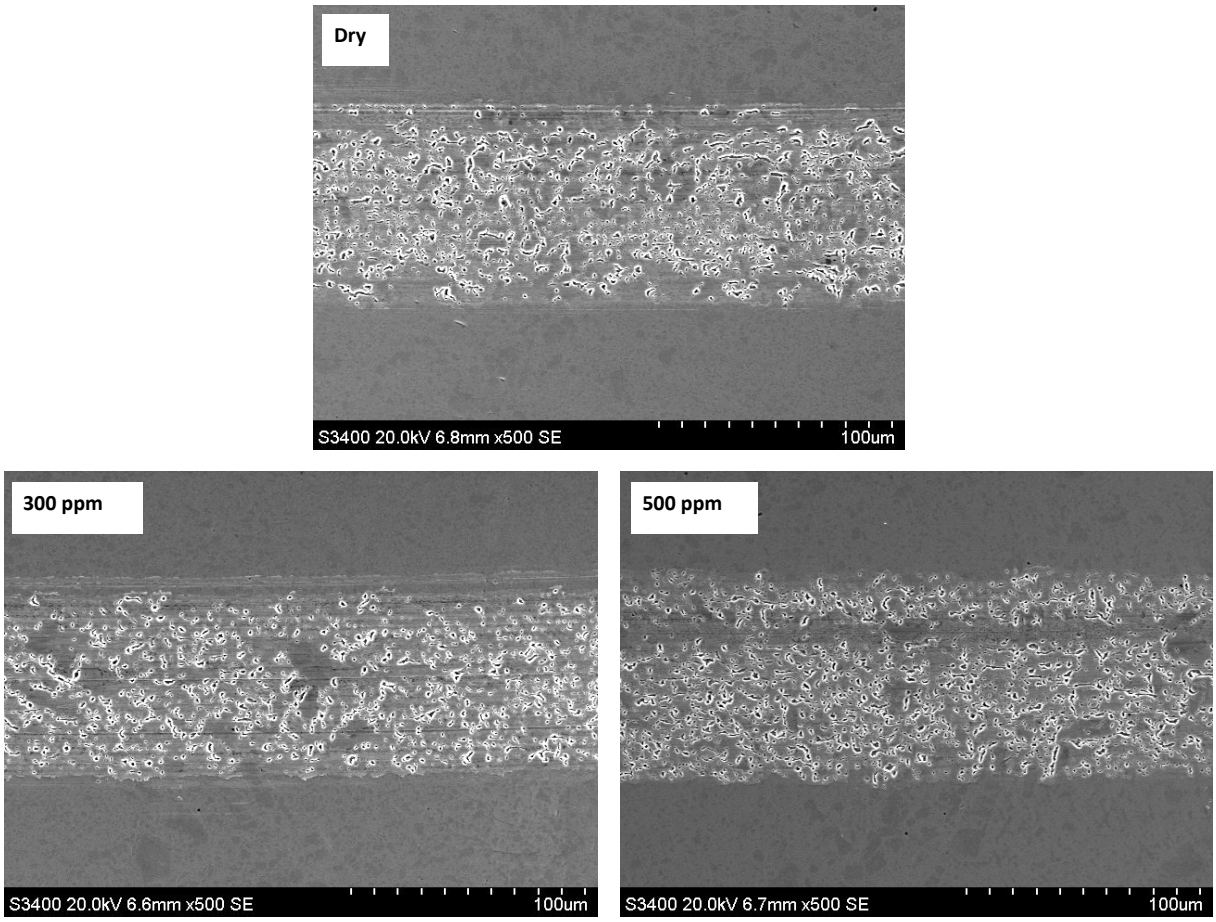

Figure 4.20: SEM images of the stainless steel samples from testing with PAG lubricant, both clean and contaminated with 300 and 500 ppm seawater.

The wear tracks formed from testing with clean and contaminated PAG on stainless steel, is shown in Figure 4.20. The pitting can clearly be seen in all the images. Other than this, abrasive wear can be seen, but it do not look like the amount of wear increases as a function of seawater content, as it did for PAG.

Silicon carbide

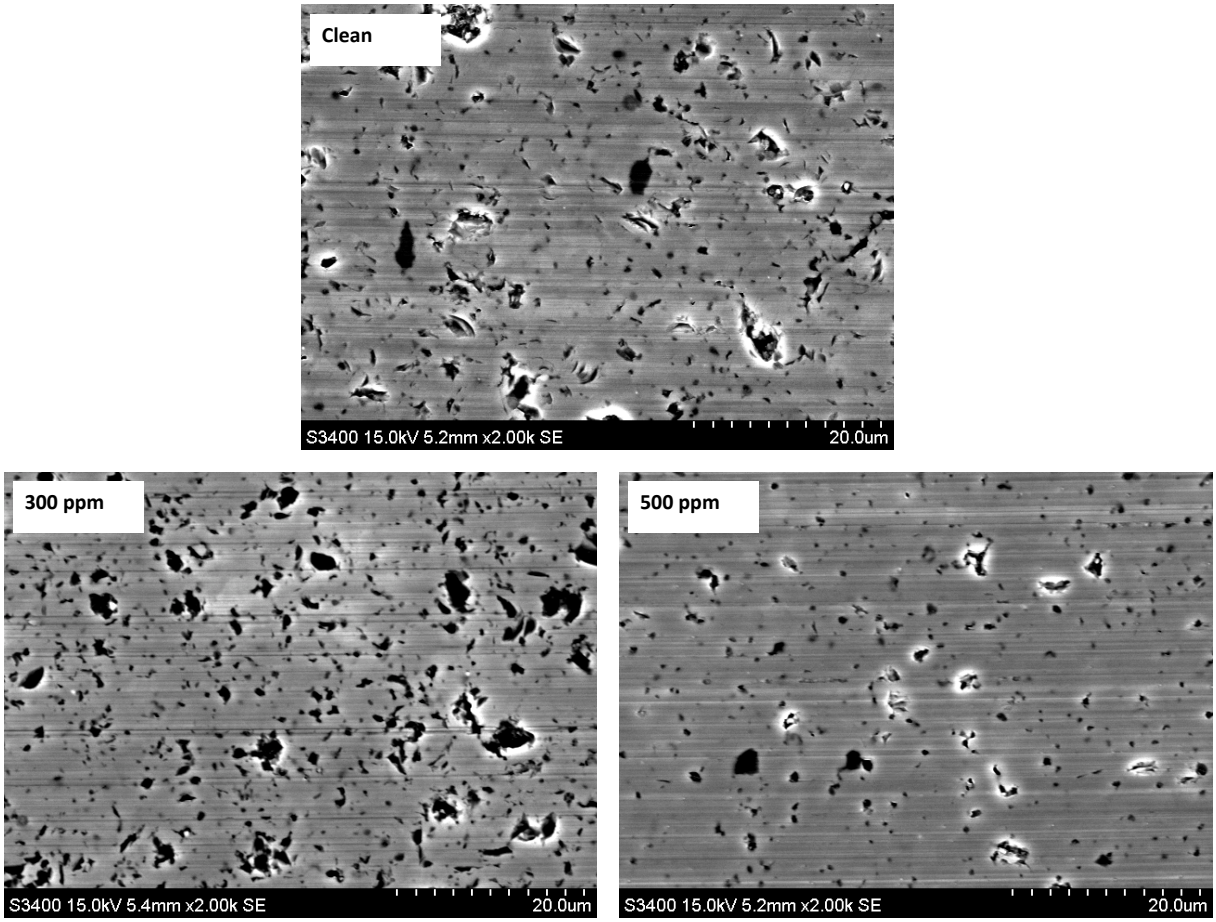

Figure 4.21: SEM images of the silicon carbide samples from testing with PAO lubricant, both clean and contaminated with 300 and 500 ppm seawater.

The wear track on silicon carbide with clean and contaminated PAO, is shown in Figure 4.21. The abrasive wear can clearly be seen, but no other types of wear can be detected. This might indicate that the water-in-oil emulsion has not influenced the wear.

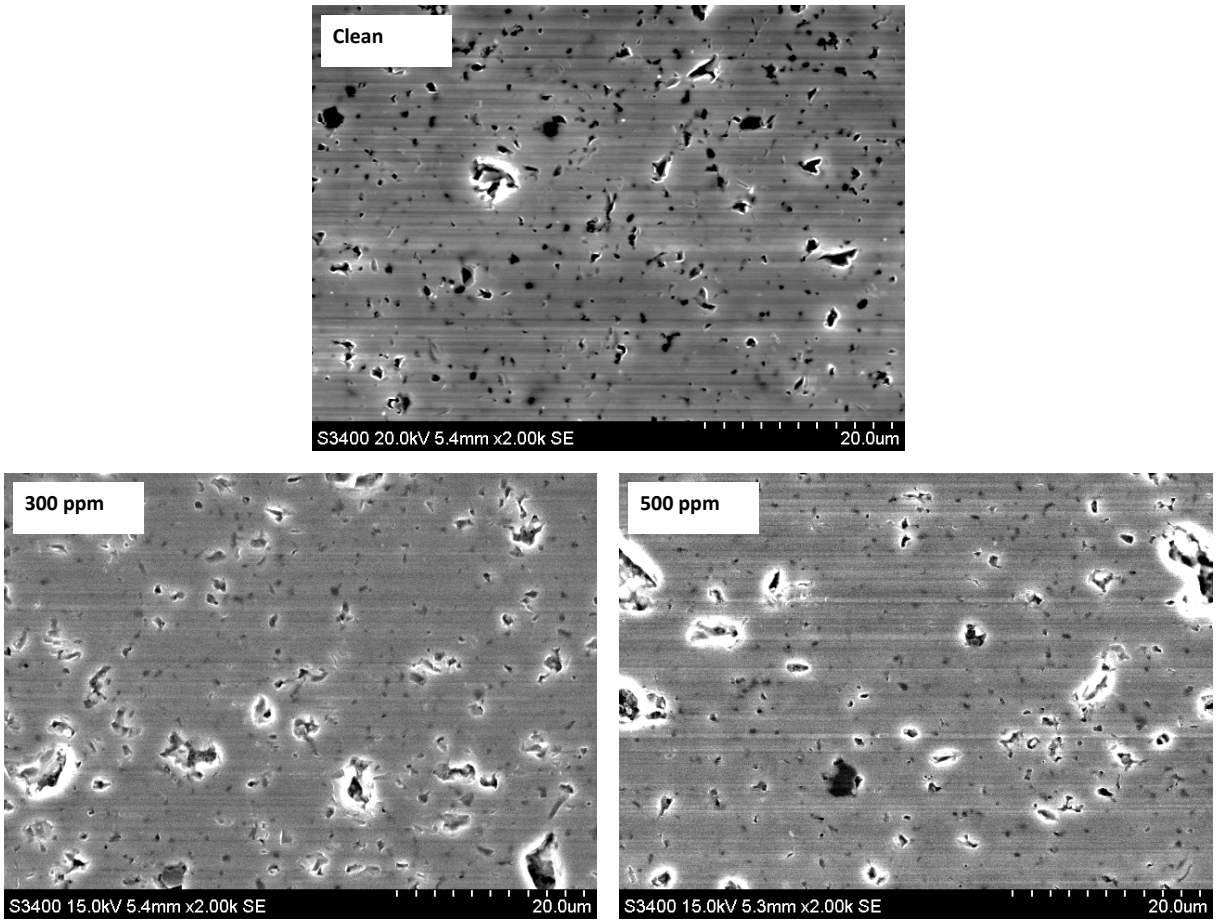

Figure 4.22: SEM images of the silicon carbide samples from testing with PAG lubricant, both clean and contaminated with 300 and 500 ppm seawater.

In Figure 4.22 some of the wear tracks on silicon carbide from testing with PAO, both clean and lubricated, are shown. Only abrasive wear can be seen.

4.4.5 Effect on volume loss

The volume loss on the stainless steel samples were estimated as described in section 3.4.2, and the result is presented in Figure 4.23. As it can be seen the volume loss was less for all the tests performed with the PAG lubricant, regardless of the contamination level.

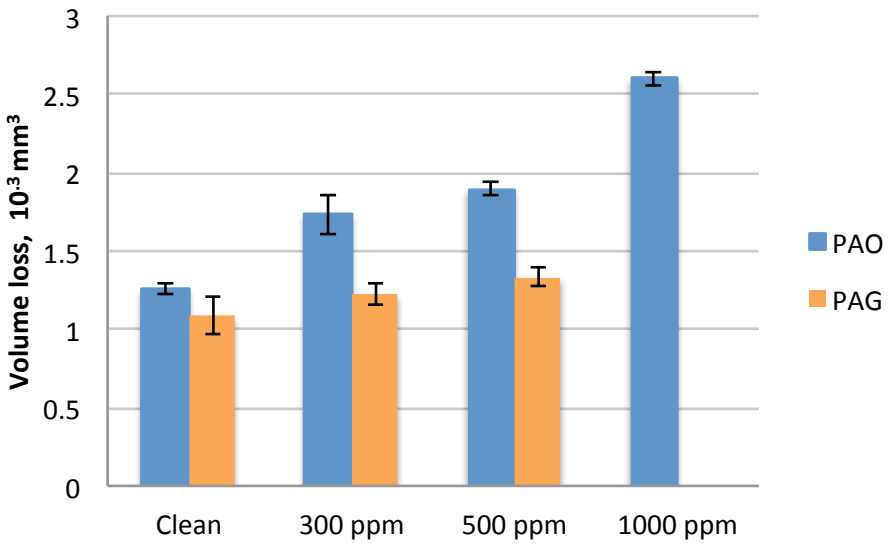

Figure 4.23: Measured volume loss for stainless steel lubricated with PAO and PAG with different amounts of seawater content

Further it can be seen that as the contamination level increases in the PAO lubricant, the wear loss increases. This can be explained by the increasing amount of abrasive wear. For the PAG lubricant, the wear also increases with increasing contamination level.

In Figure 4.24 the volume loss is plotted as a function of the contamination level, and it can be seen that the increase is approximately linear for both the lubricants. However, the slope of the increase appears to be higher for the PAO lubricant than for the PAG. This might be because PAO forms an emulsion with seawater, whereas it is dissolved in PAG.

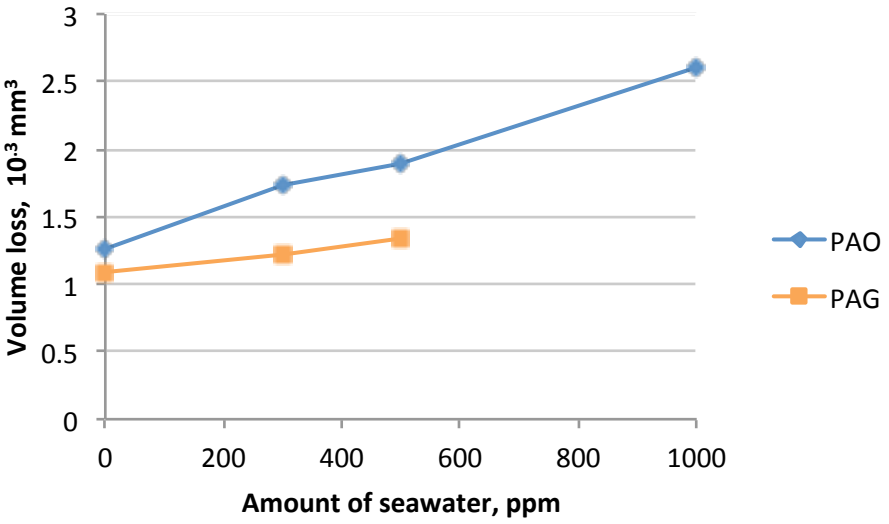

Figure 4.24: Volume loss as a function of seawater content for stainless steel lubricated with PAO and PAG

5 Conclusions

For dry tribological testing COF was found to be mush less for self-mated silicon carbide than for self-mated stainless steel. This is as expected, since silicon carbide has shown outstanding tribological properties in previous work.

Clean PAO gave a lower COF than PAG for tests performed on the stainless steel. With PAO, two-body abrasive wear and plastic deformation were detected. This was also detected for the tests performed with PEG as lubricant, in addition to pitting. The pitting was found to be entirely wear induced. Most likely, some of the additives in the additive package react with the metal surface of this specific material. In order to address this phenomenon in more detail, further tests have to be performed. Also, investigation of the additive package should be done to explain the results.

When PAO was contaminated with small amounts of seawater, it formed an emulsion. The tribological testing of stainless steel samples, gave unstable friction coefficients. The standard deviation for these tests increased with increasing seawater content. Further, it was found that the amount of abrasive wear, and the wear volume loss, increased as the contamination level increased. This might be due to tribocorrosion.

The PAG showed no increase abrasive wear when the content of seawater was increased. However, the calculated wear volume loss shoved an increase, but nor as much as for the PAG lubricant. No trend in COF as a function of seawater content could be found, even though the result where more stable than for PAO. The seawater was dissolved in the PAG lubricant.

For self-mated silicon carbide testing only abrasive wear could be found for both dry contact, and lubricated. The results from PAO contaminated with seawater, showed a clear increase in COF as a function of seawater content. Further, the COF all stabilized after the running-in period. PAG showed no such trend with increasing amounts of seawater, but the standard deviation of the measurements increased.

6 Further work

The most obvious

- Silicon carbinde layer on top of the SS – tribological testing
- Does the seawater bind to the surface and contribute to wear/lubrication?
- Analyze the lubricant used for the tests – wear particles? Dissolved?
- What happens to the additive package?
- Viscosity measurements
-

7 References

1. Nosonovsky M, Bhushan B. Green Tribology: Biomimetics, Energy Conservation and Sustainability. Berlin, Heidelberg: Springer Berlin Heidelberg; 2012.
2. Hau E, Renouard H. Wind Turbines: Fundamentals, Technologies, Application, Economics. Berlin, Heidelberg: Springer Berlin Heidelberg; 2006.
3. Czichos H. Tribology: a systems approach to the science and technology of friction, lubrication and wear. Amsterdam: Elsevier; 1978. XIII, 400 s. p.
4. Stachowiak GW, Batchelor AW. Engineering tribology. Amsterdam: Elsevier Butterworth-Heinemann; 2005. xxiv, 801 s. p.
5. Van Beek A, Delft TU. Advanced Engineering Design: Lifetime Performance and Reliability: TU Delft; 2006.
6. Bhushan B. Modern tribology handbook. Boca Raton, Fla.: CRC Press; 2001. 2 b. p.
7. Landolt D. Corrosion and surface chemistry of metals. Lausanne, Switzerland: EPFL Press; 2007. x, 622 s. p.
8. Blau PJ. Friction science and technology: from concepts to applications. Boca Raton: CRC Press; 2009. xiv, 420 s. p.
9. Revie RW, Uhlig HH. Corrosion and corrosion control: an introduction to corrosion science and engineering. Hoboken. N.J.: Wiley-Interscience; 2008. XX, 490 s. p.
10. Greaves M. Pressure viscosity coefficients and traction properties of synthetic lubricants for wind turbine gear systems. Lubrication Science. 2012;24(2):75-83.
11. Lainé E, Olver AV, Beveridge TA. Effect of lubricants on micropitting and wear. Tribology International. 2008;41(11):1049-55.
12. Williams JA. Engineering tribology. Cambridge: Cambridge University Press; 2005. XIX, 488 s. p.
13. Rudnick LR. Synthetics, mineral oils, and bio-based lubricants: chemistry and technology. Boca Raton: CRC/Taylor & Francis; 2006. 928 s. p.
14. Booser ER. CRC handbook of lubrication and tribology, Vol. 3, Monitoring, materials, synthetic lubricants and applications. Boca Raton, Fla.: CRC Press; 1994. 619 s. p.
15. Szeri AZ. Fluid film lubrication. Cambridge: Cambridge University Press; 2011. 1 online resource (xv, 547 s.) p.
16. Bloch HP. Practical lubrication for industrial facilities. Lilburn, GA: Fairmont Press; 2000. xiii, 612 s. p.
17. Fitch JC, Jaggernauth S. Moisture-The second most destructive lubricant contaminate and its effects on bearing life. Courtesy of Noria Corporation, P/PM Technology. 1994:50-3.
18. Mørk PC. Overflate og kolloidkjemi: grunnleggende prinsipper og teorier. Trondheim: Norges teknisk-naturvitenskapelige universitet, Instituttfor kjemisk prosessteknologi; 2004. X, 307 s. p.
19. Hamaguchi H, Spikes HA, Cameron A. Elastohydrodynamic properties of water in oil emulsions. Wear. 1977;43(1):17-24.
20. Benner JJ, Sadeghi F, Hoeprich MR, Frank MC. Lubricating Properties of Water in Oil Emulsions. Journal of Tribology. 2006;128(2):296-311.
21. A/S CCJ. Clean Oil Guide. 2011; Available from: http://www.cjc.dk/fileadmin/user_upload/pdf/CJC_Brochures/Clean_Oil_Guide.pdf.

22. Beran E. Effect of chemical structure on the hydrolytic stability of lubricating base oils. Tribology International. 2010;43(12):2372-7.
23. Callister WD, Rethwisch DG. Materials science and engineering: an introduction. New York: Wiley; 2007. XXV, 721, [82] s. p.
24. Cardarelli F. Materials Handbook: A Concise Desktop Reference. London: Springer-Verlag; 2008.
25. Zum Gahr KH, Blattner R, Hwang DH, Pöhlmann K. Micro- and macro-tribological properties of SiC ceramics in sliding contact. Wear. 2001;250(1–12):299-310.
26. Presser V, Krummhauer O, Nickel KG, Kailer A, Berthold C, Raisch C. Tribological and hydrothermal behaviour of silicon carbide under water lubrication. Wear. 2009;266(7–8):771-81.
27. Erickson LC, Blomberg A, Hogmark S, Bratthäll J. Tribological characterization of alumina and silicon carbide under lubricated sliding. Tribology International. 1993;26(2):83-92.
28. Kato K. Tribology of Ceramics and Hard Coatings. Materialwissenschaft und Werkstofftechnik. 2003;34(10-11):1003-7.
29. Tomizawa H, Fischer TE. FRICTION AND WEAR OF SILICON-NITRIDE AND SILICON-CARBIDE IN WATER - HYDRODYNAMIC LUBRICATION AT LOW SLIDING SPEED OBTAINED BY TRIBOCHEMICAL WEAR. Asle Transactions. 1987;30(1):41-6.
30. Chen M, Kato K, Adachi K. Friction and wear of self-mated SiC and Si3N4 sliding in water. Wear. 2001;250:246-55.
31. Andersson P. Water-lubricated pin-on-disc tests with ceramics. Wear. 1992;154(1):37-47.

Appendix A: Calculation of seawater volume

Volume lubricant: 100 ml

Table **Feil! Det er ingen tekst med den angitte stilen i dokumentet.**.1: Constants used in the calculations

Constants		
Density seawater	1,02	g/cm3
Density PAO	0,85	g/ml
Mass PAO	85	g
Density PEG	1,067	g/cm3
Mass PEG	106,7	g

Table **Feil! Det er ingen tekst med den angitte stilen i dokumentet.**.2: Calculation of seaweter content

	Seawater content (ppm)	**Weight** (g)	**Volume** (ml)	**Volume** (µl)
PAO	100	0,085	0,0833	83
	300	0,255	0,250	250
	500	0,425	0,417	417
	1000	0,850	0,833	833
PEG	300	0,320	0,300	300
	500	0,534	0,500	500

Appendix B: Tribological testing and characterization of wear

B.1 Stainless steel, dry contact

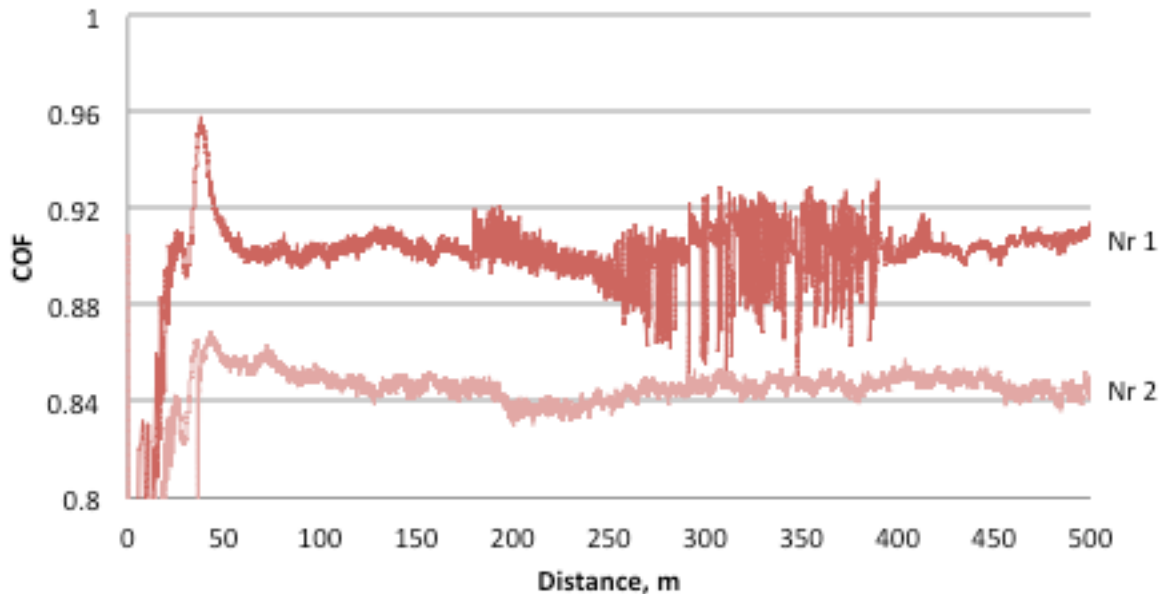

Figure B.1: Dry contact on stainless steel

Nr 2 is used as a measure of dry contact due to all the noise in test nr 1

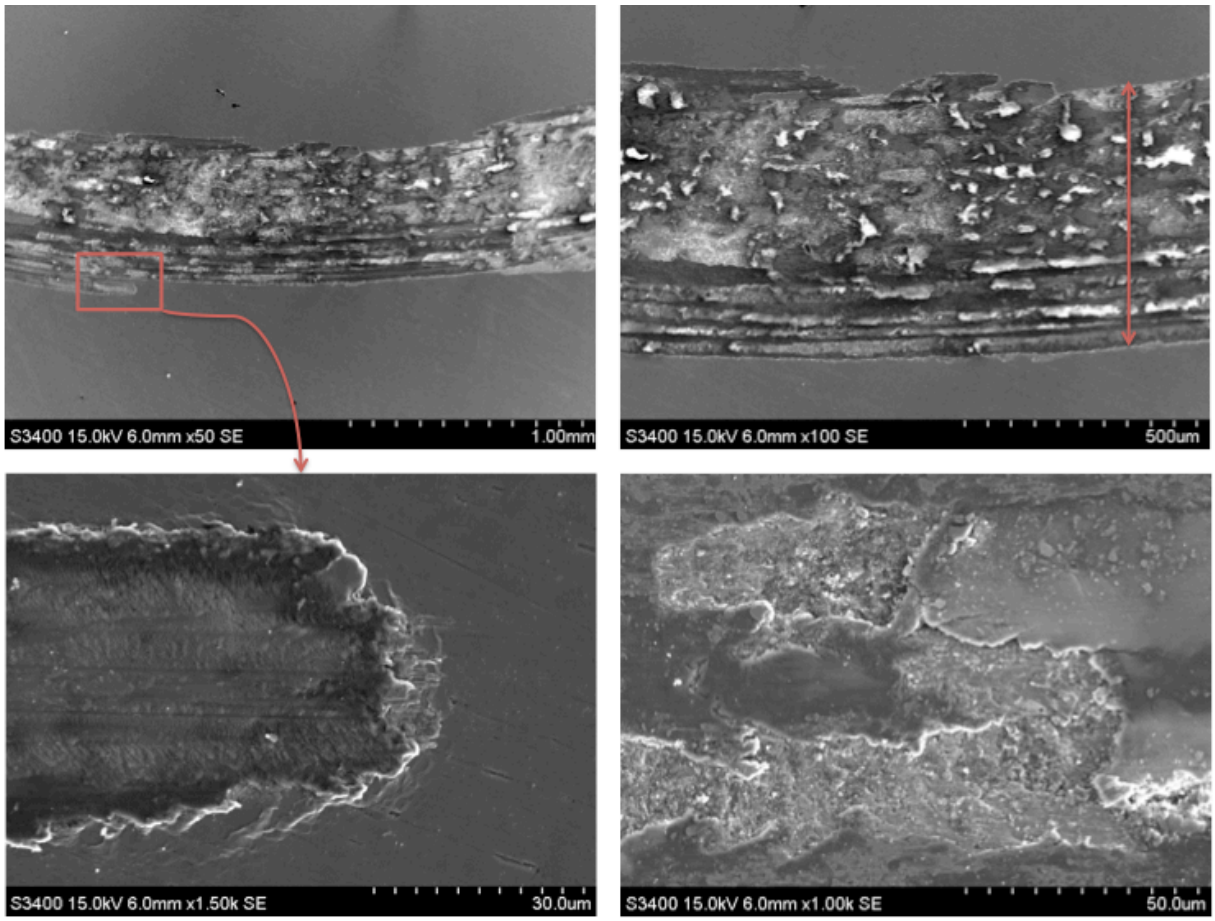

Figure B.2: SS, dry contact nr 1

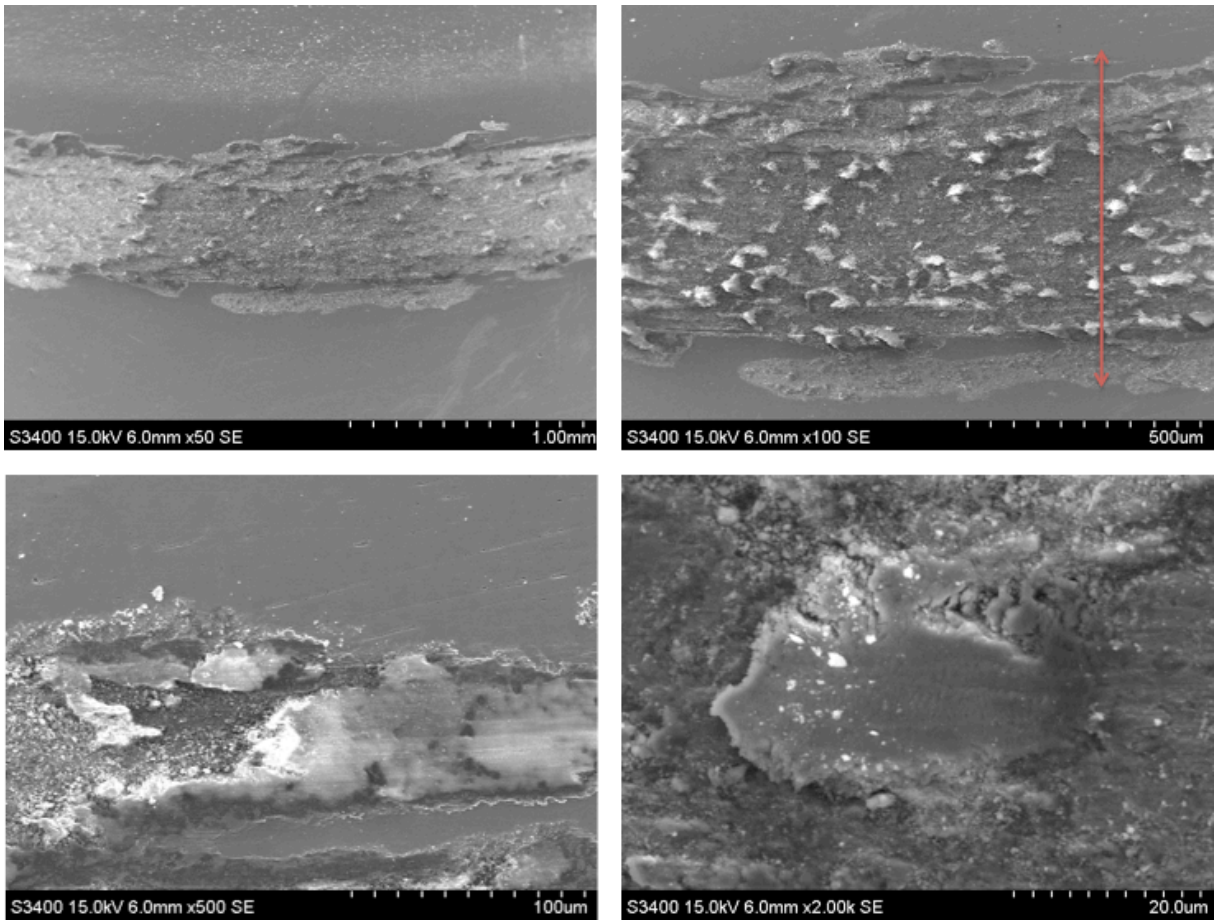

Figure B.3: SS, dry contact nr 2

B.2 Silicon carbide, dry contact

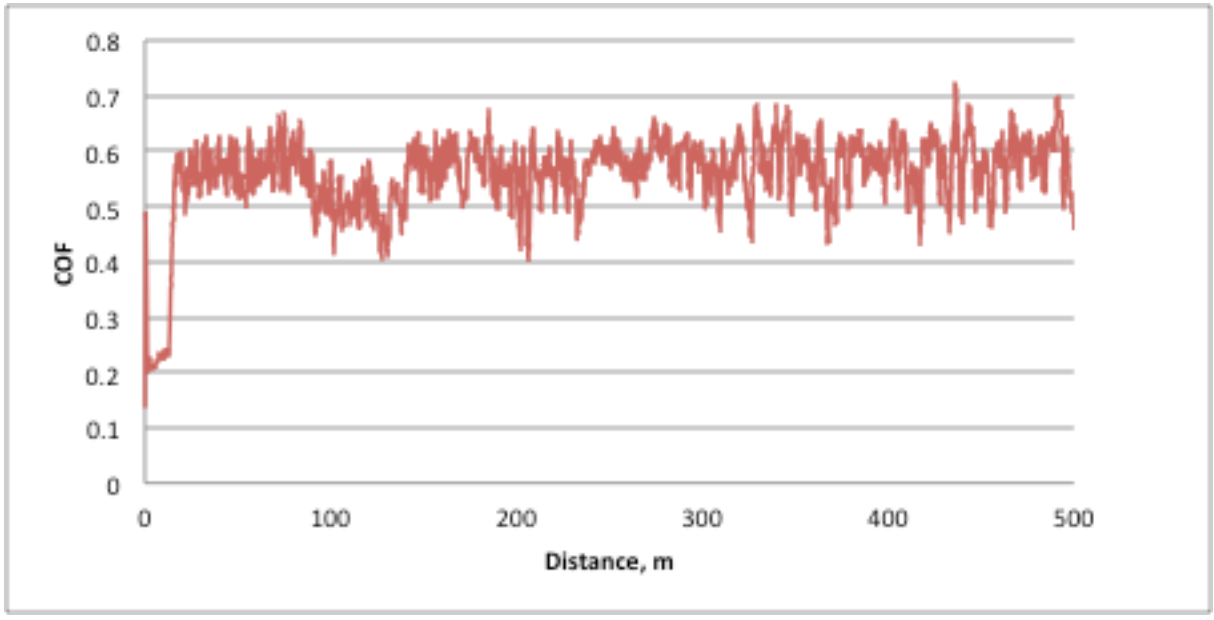

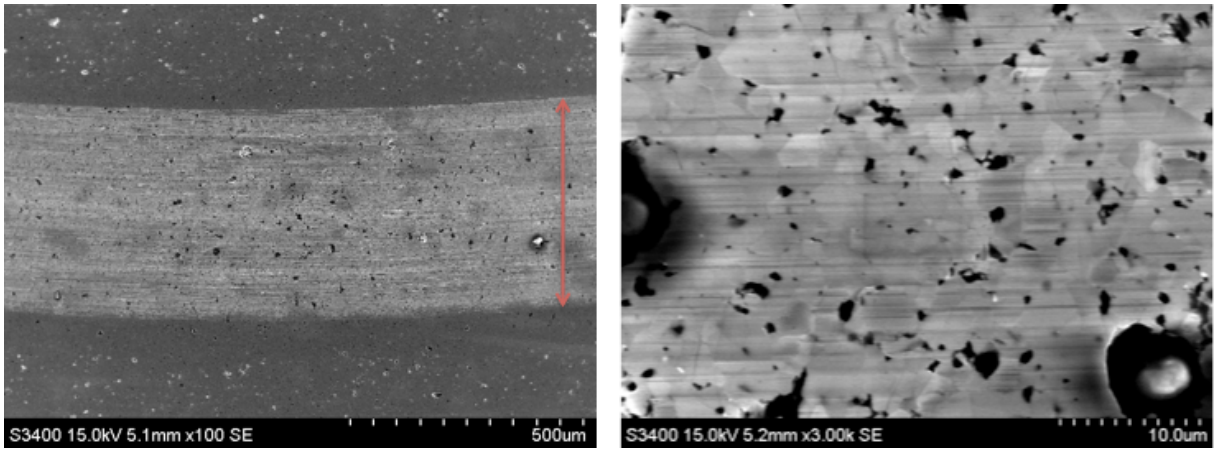

Figur B.1: SiC dry contact

B.3 Stainless steel, seawater

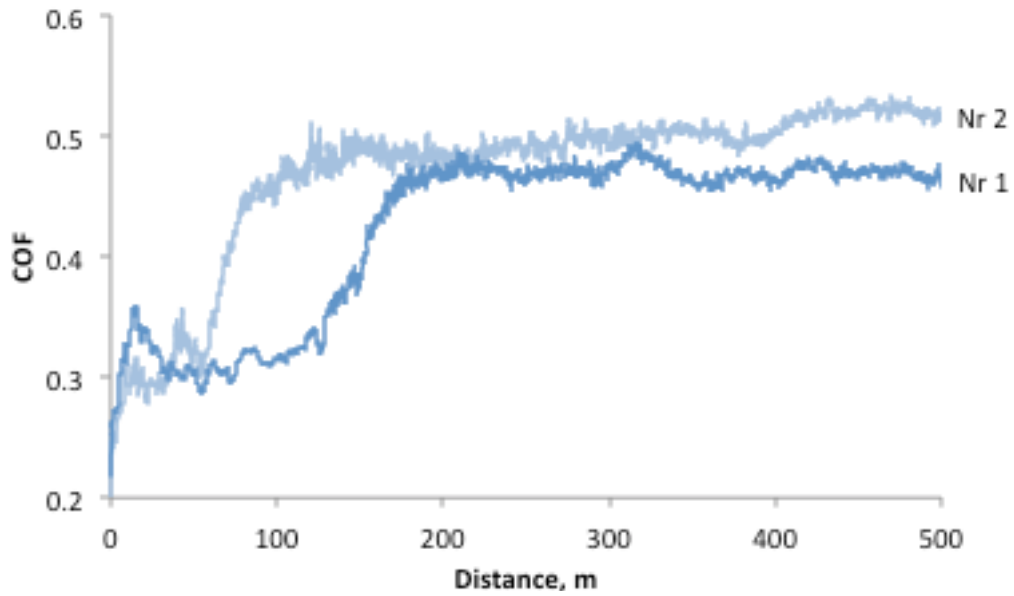

Figure B.4: COF for wear in seawater on stainless steel

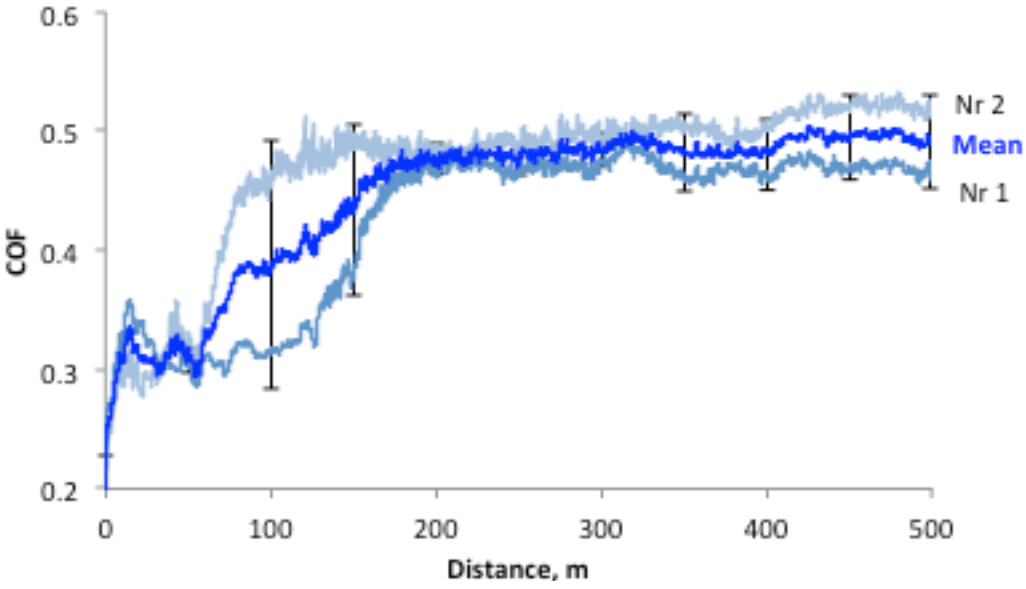

Figure B.5: SS in seawater with calculated mean value and standard deviation

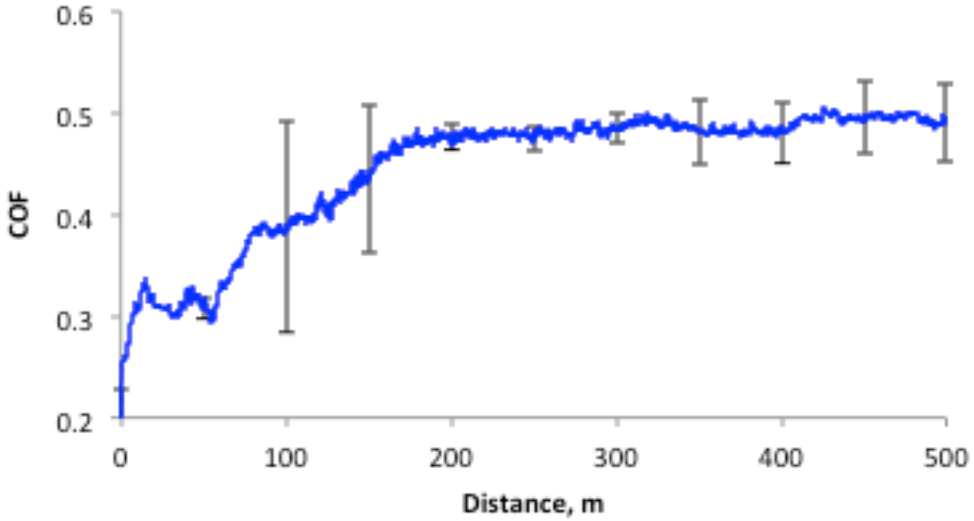

Figure B.6: Mean value of COF for stainless steel in seawater

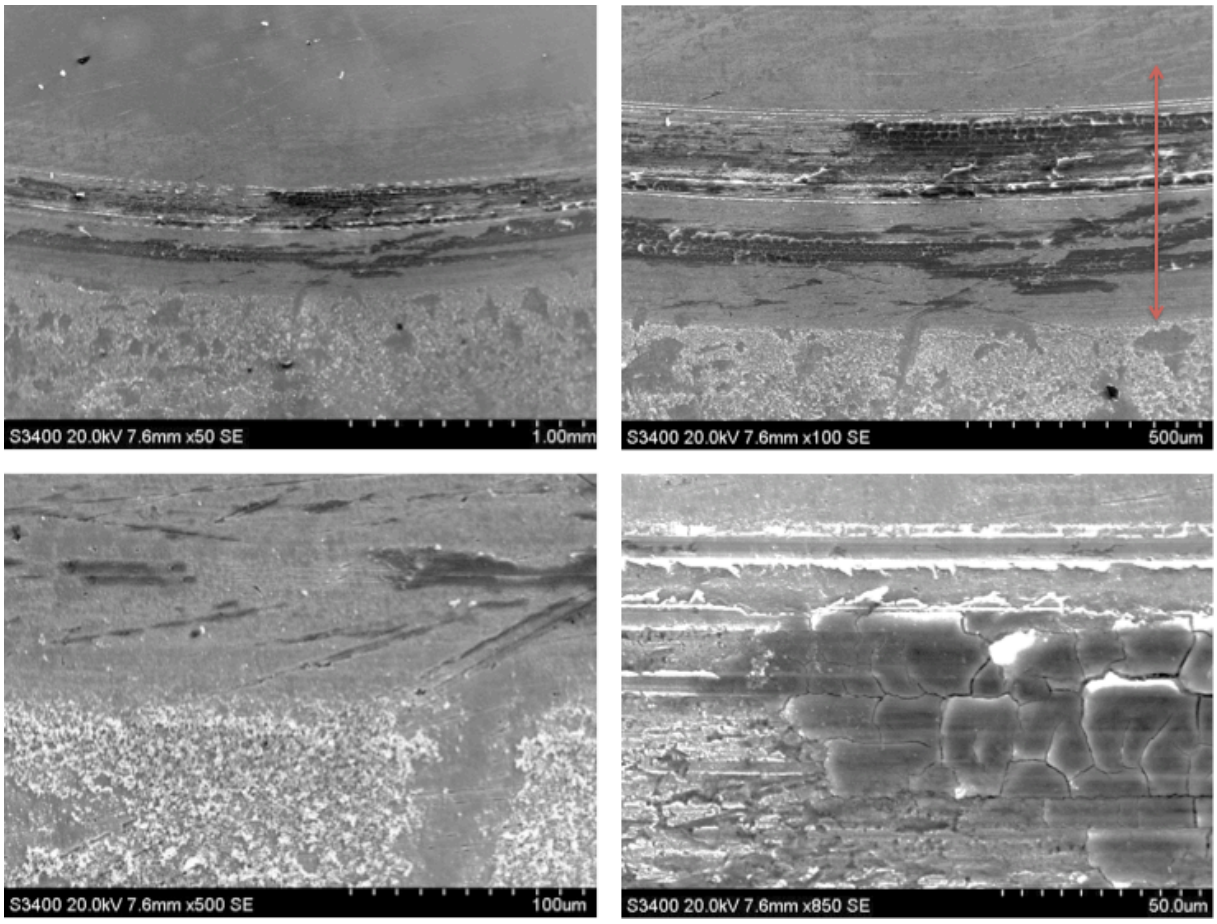

Figure B.7: SS Dry nr 1

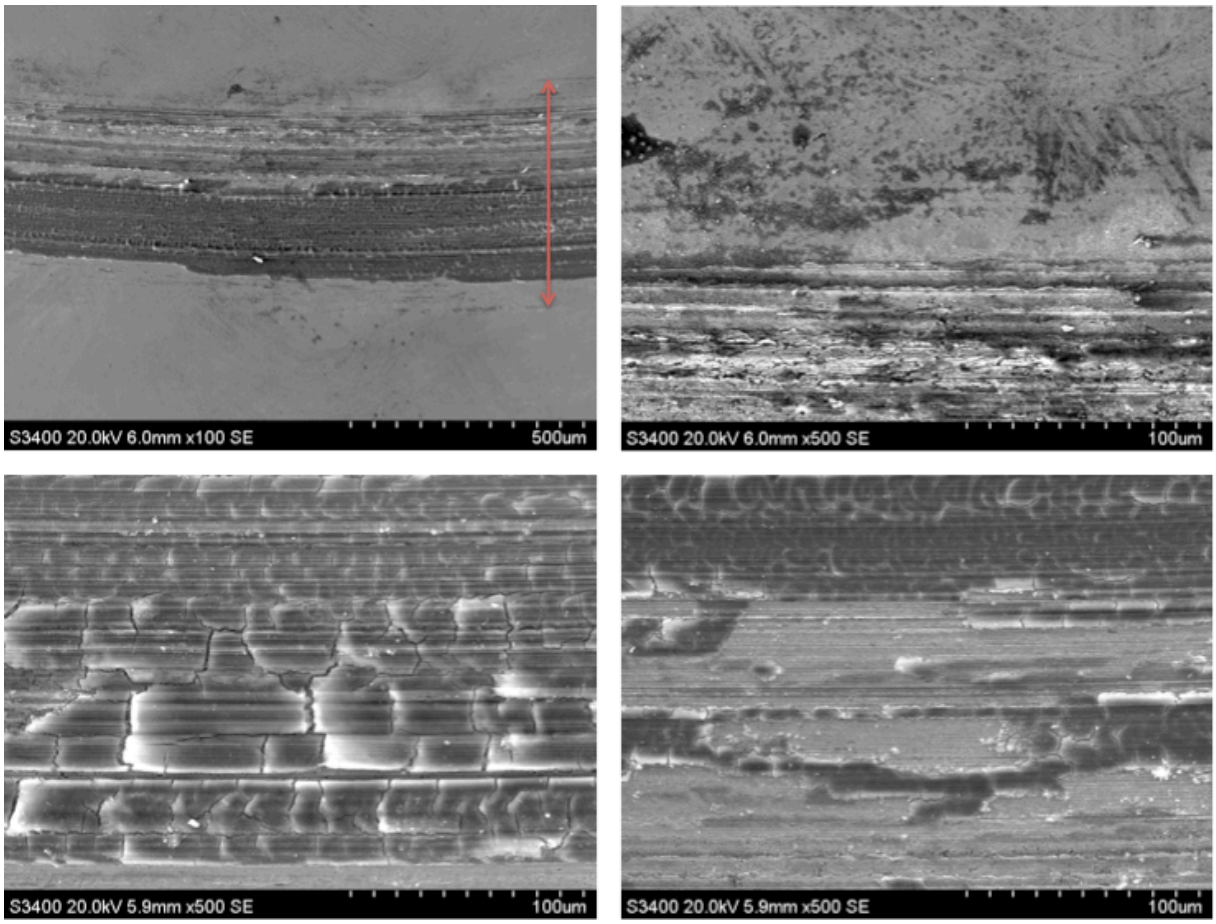

Figure B.8: SS Dry nr 2

B.4 Silicon carbide, seawater

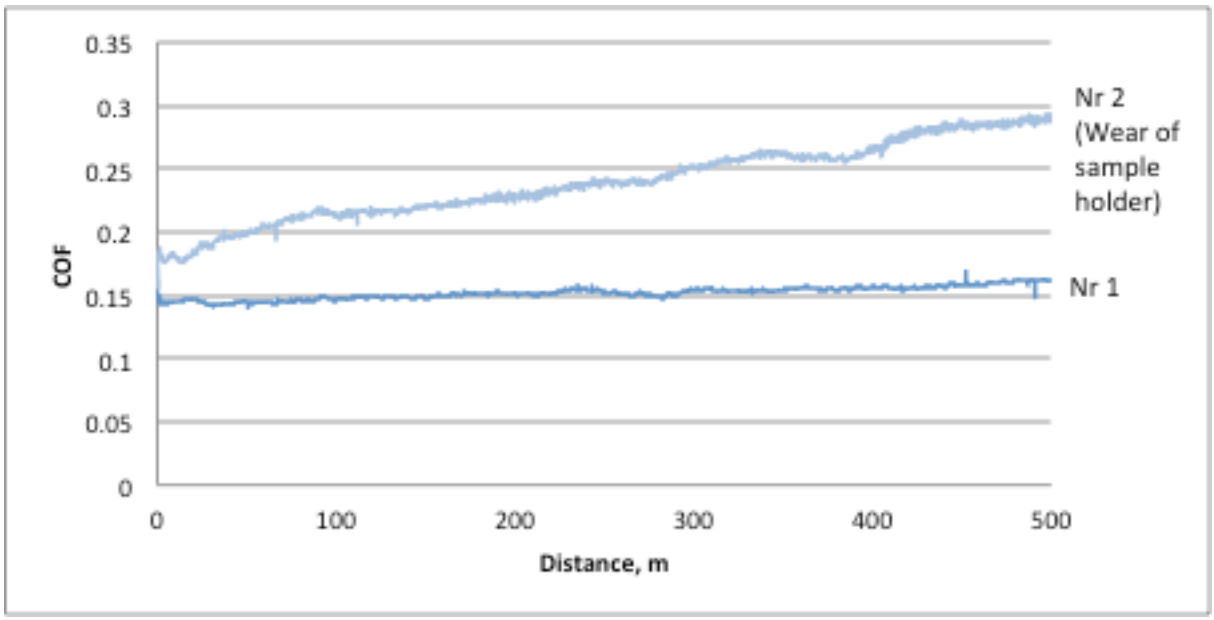
0.35
0.3
0.25
0.2
0.15
0.1
0.05
0
COF
0
100
200
300
400
500
Distance, m
Nr 2 (Wear of sample holder)
Nr 1

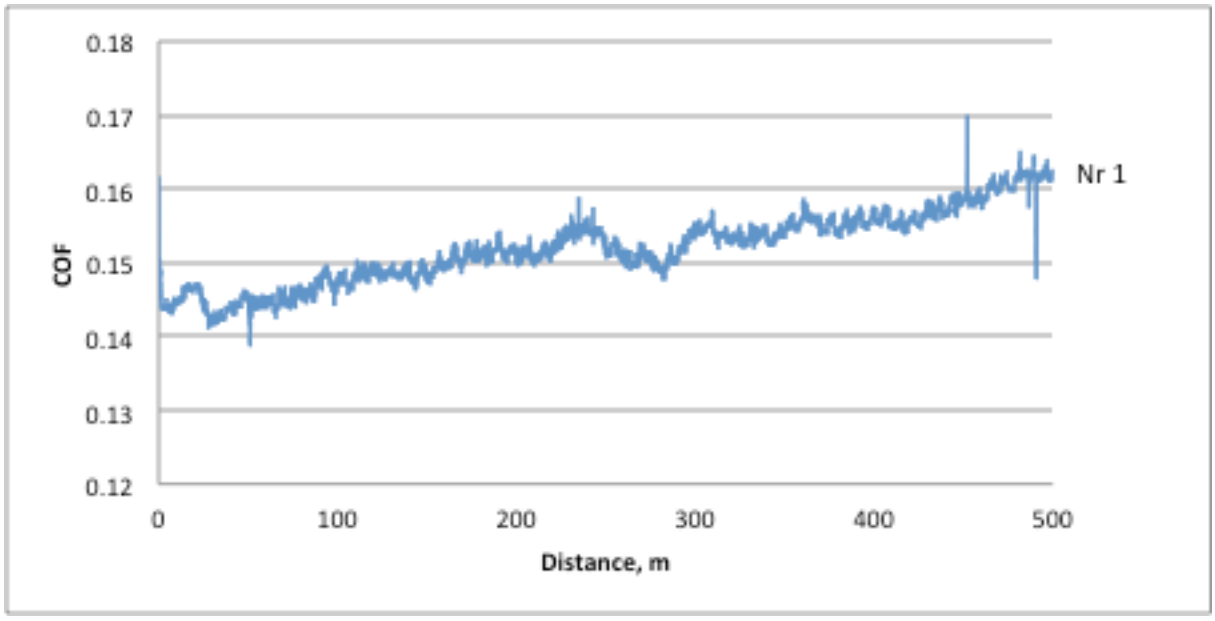
0.18
0.17
0.16
0.15
0.14
0.13
0.12
COF
0
100
200
300
400
500
Distance, m
Nr 1

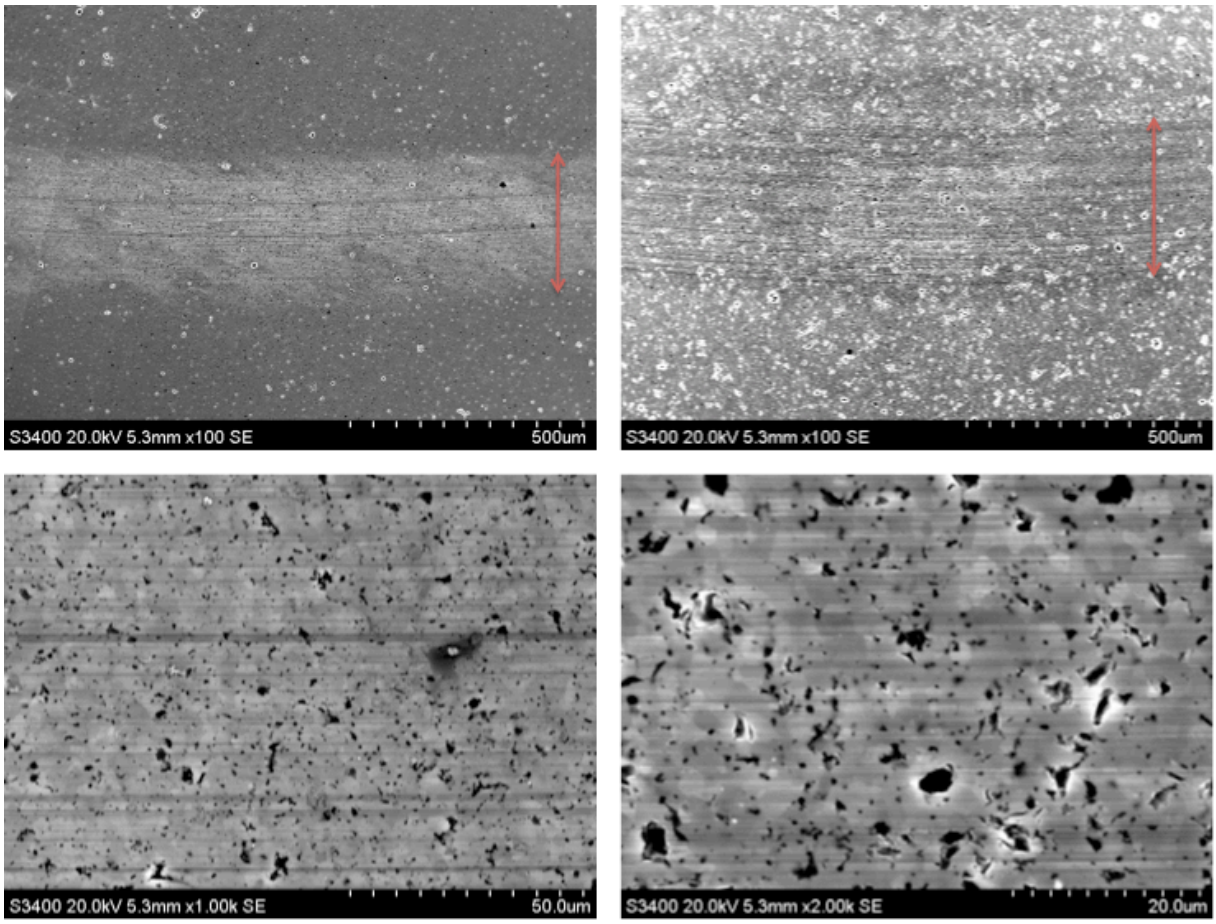

Figur B.2: SiC Seawater Left nr 1, right nr 2

B.5 Stainless steel, clean PAO

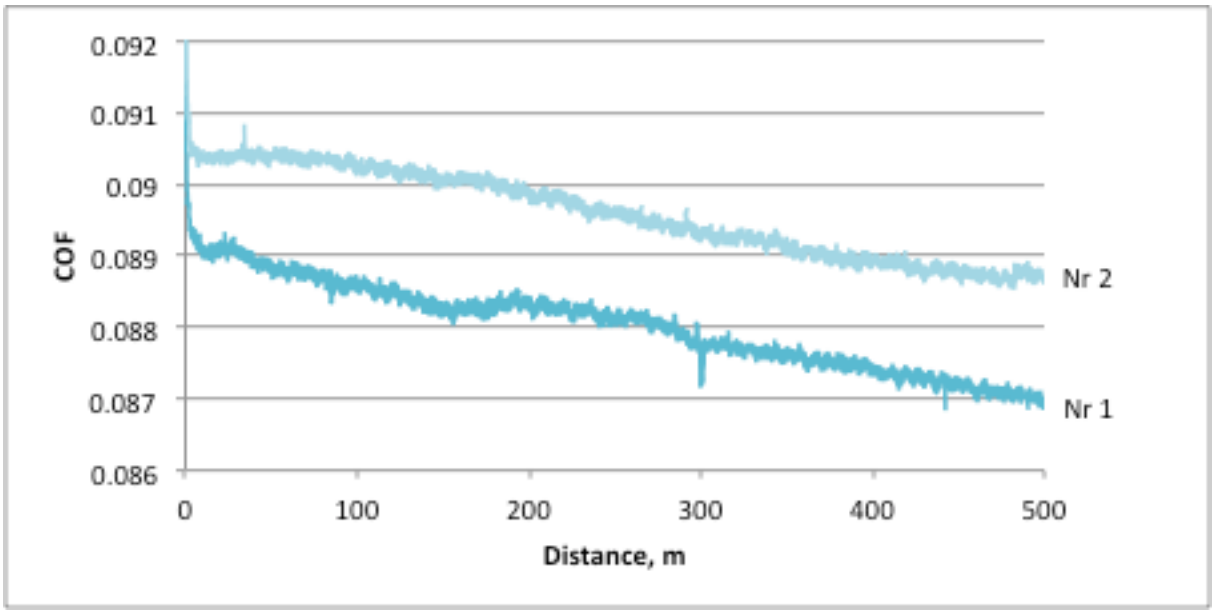

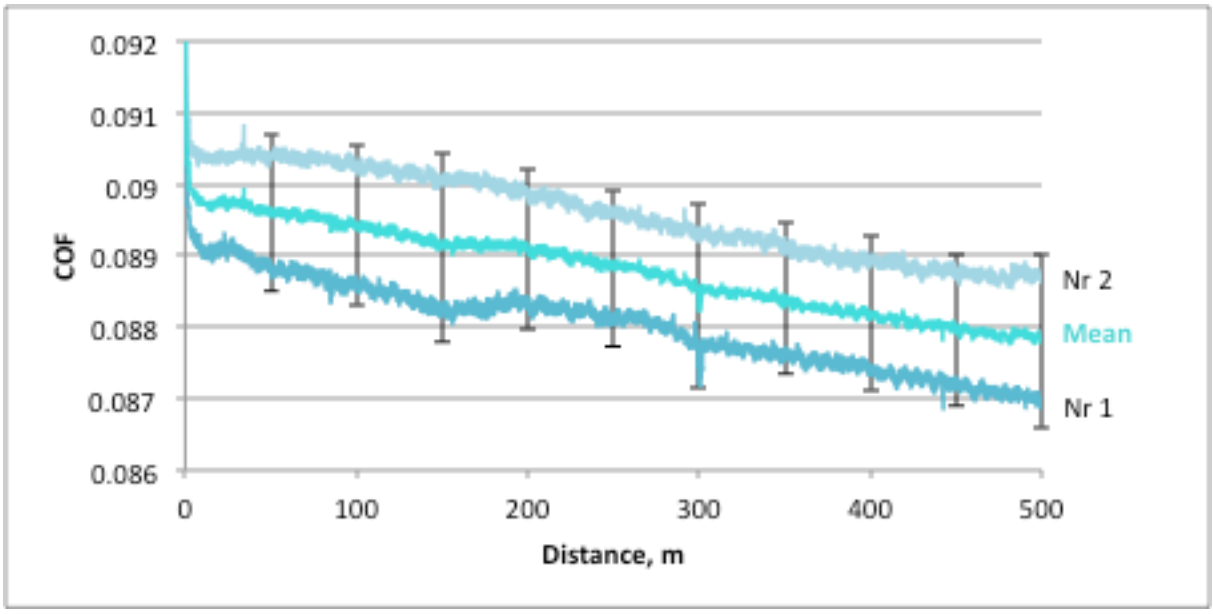

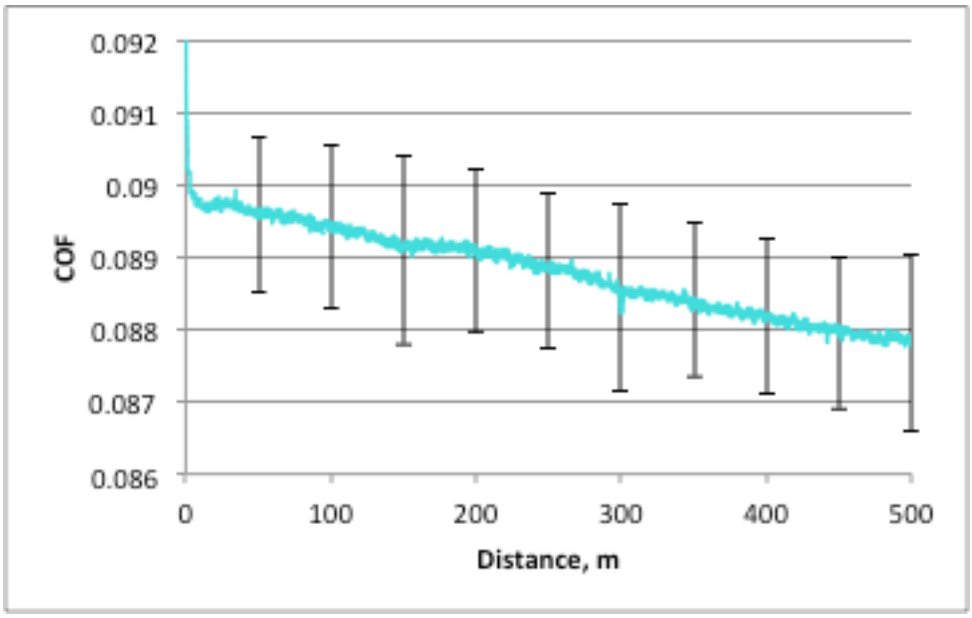

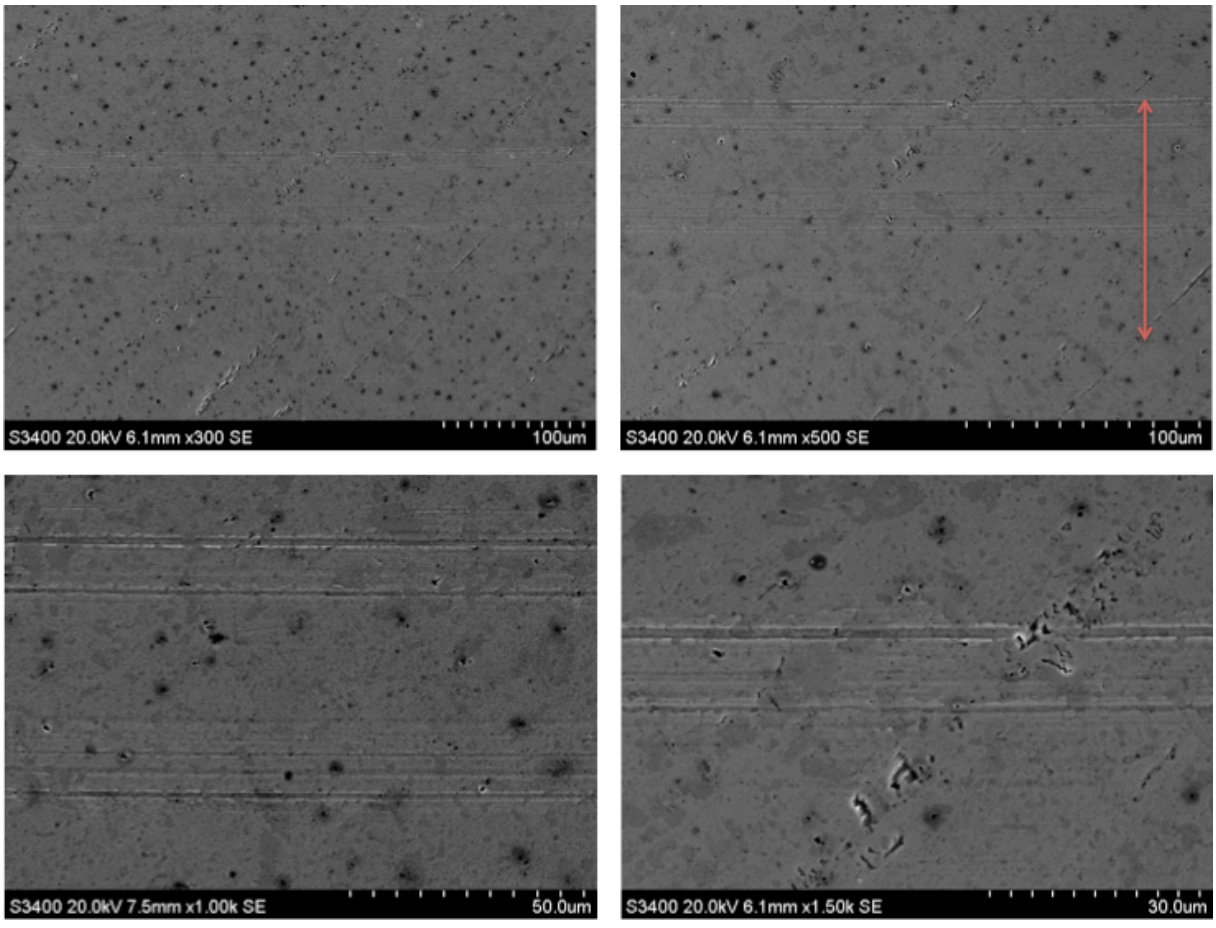

Figure B.9: SS clean PAO nr 1

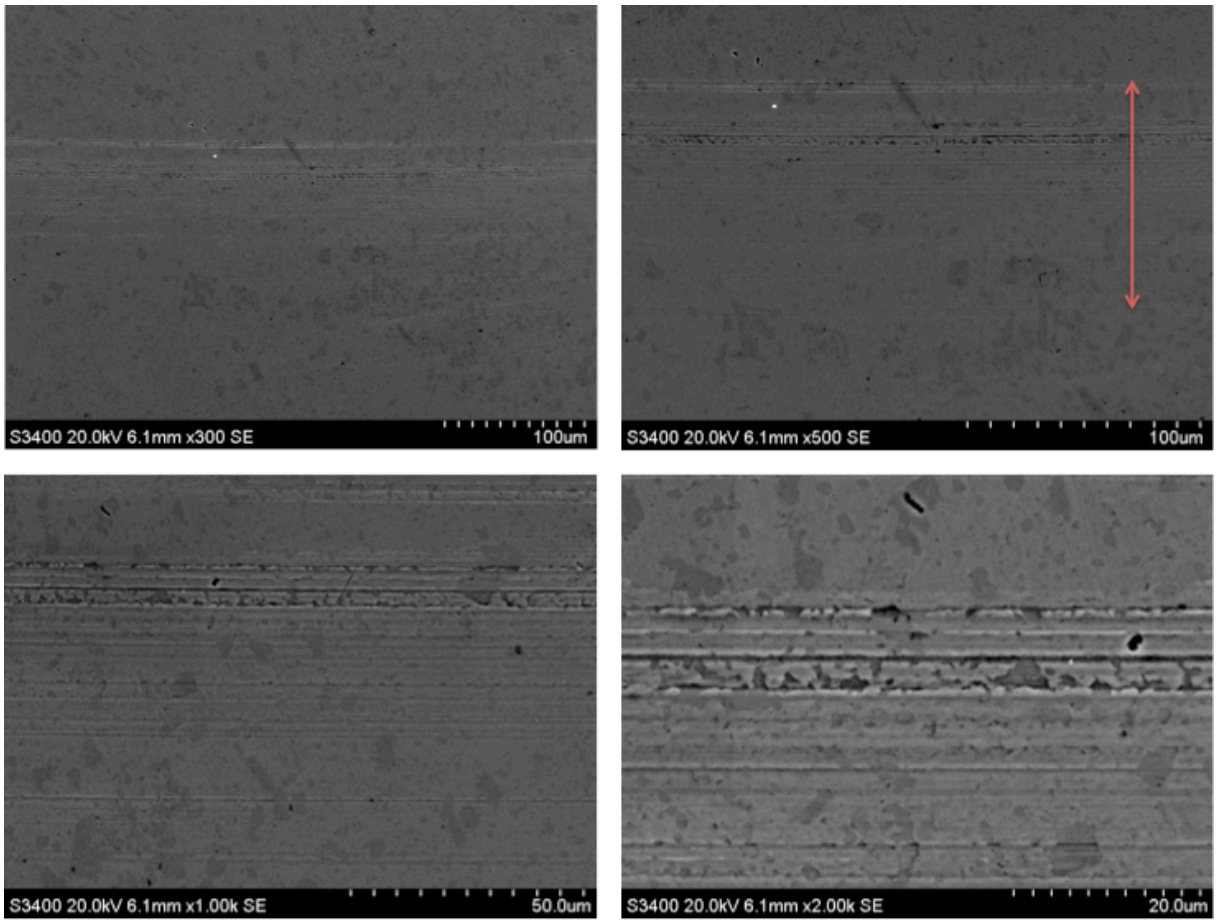

Figure B.10: SS clean PAO nr 2

B.6 Stainless steel, PAO 100 ppm

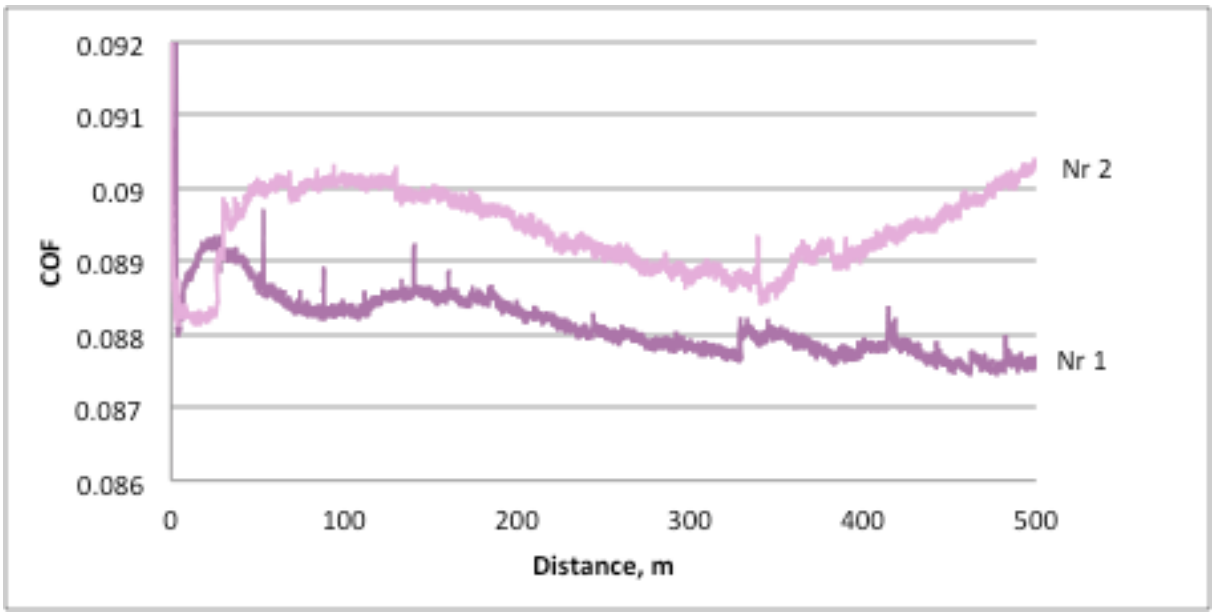
0.092
0.091
0.09
0.089
0.088
0.087
0.086
COF
0
100
200
300
400
500
Distance, m
Nr 2
Nr 1

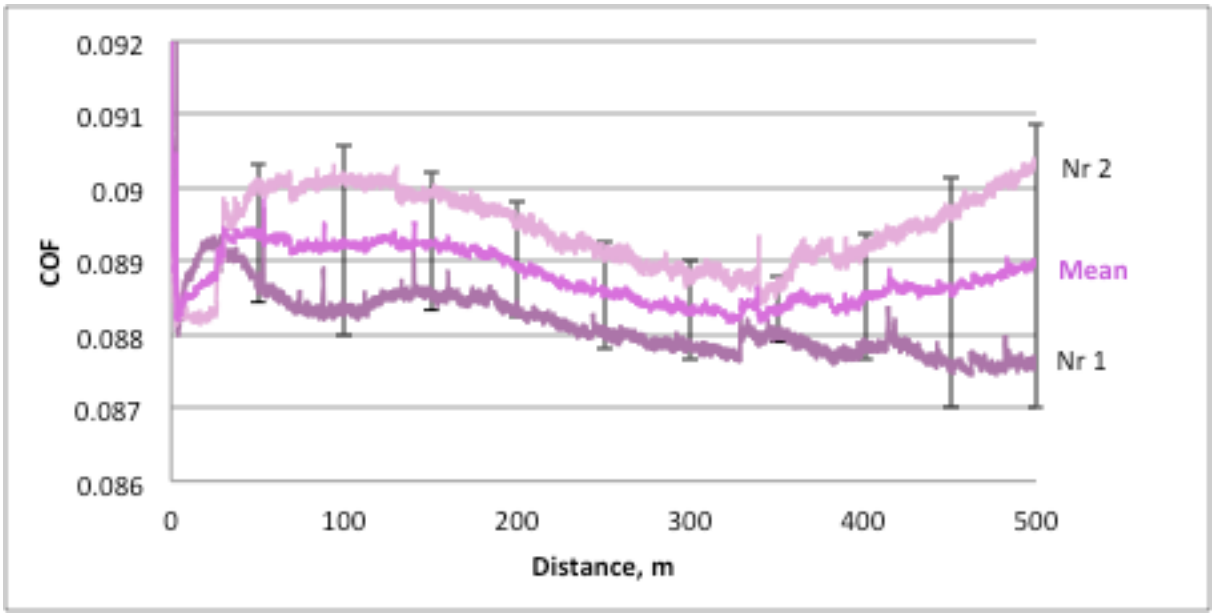
0.092
0.091
0.09
0.089
0.088
0.087
0.086
COF
0
100
200
300
400
500
Distance, m
Nr 2
Mean
Nr 1

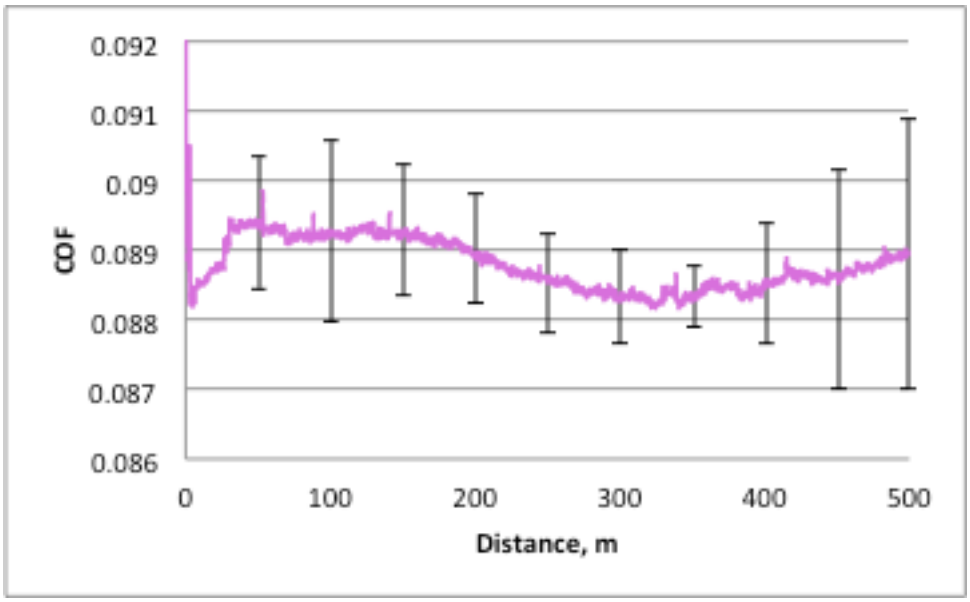
0.092
0.091
0.09
0.089
0.088
0.087
0.086
COF
0
100
200
300
400
500
Distance, m

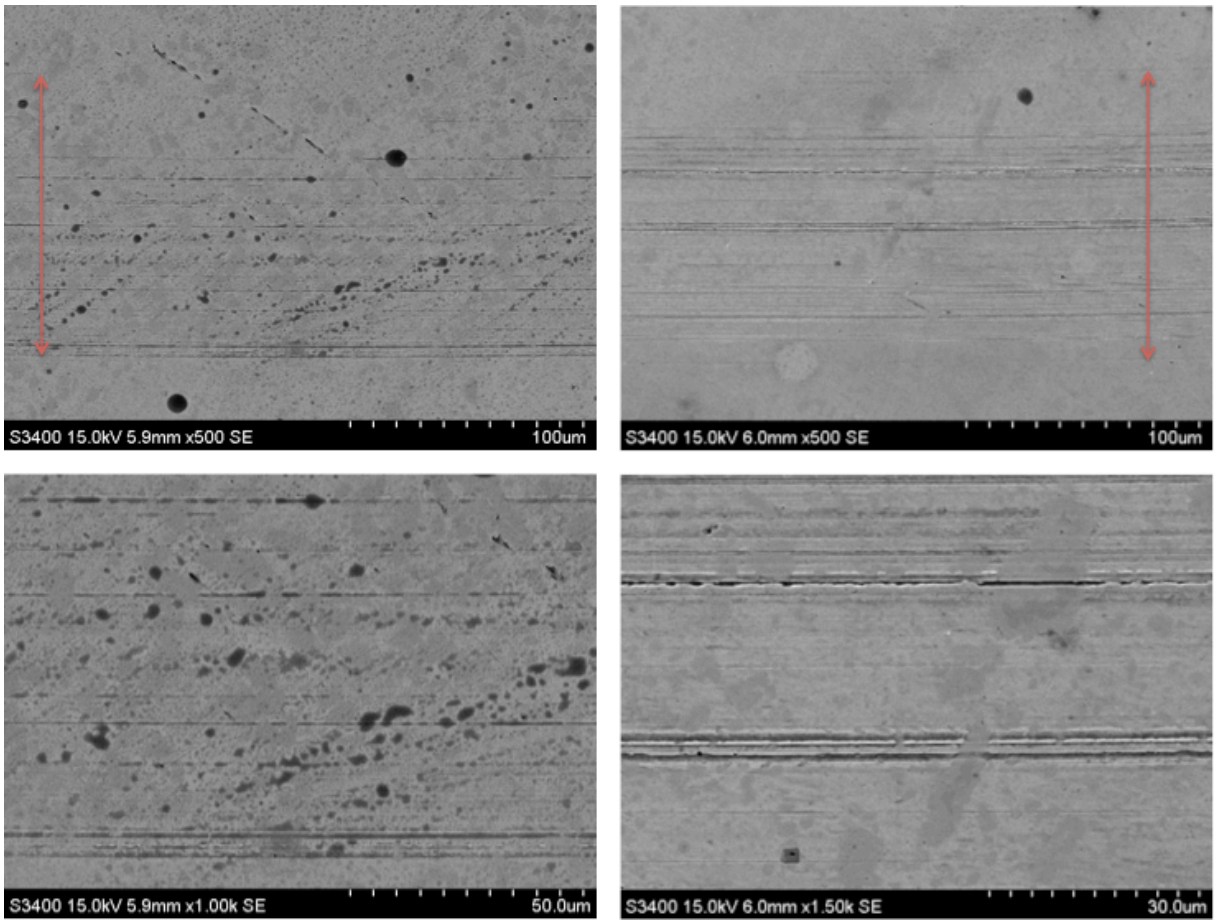

Figure B.11: SS PAO 100 ppm. The red line indicate the width of the wear track. The images to the left is from test nr 1, and the images to the right is from test nr 2

B.7 Stainless steel, PAO 300 ppm

B.8

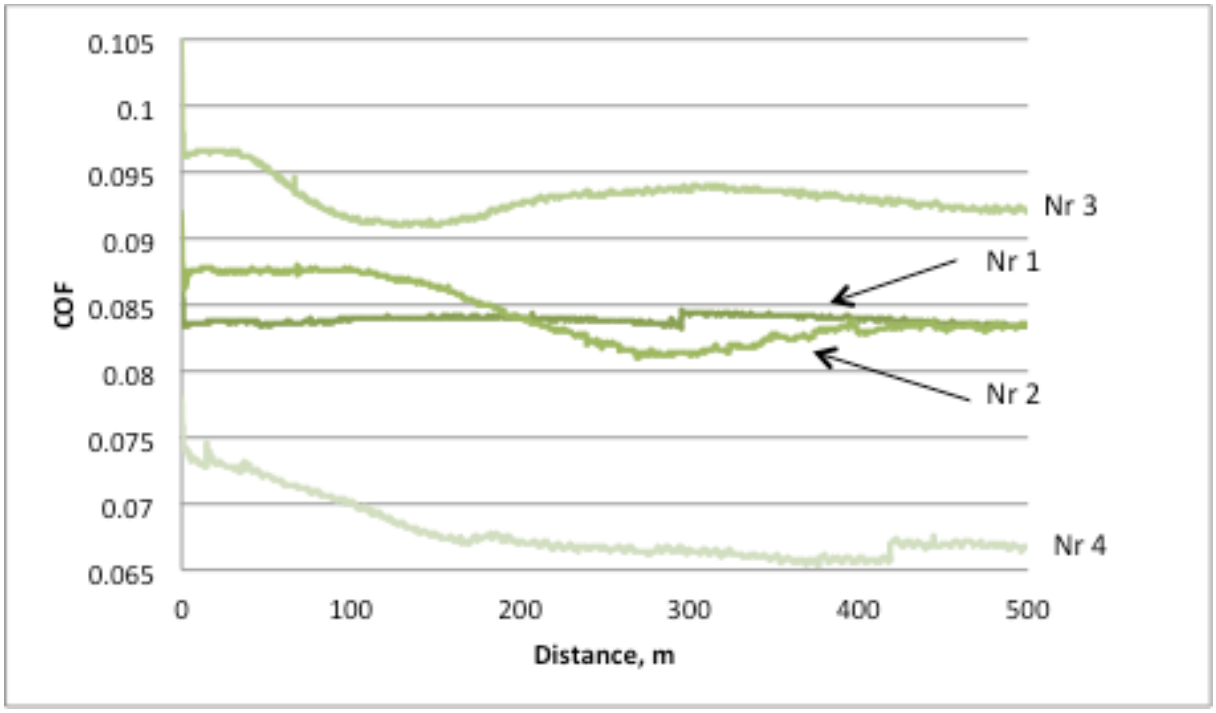

Figure B.12: PAO 300 ppm on SS

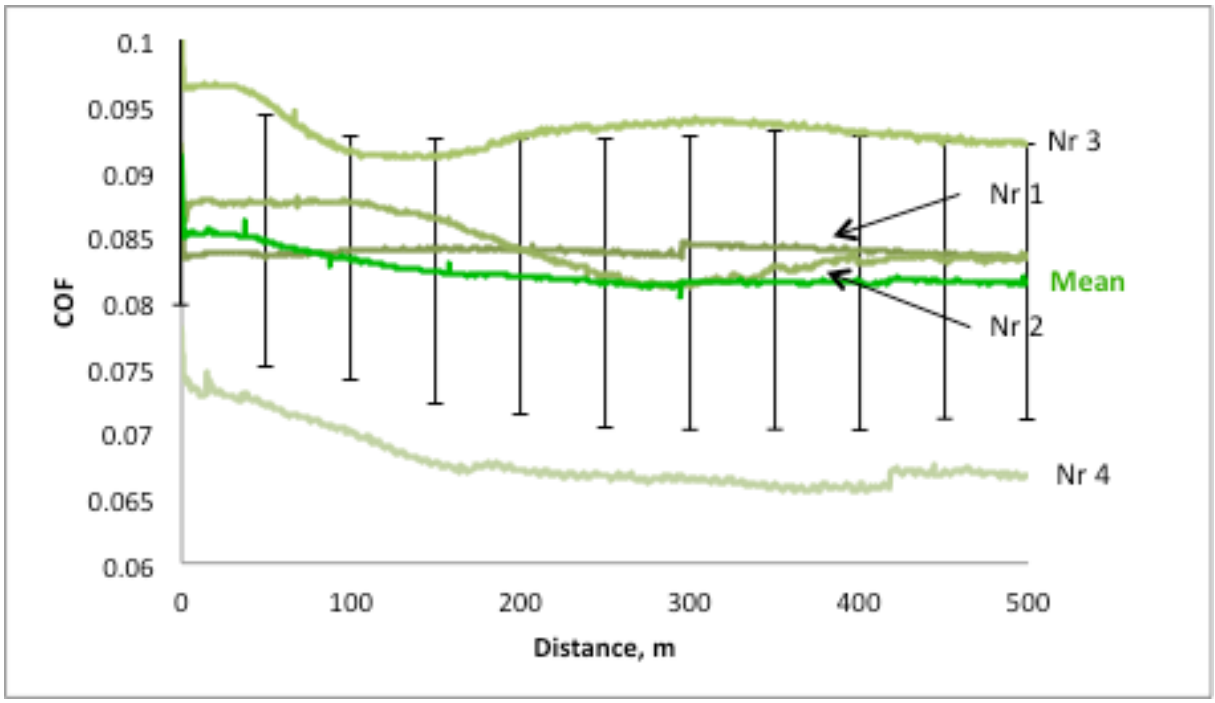

Figure B.13: PAO 300 ppm on SS with Mean and std dev

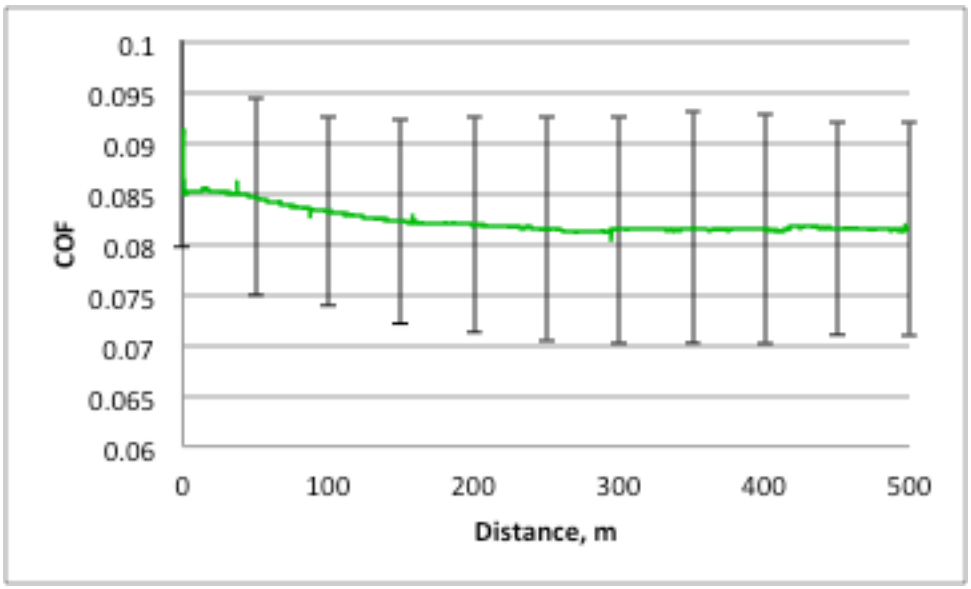

Figure B.14: PAO 300 ppm MEAN with std.dev

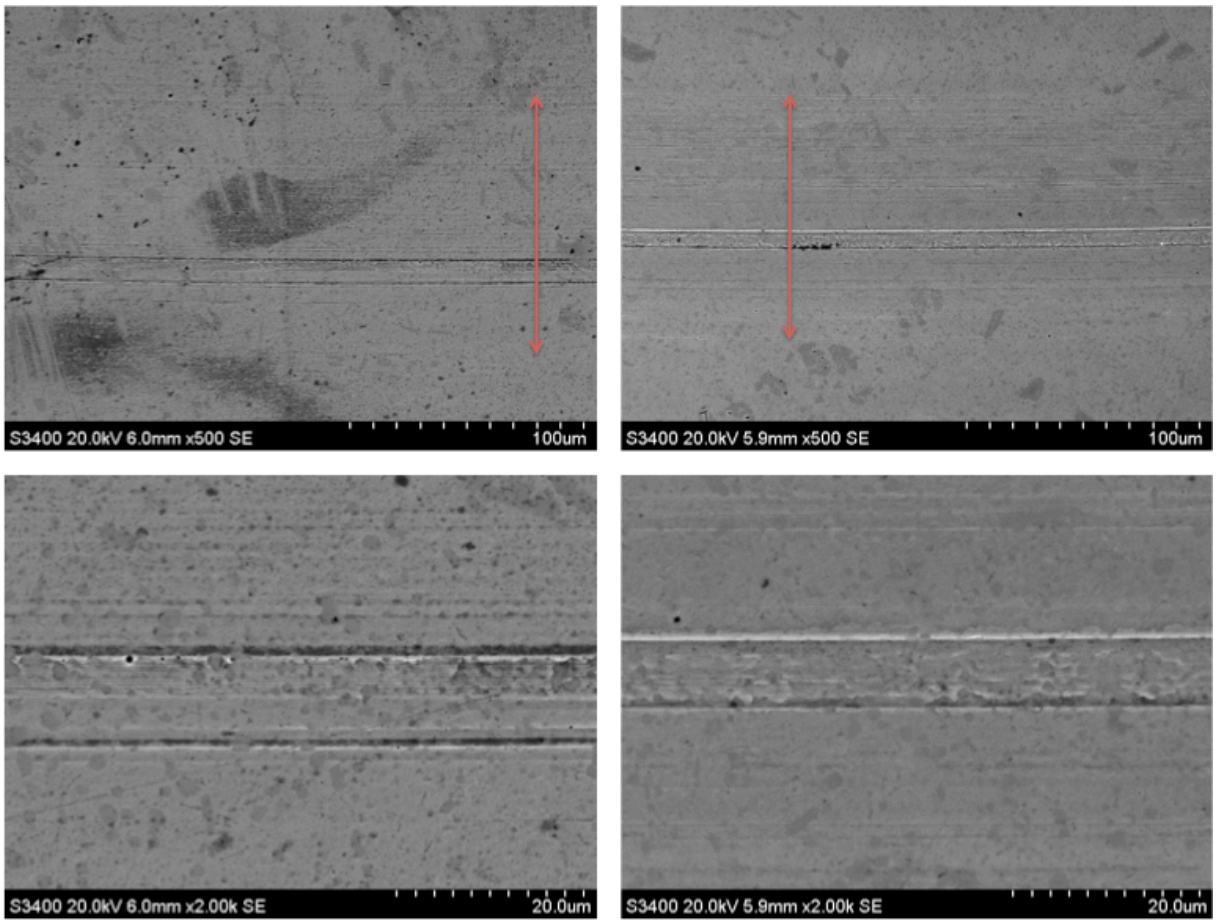

Figure B.15: SS PAO 300 ppm. Left nr 1, right nr 2

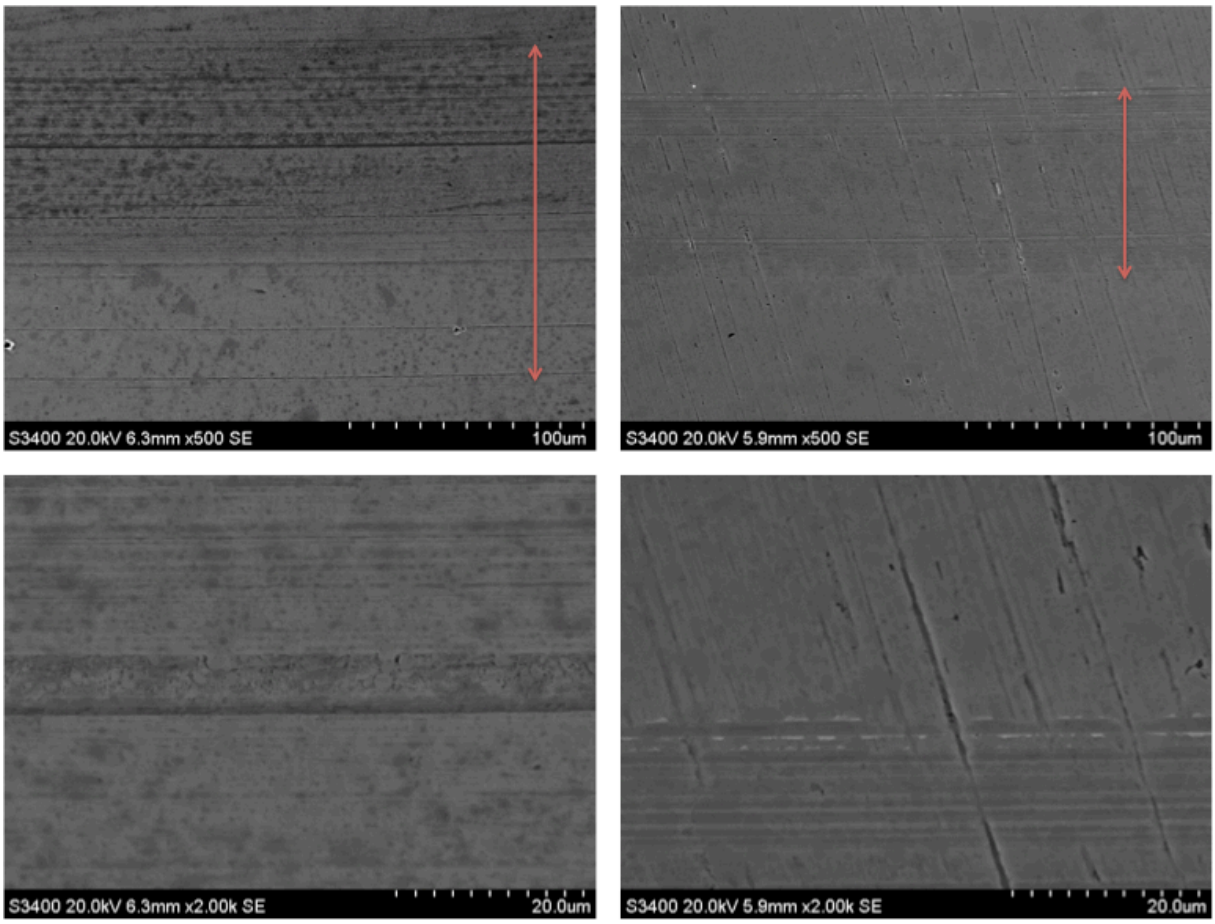

Figure B.16: SS PAO 300 ppm. Left nr 3, right nr 4

B.9 Stainless steel, PAO 500 ppm

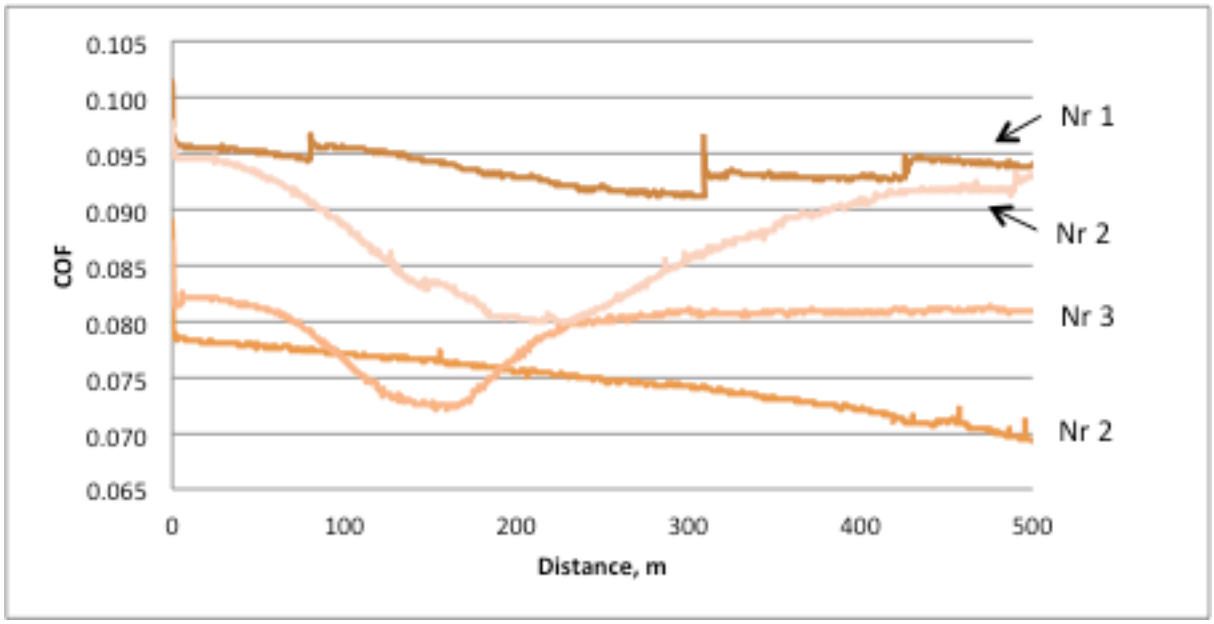

Figure B.17: PAO 500 ppm SS

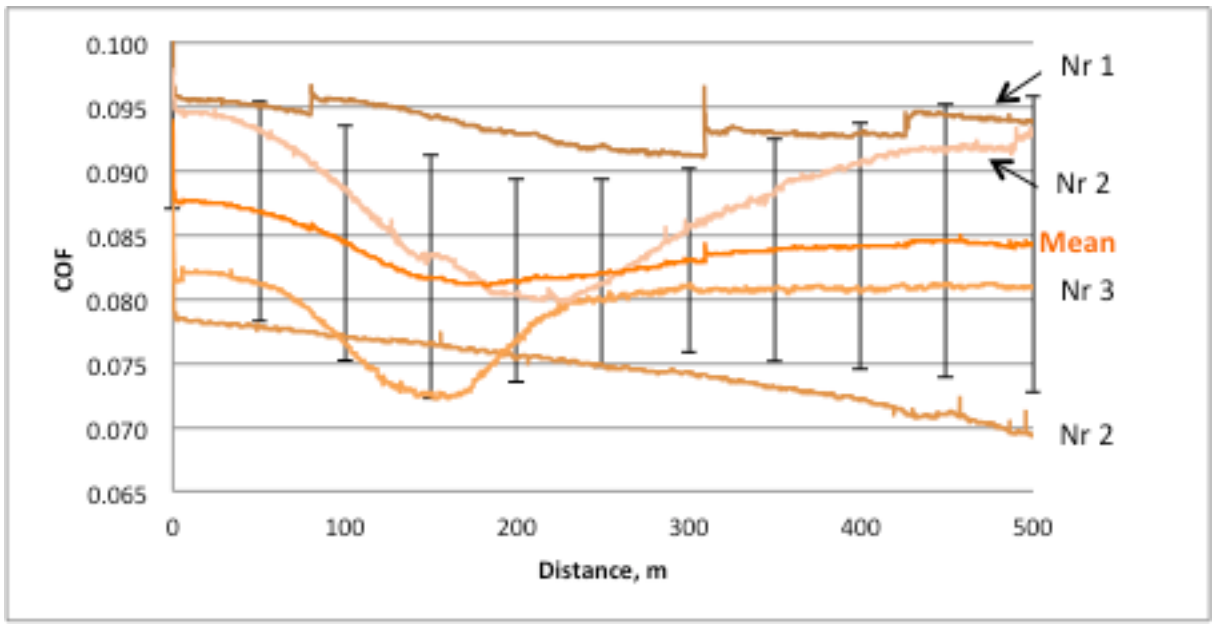

Figure B.18: PAO 500 500 ppm with Mean og std dev

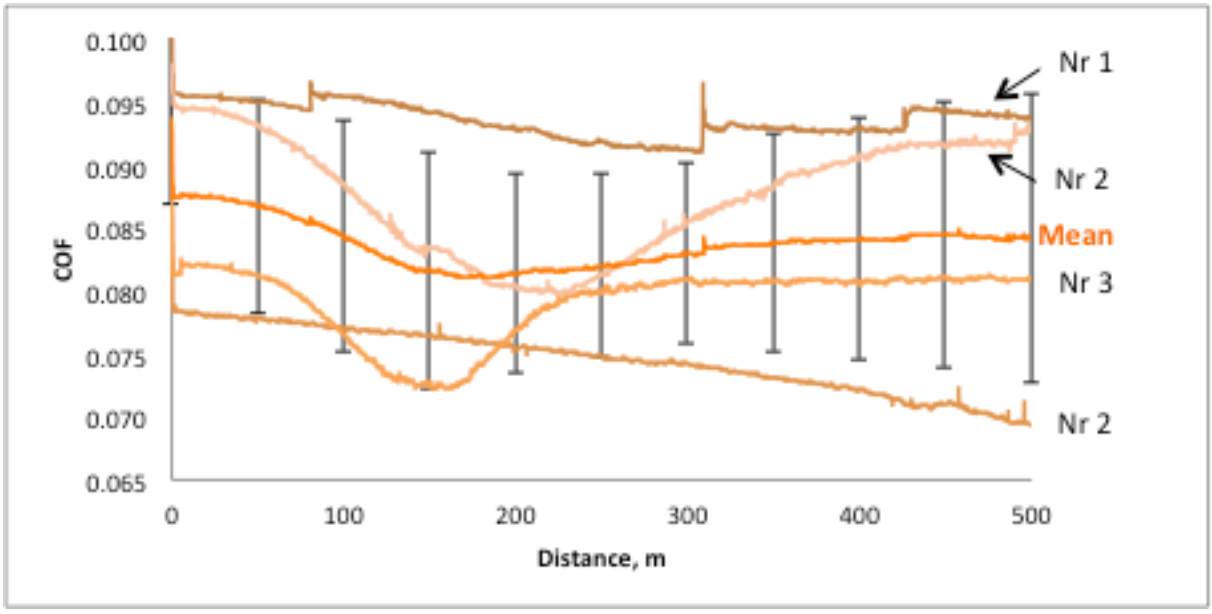

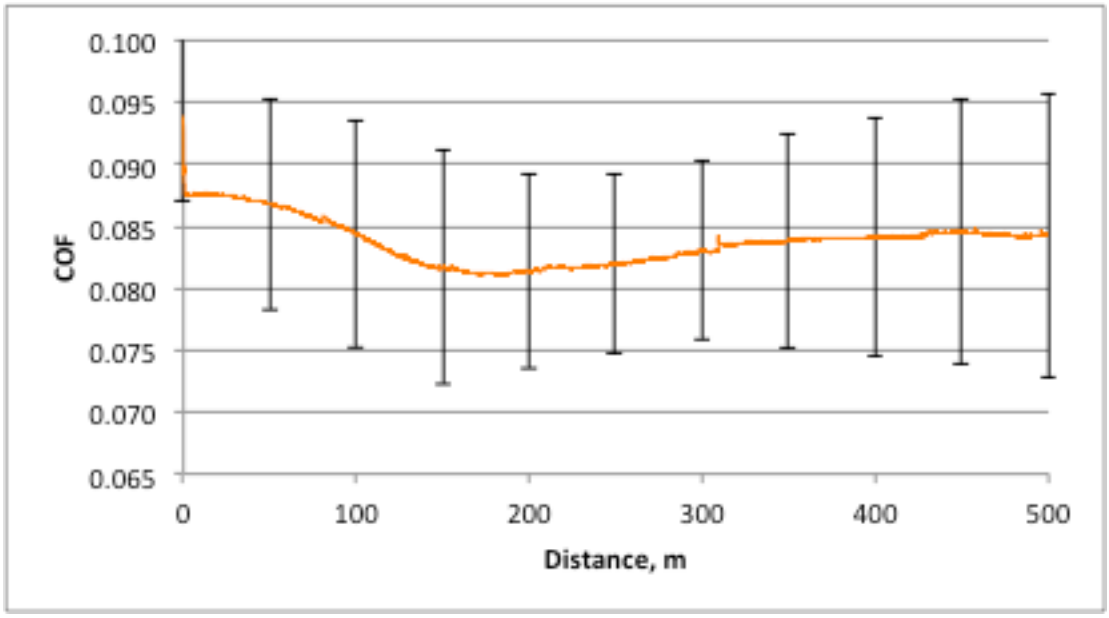

Figure B.19: PAO 500 ppm MEan with std dev

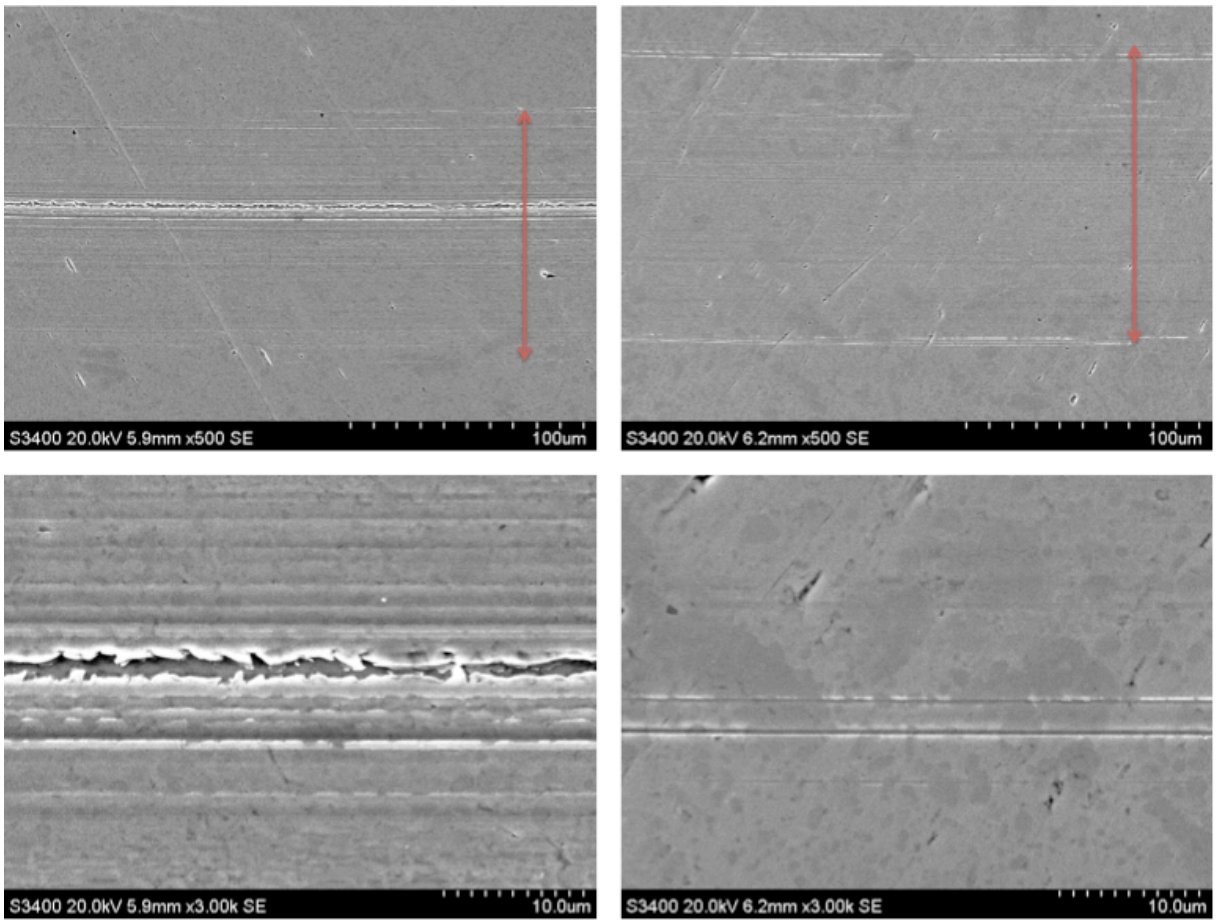

Figure B.20: SS PAO 500 ppm. Left nr 1, right nr 2

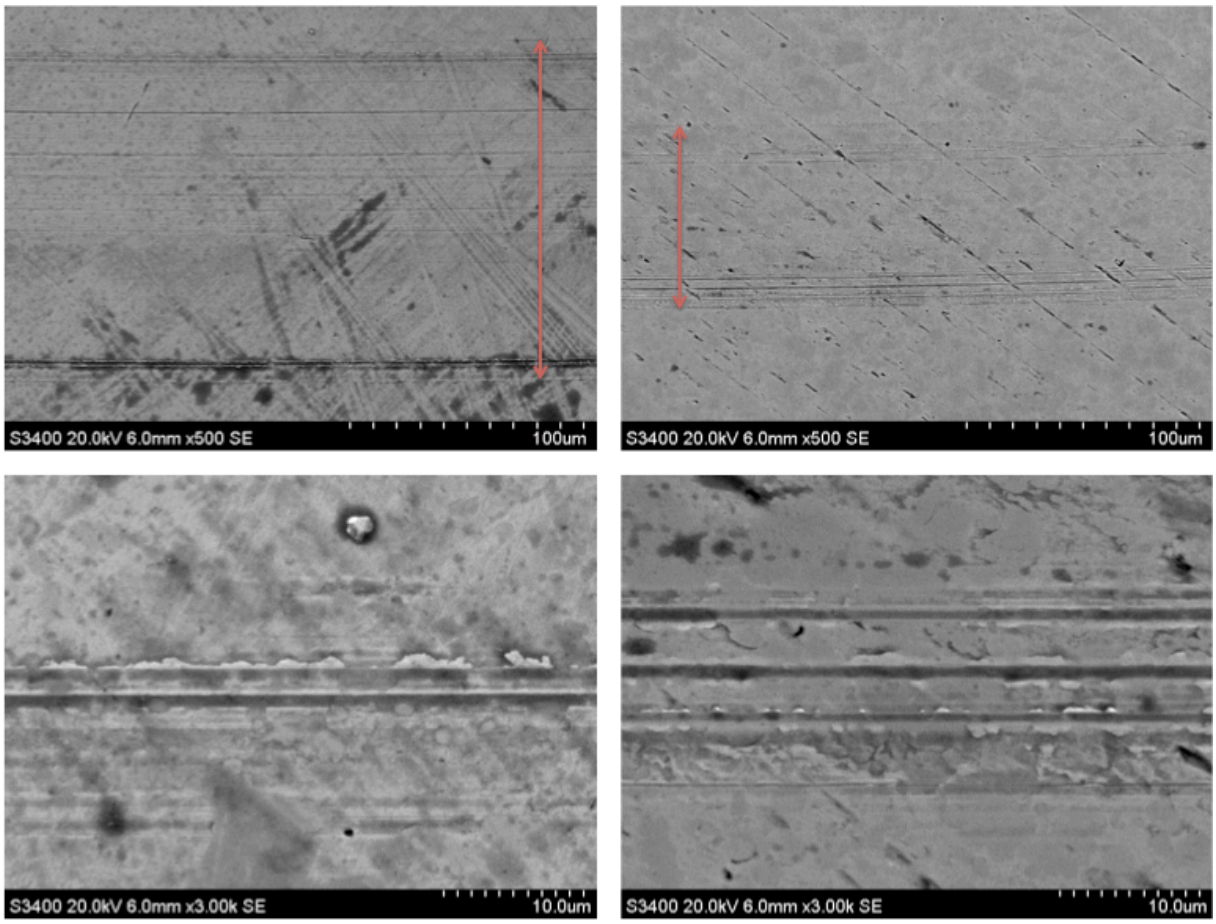

Figure B.21: SS PAO 500 ppm. Left nr 3, right nr 4

B.10 Stainless steel, PAO 1000 ppm

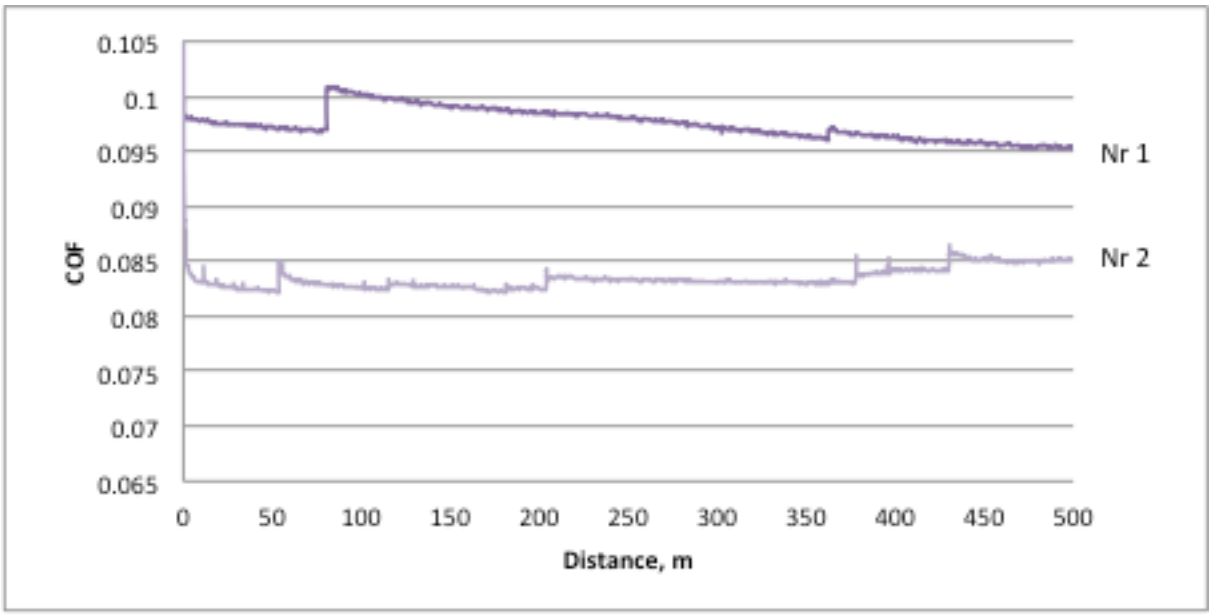

Figure B.22: PAO 1000 ppm

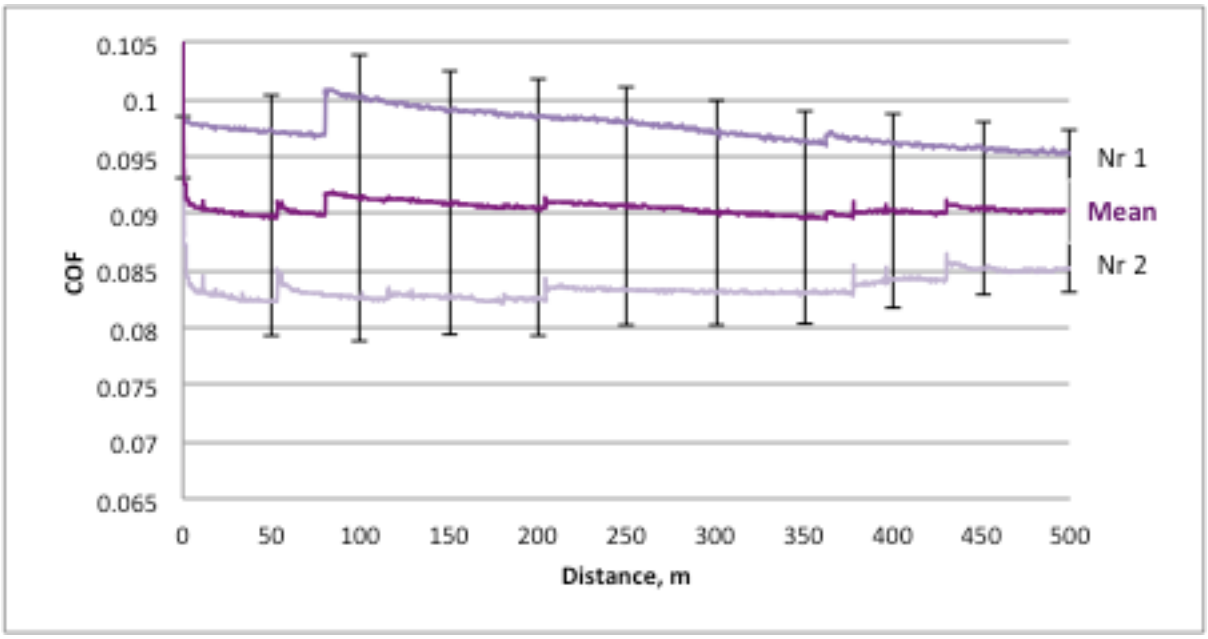

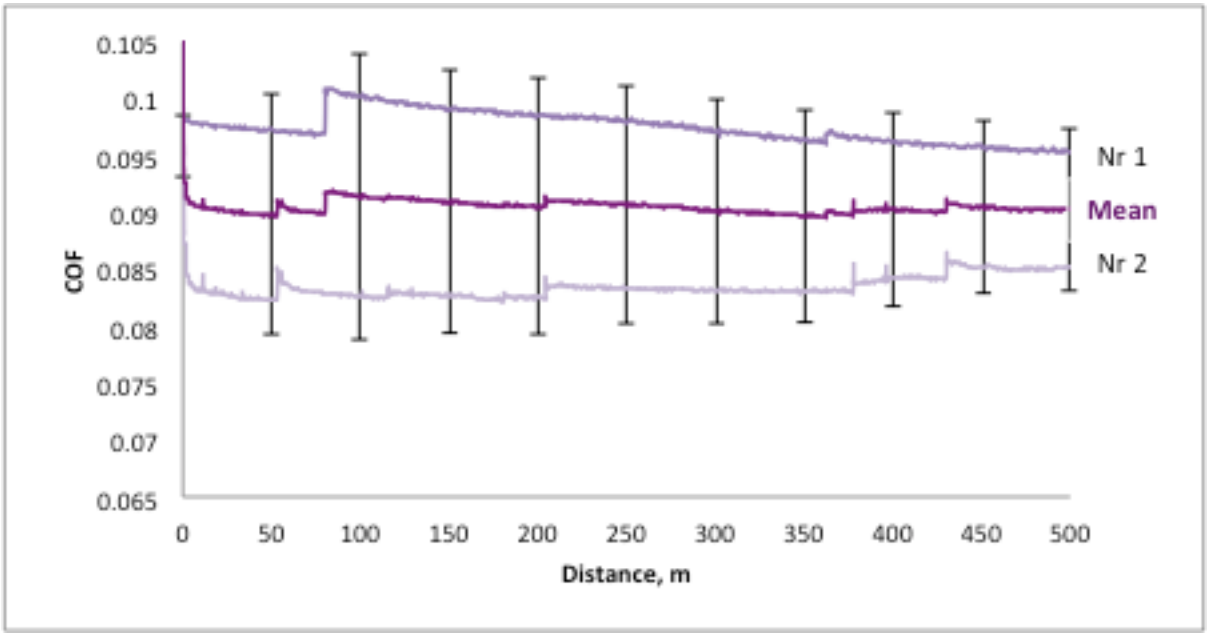

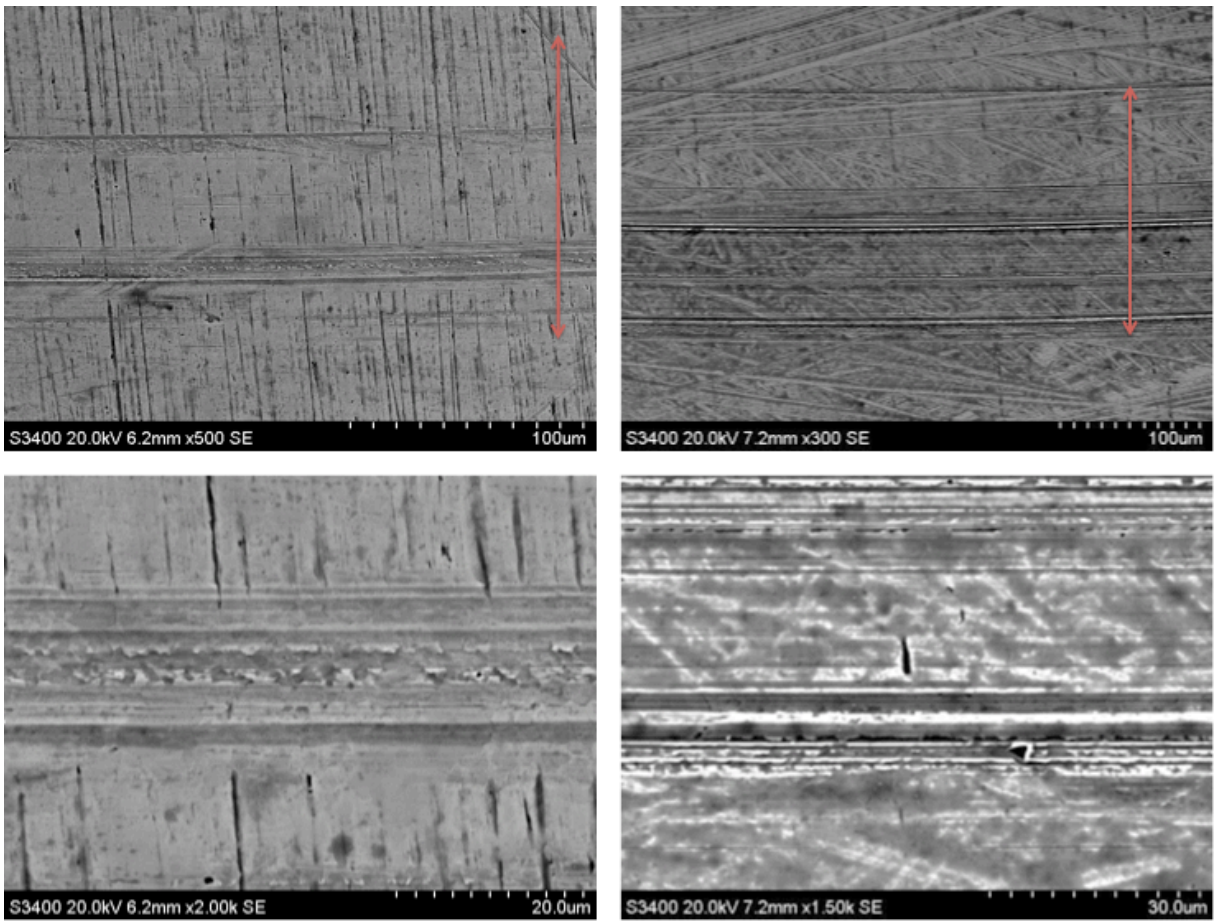

Figure B.23: PAO 1000 ppm. Left nr 1, right nr 2

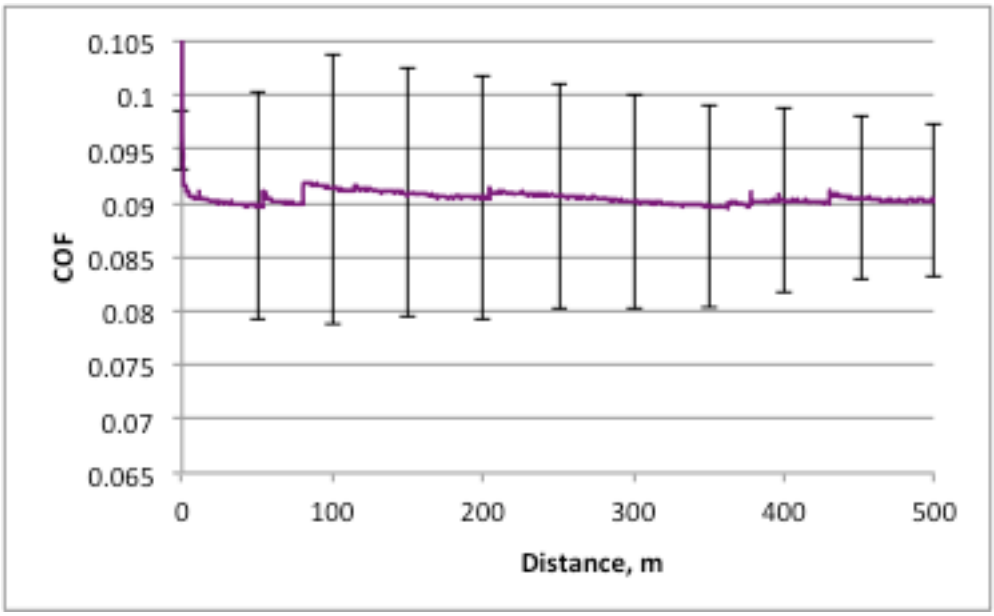

Figure B.24: PAO 1000 ppm

B.11 Stainless steel, Clean PAG

Clean:

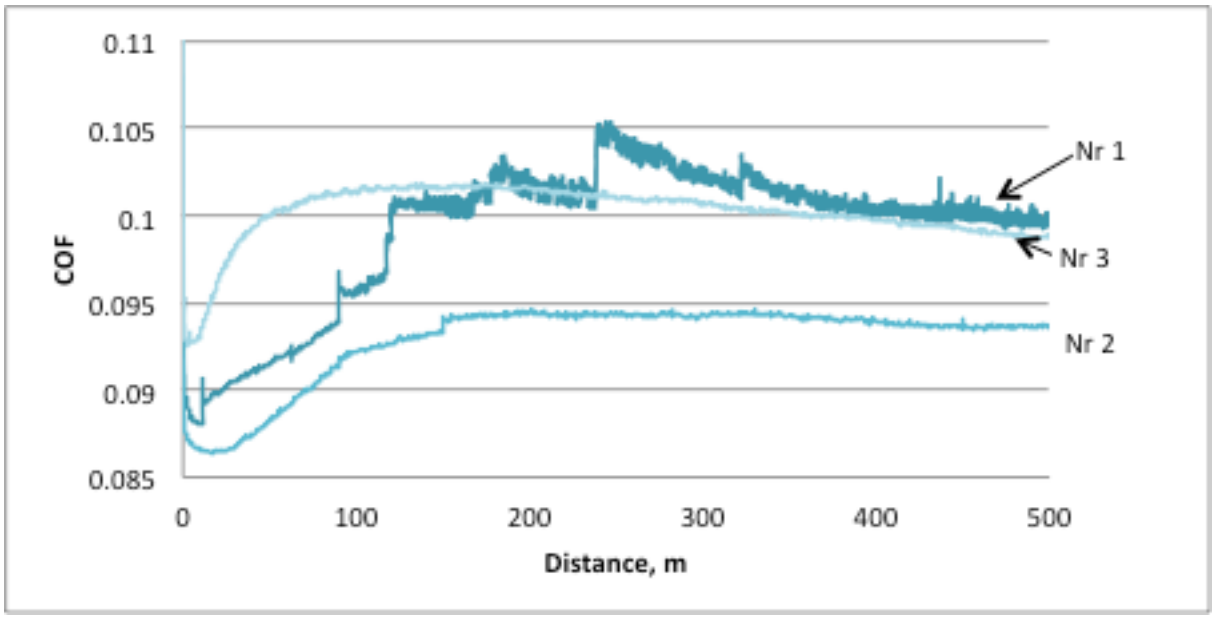

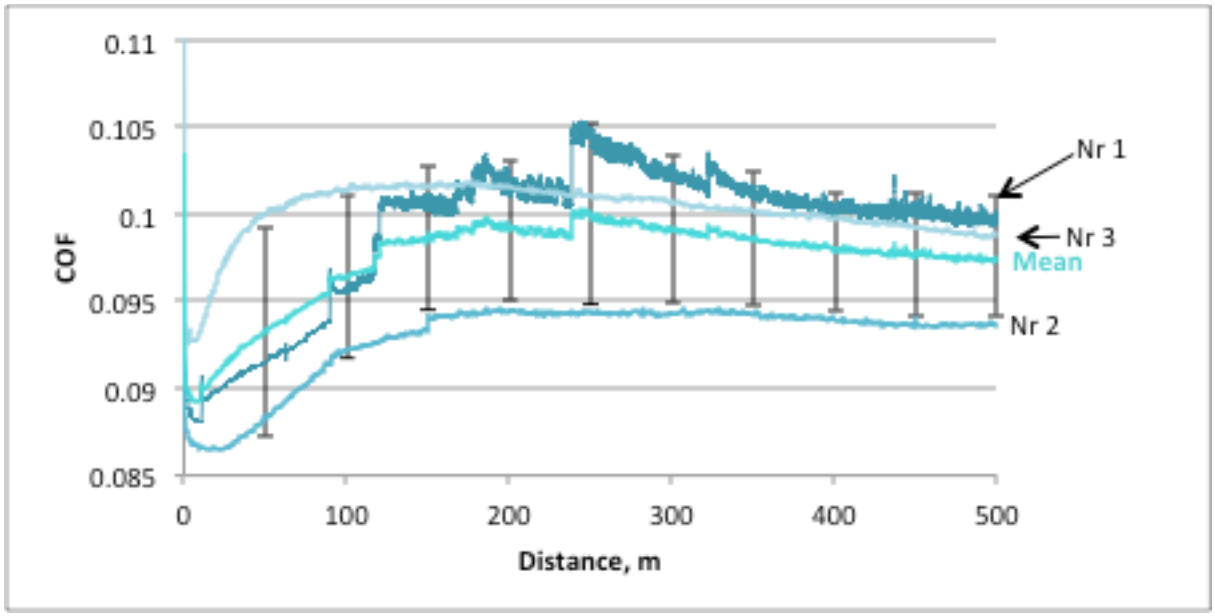

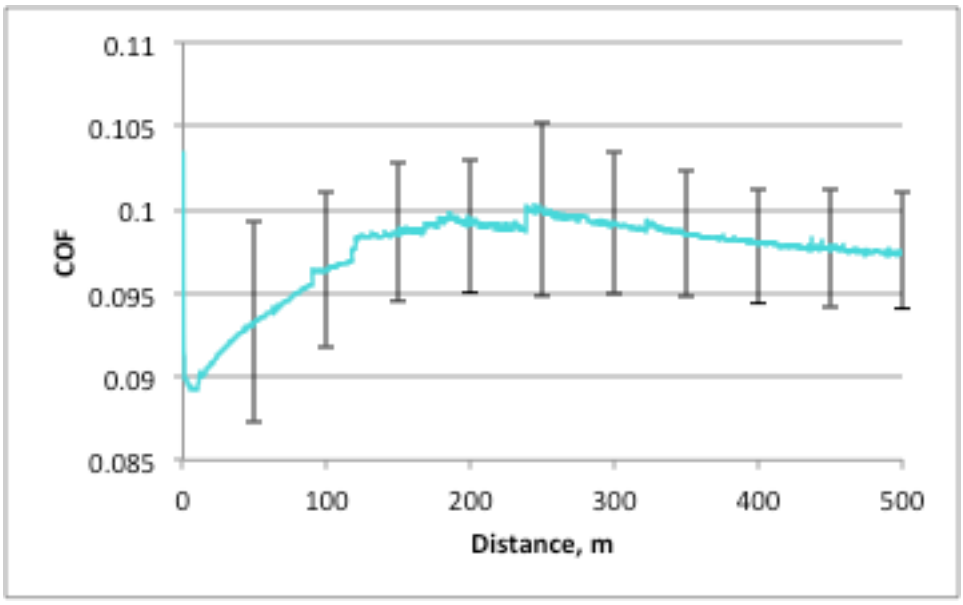

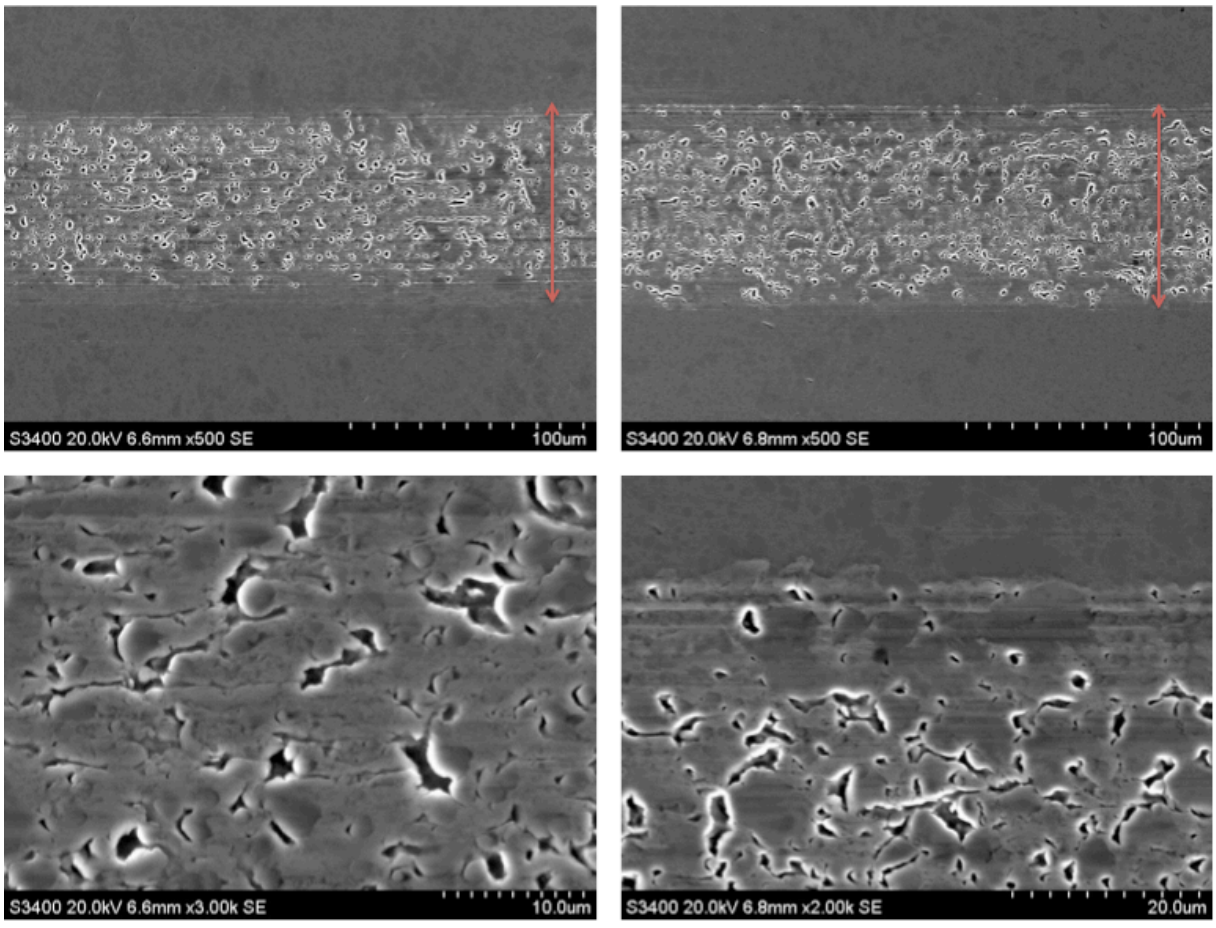

Figure B.25: SS PAG clean. Left nr 2, right nr 3

B.12 Stainless steel, PAG 300 ppm

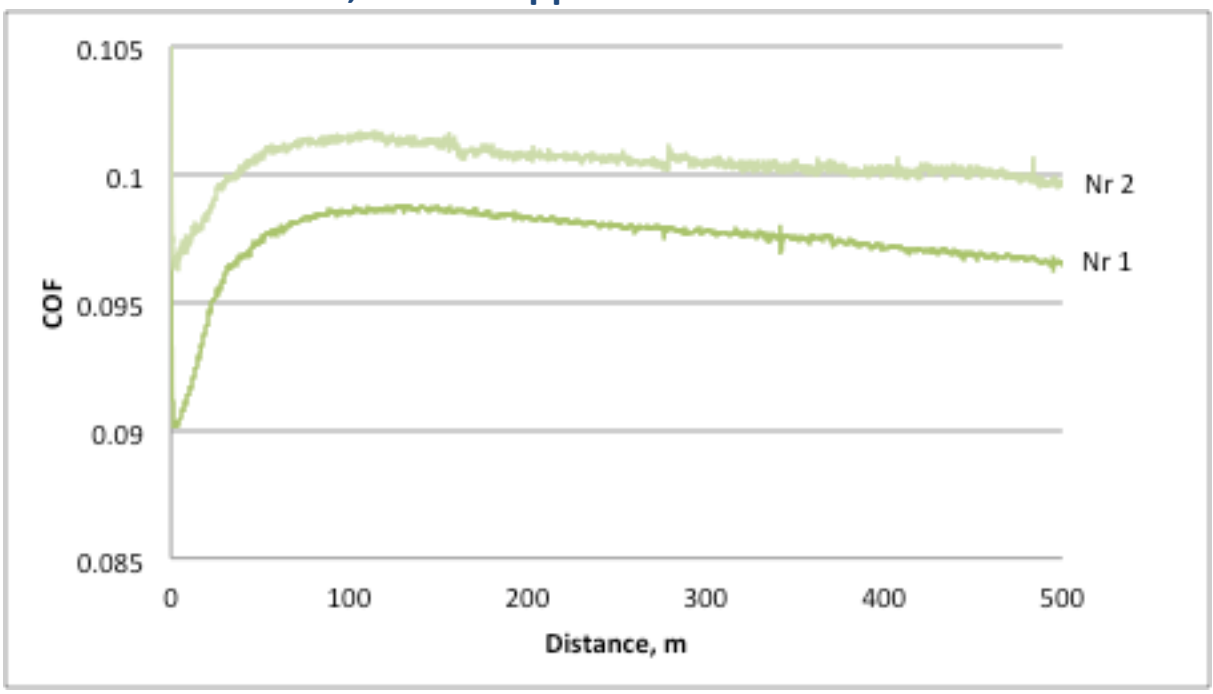

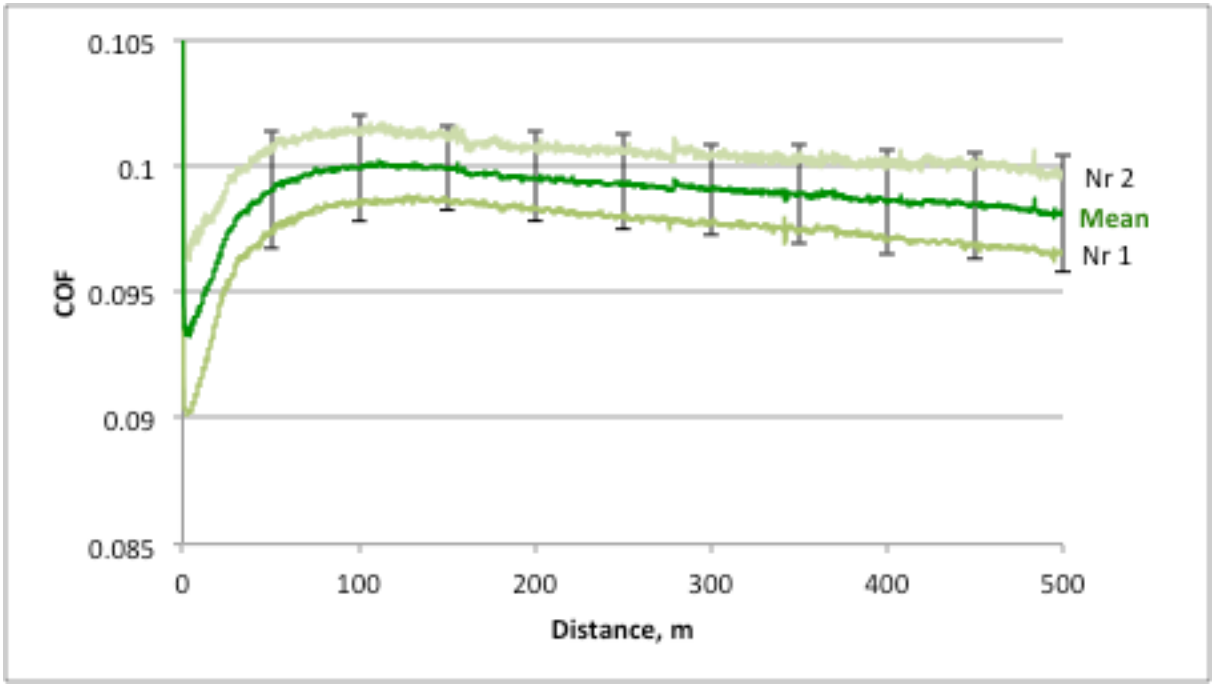

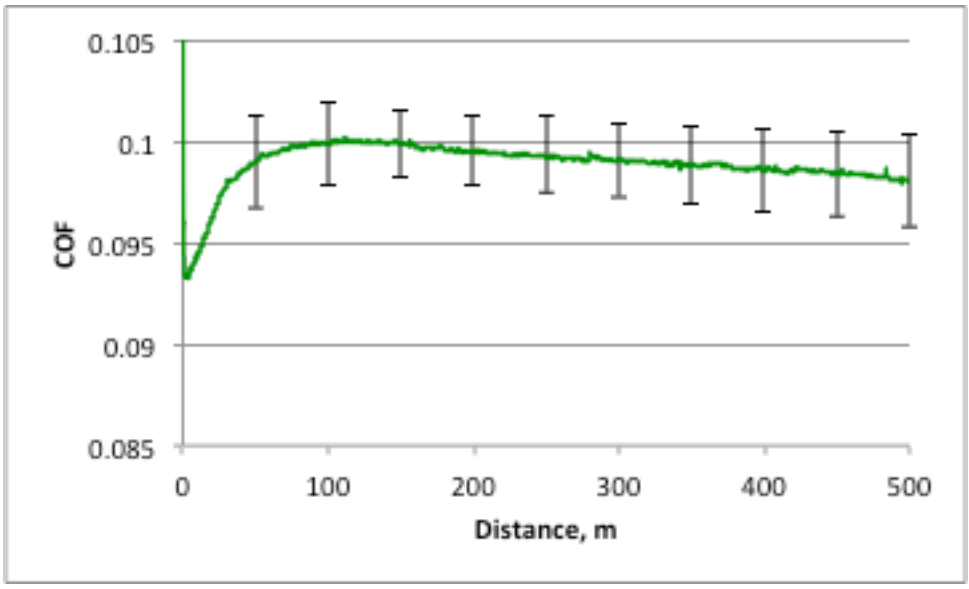

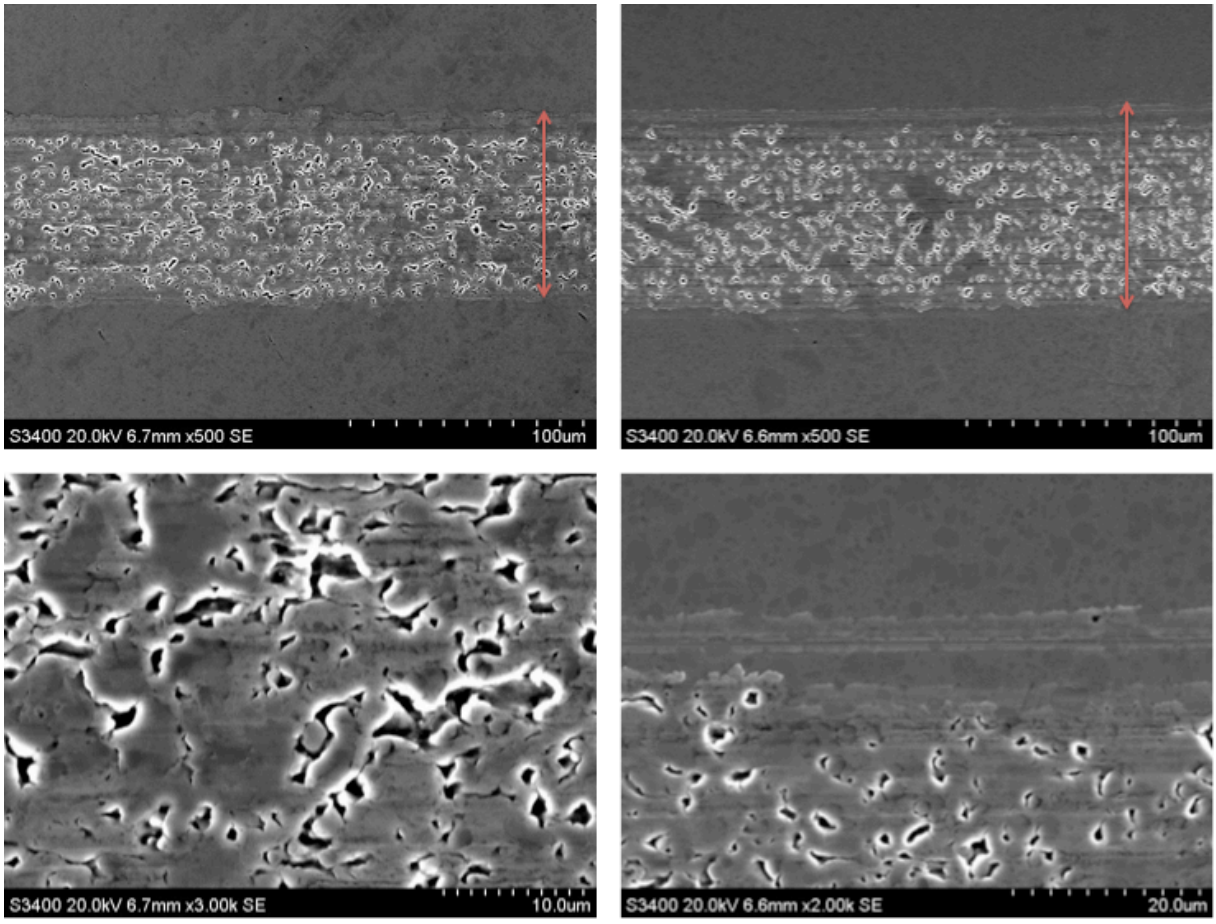

Figure B.26: SS PAG 300 ppm. Left nr 1, right nr 2

B.13 Stainless steel, PAG 500 ppm

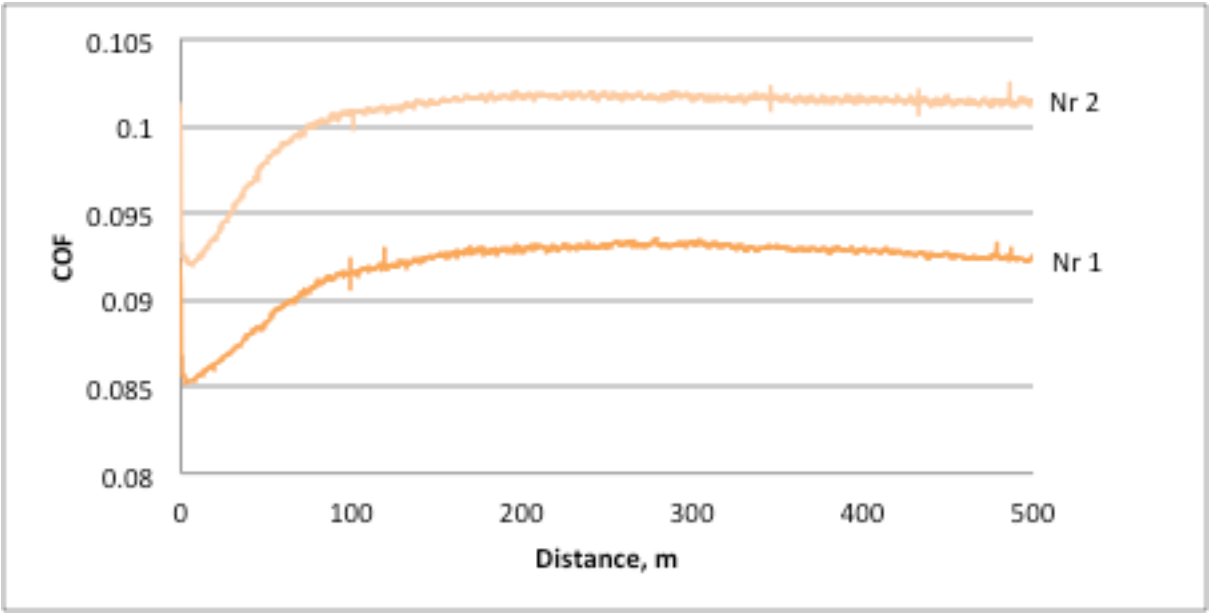

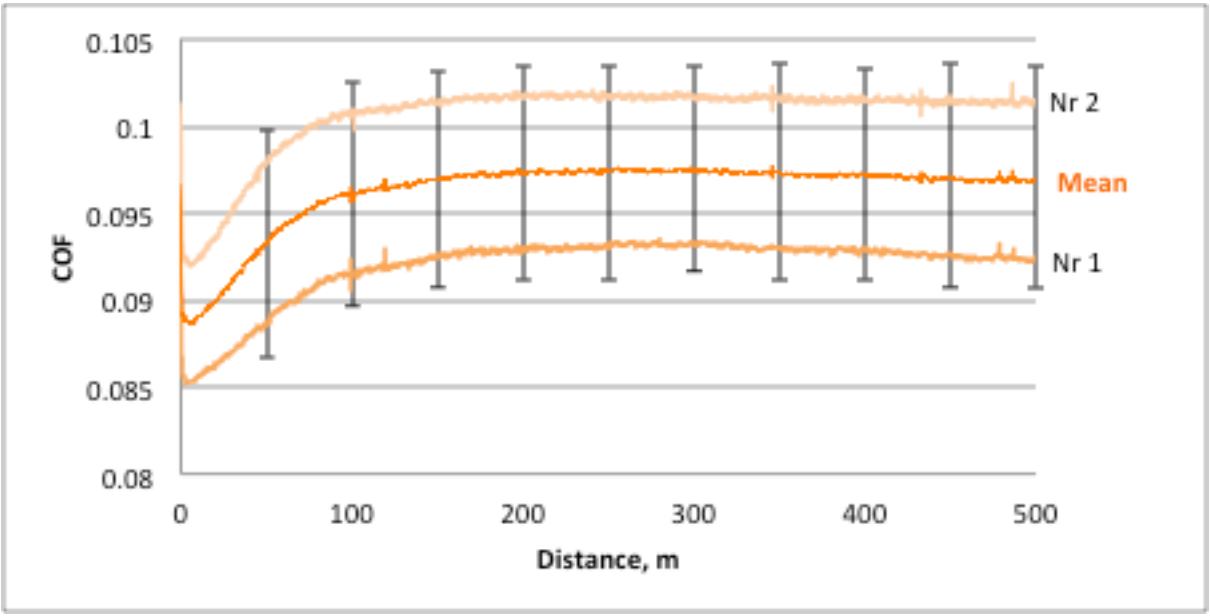

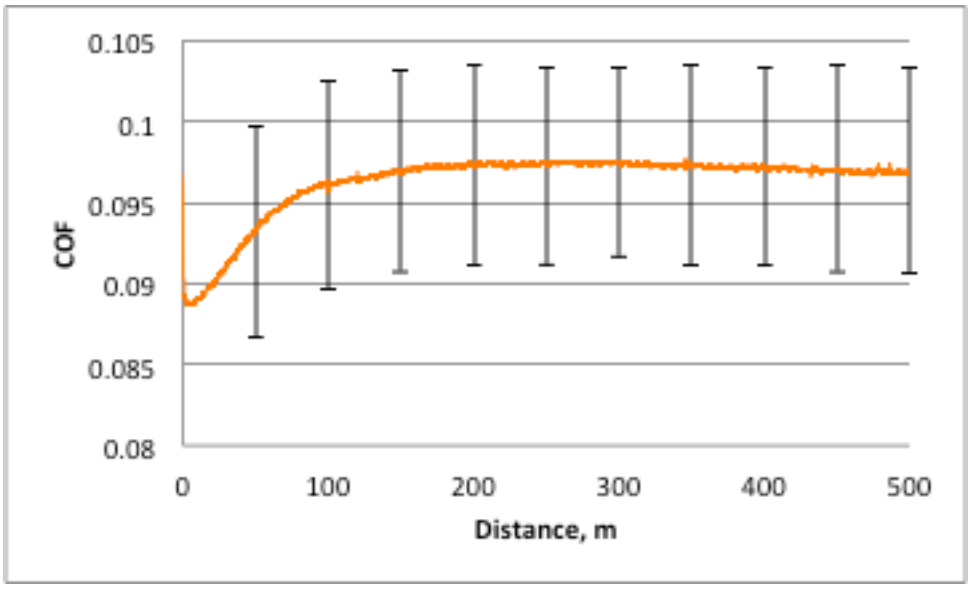

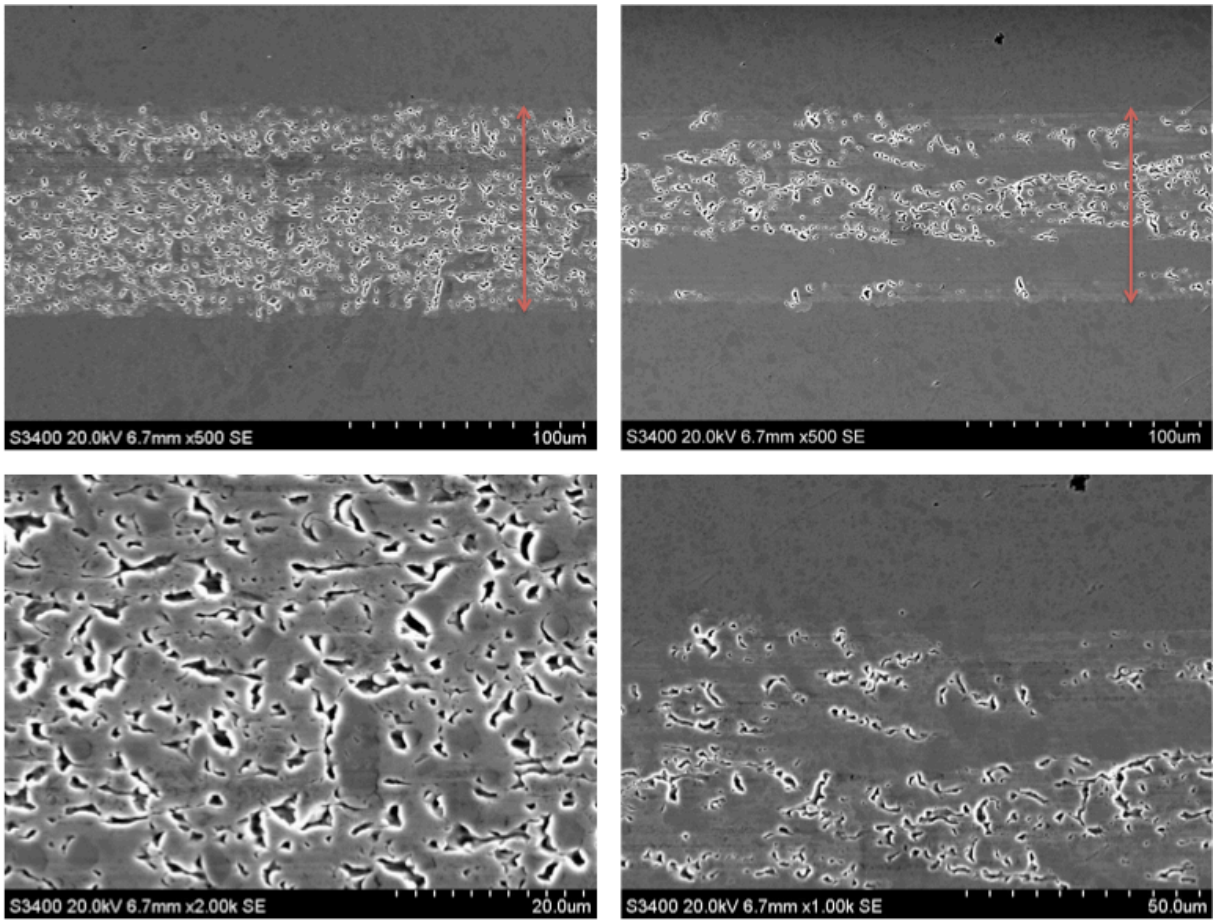

Figure B.27: SS PAO 500 ppm. Left nr 1, right nr 2

B.14 Silicon carbide, clean PAO

Clean:

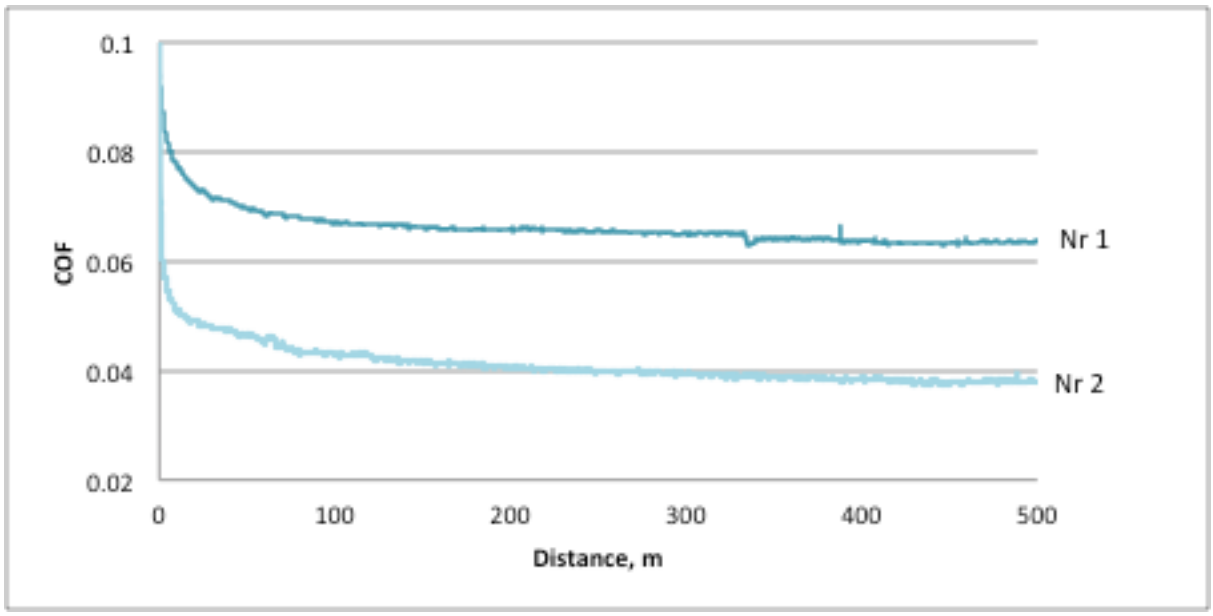

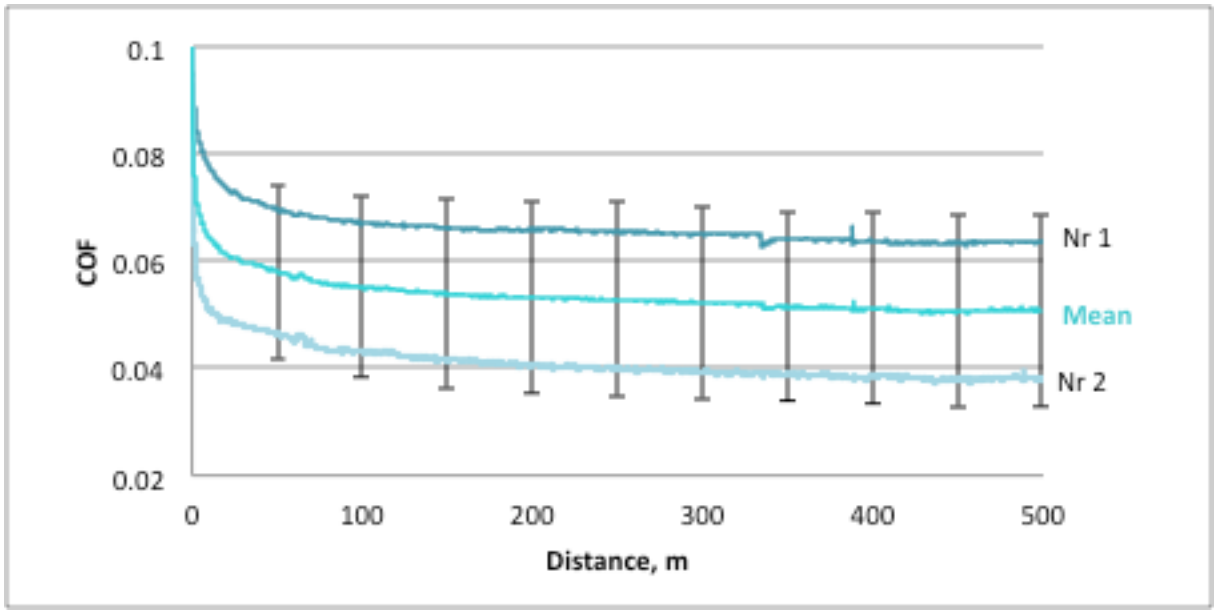

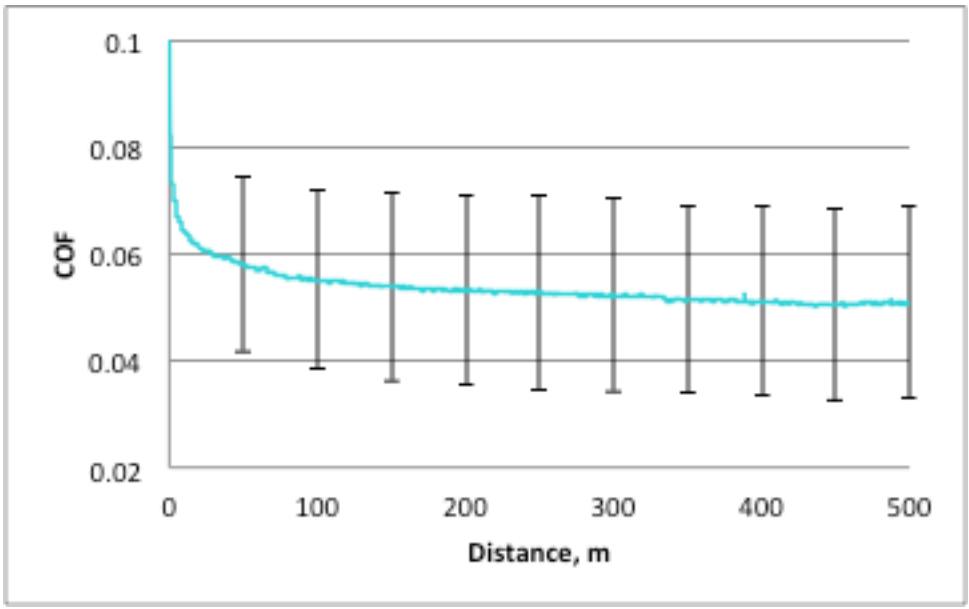

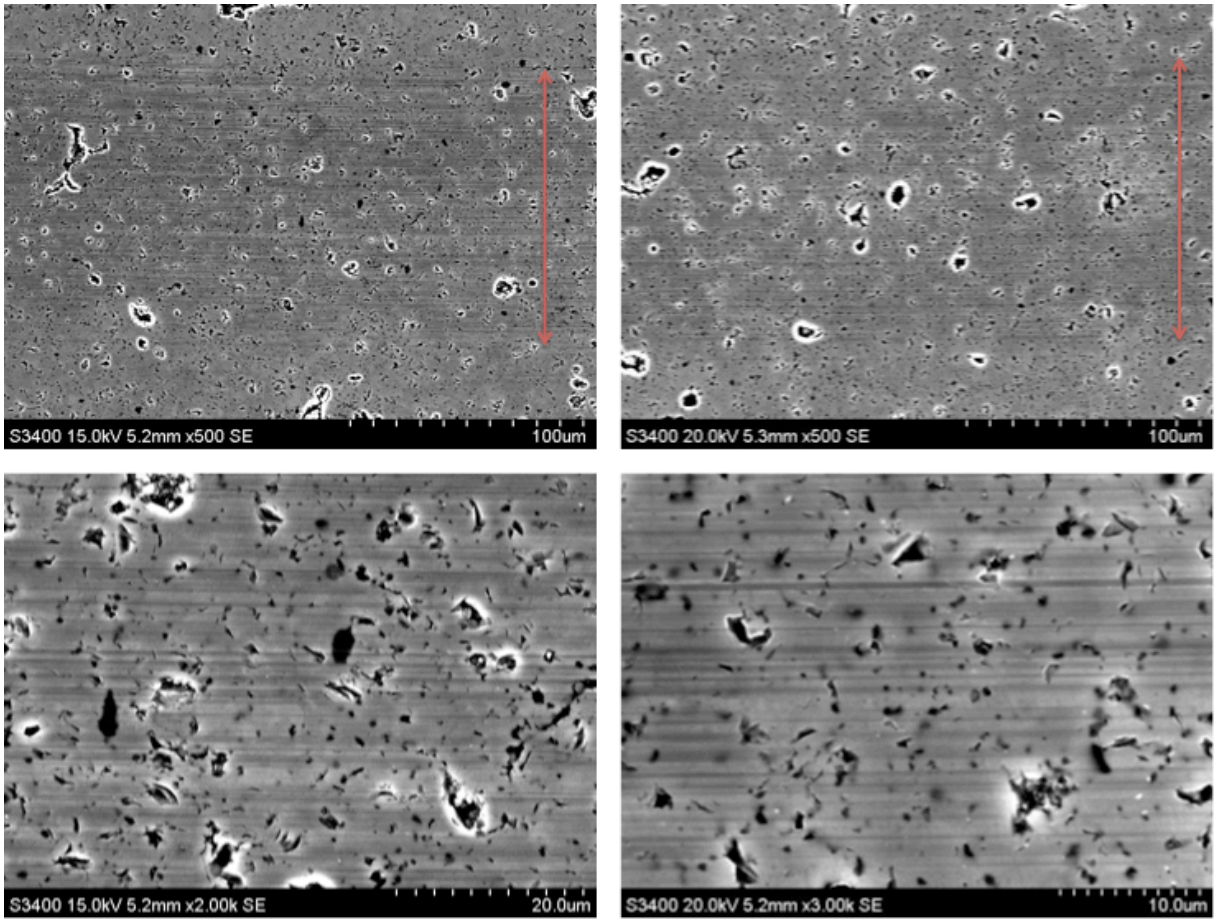

Figure B.28: SIC Clean PAO. Left nr 1, right nr 2

B.15 Silicon carbide, PAO 300 ppm

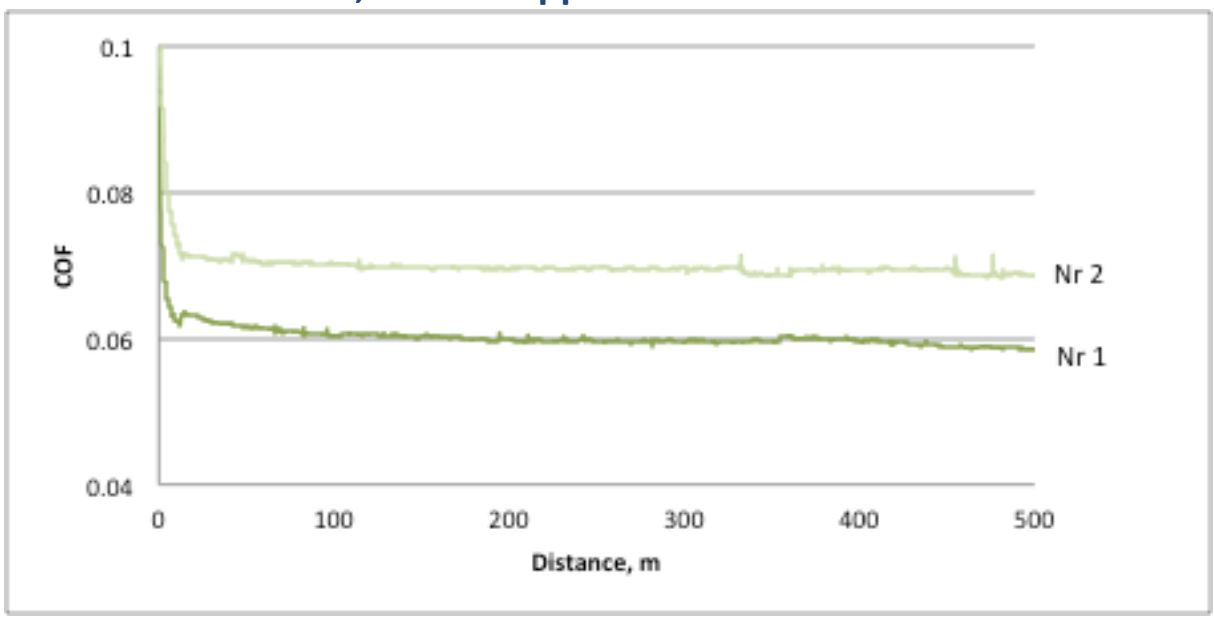

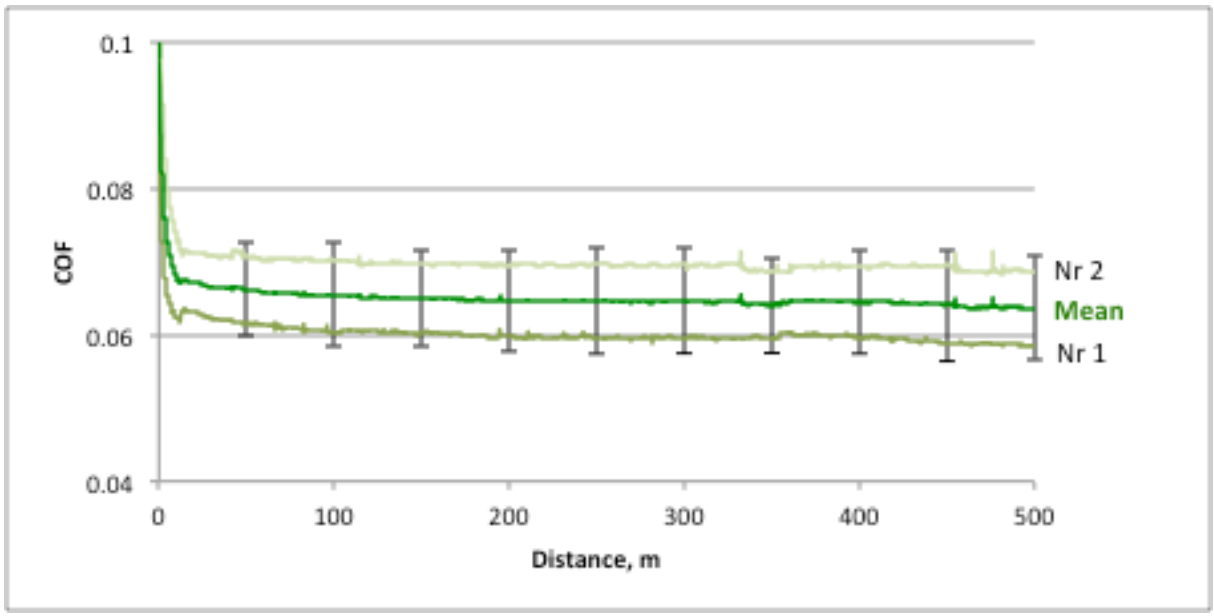

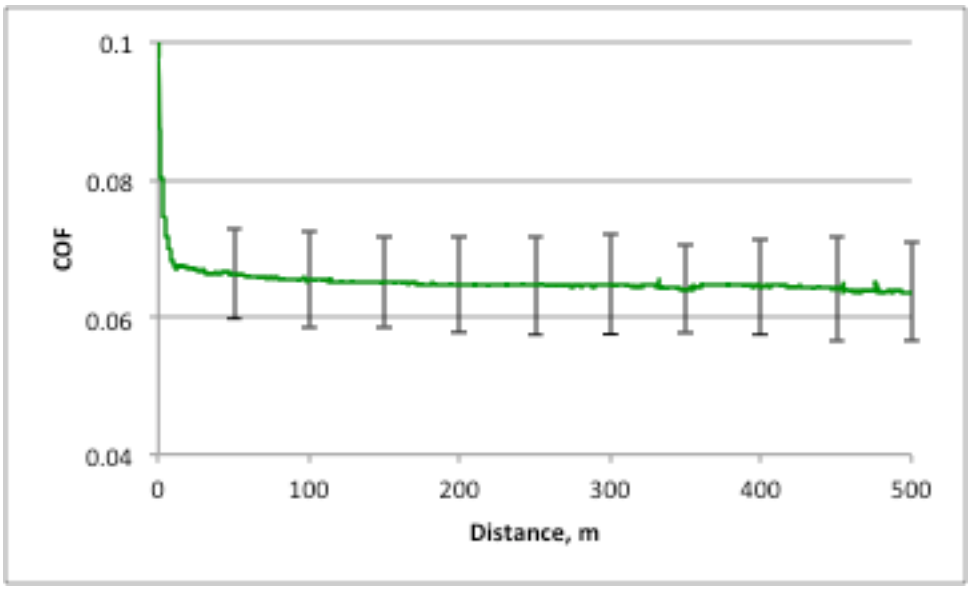

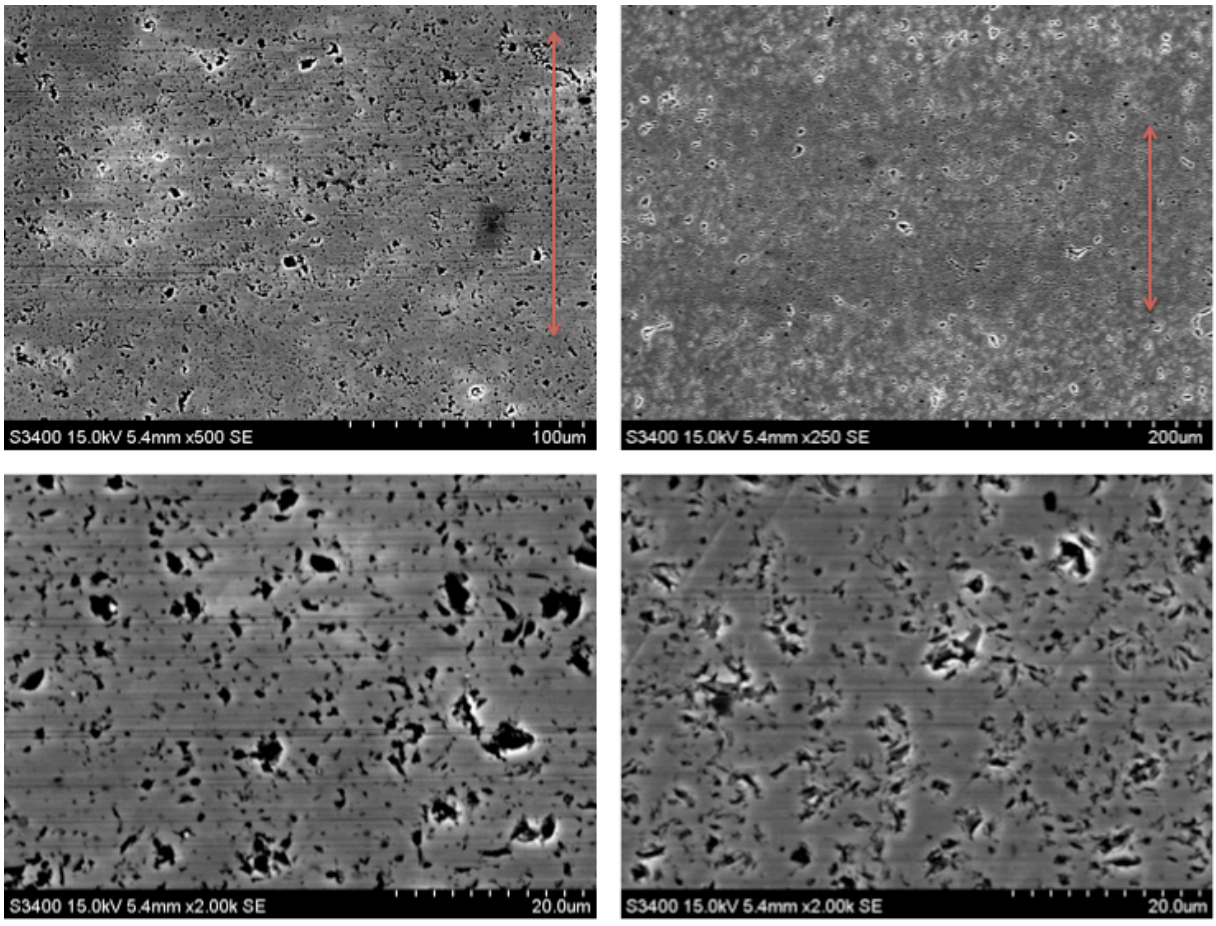

Figure B.29: SiC PAO 300 ppm. Left nr 1, right nr 2

B.16 Silicon carbide, PAO 500 ppm

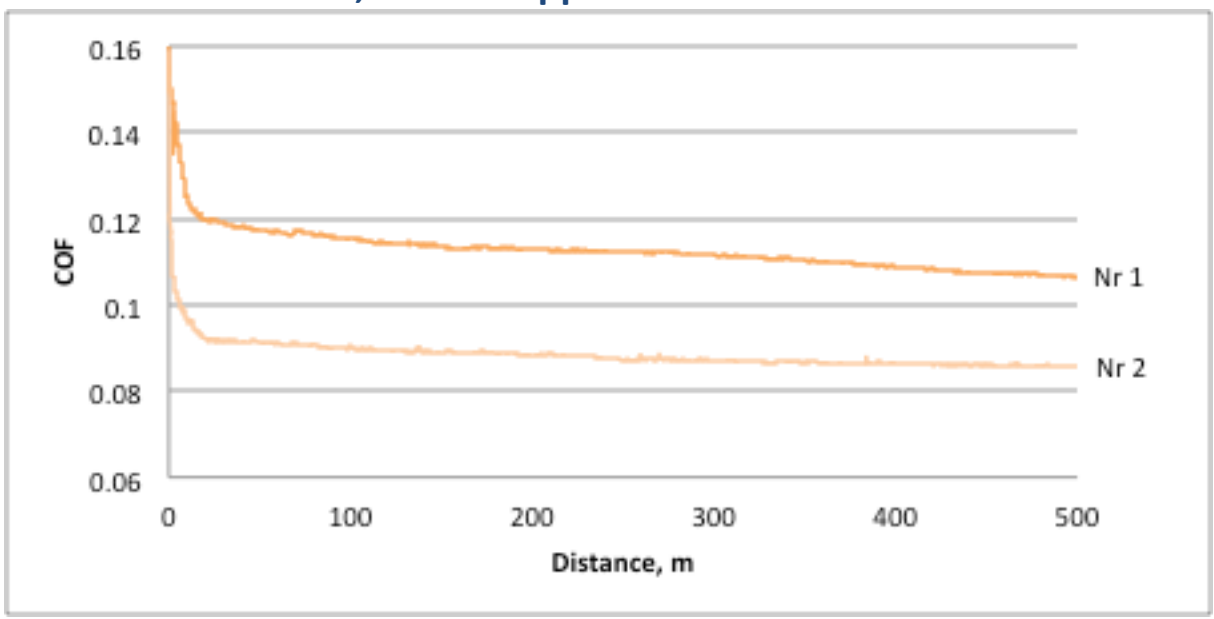

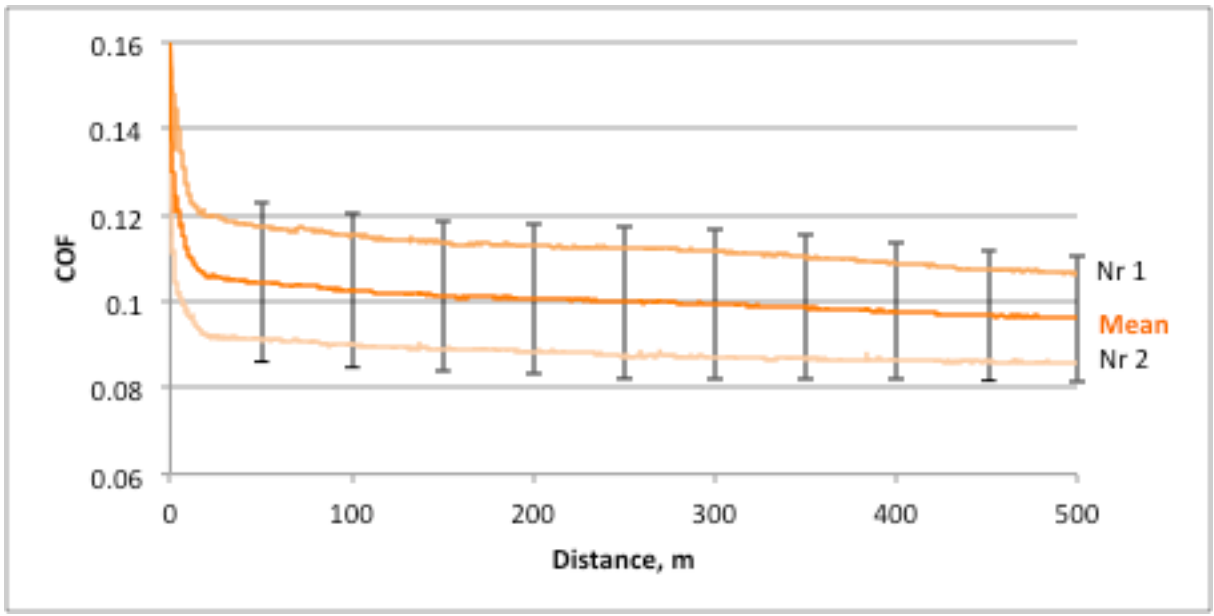

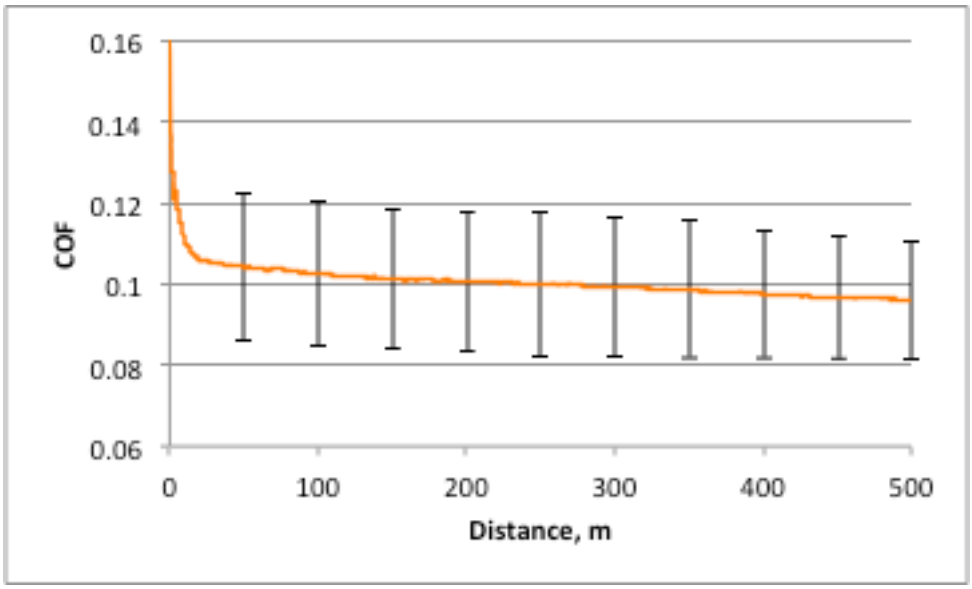

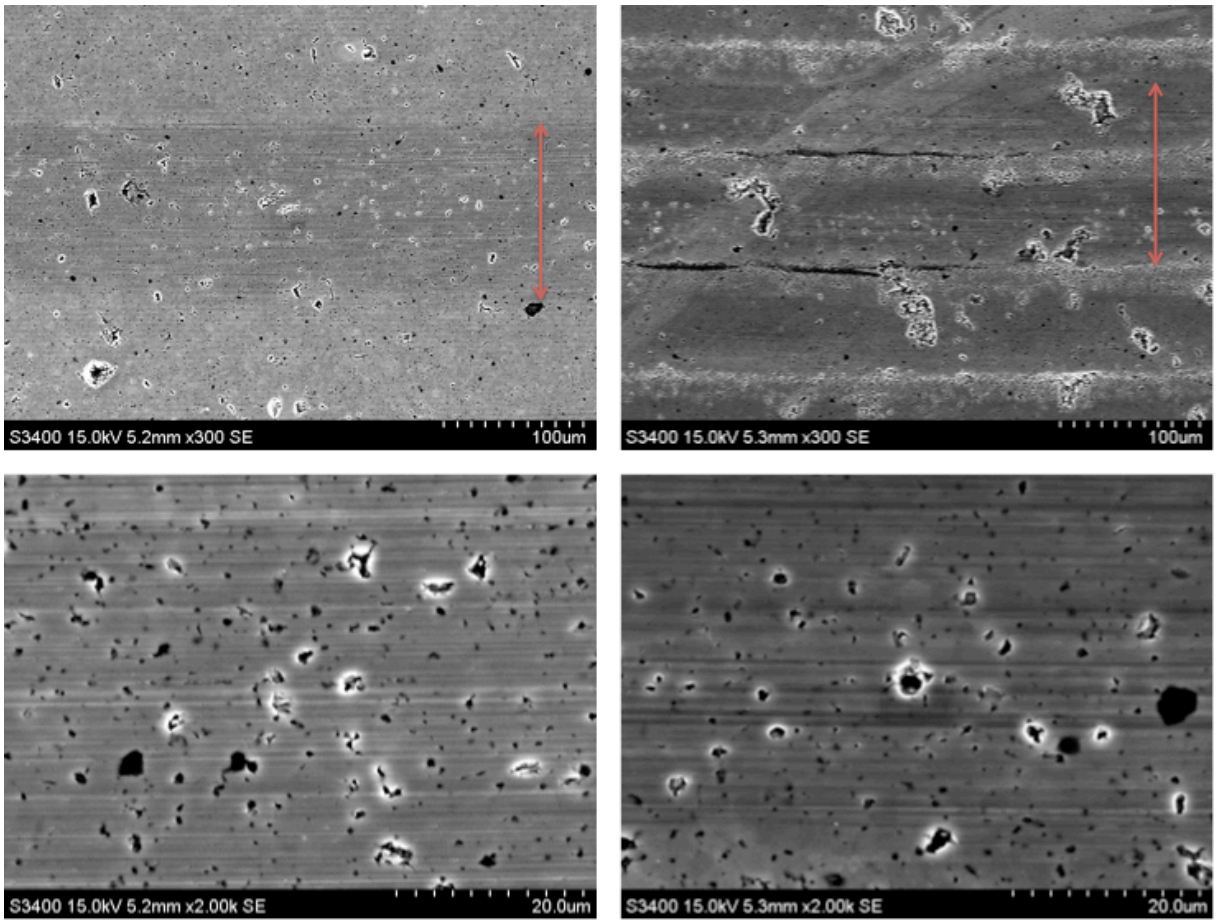

Figure B.30: SiC PAO 500 ppm. Left nr 1, right nr 2

B.17 Silicon carbide, clean PAG

Clean:

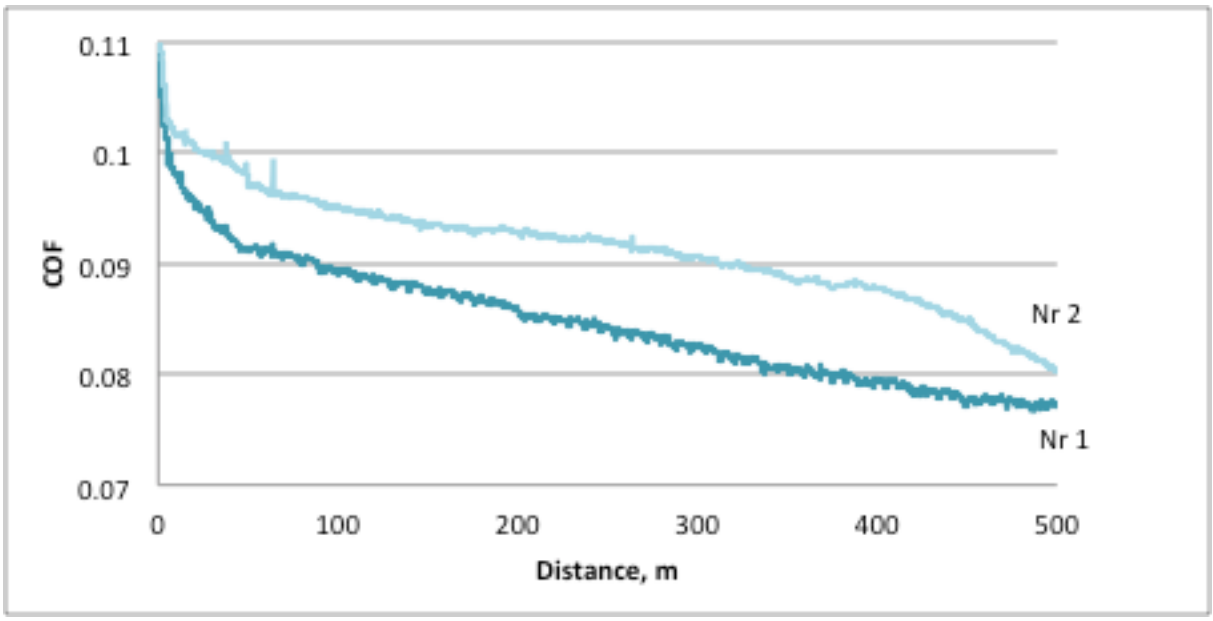

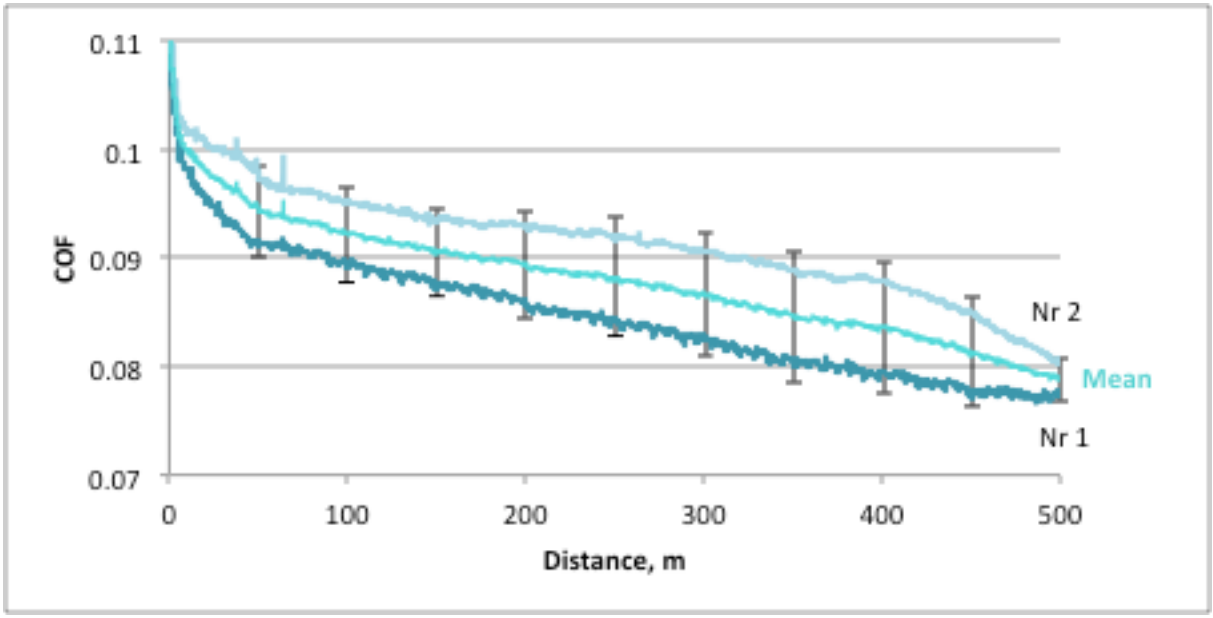

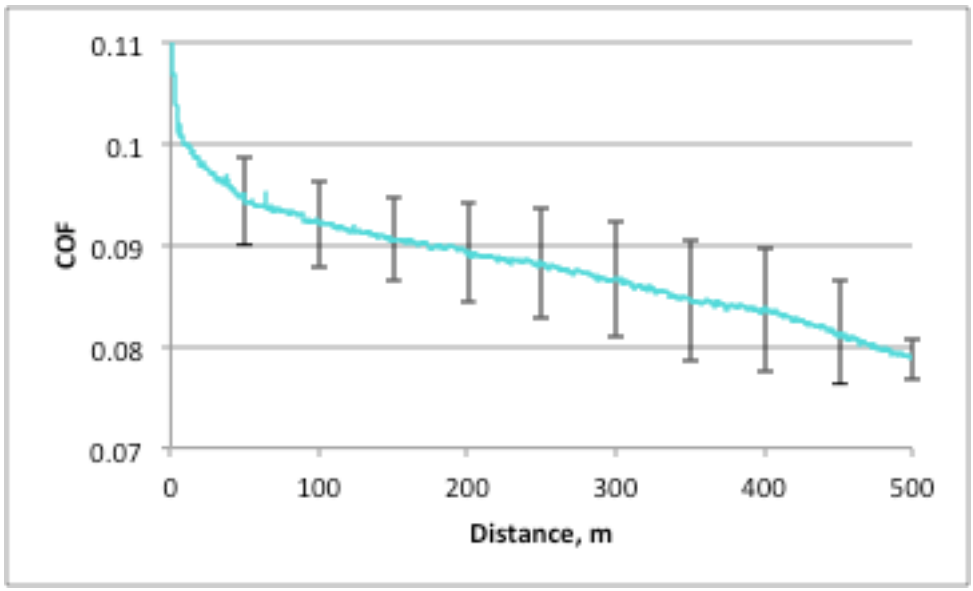

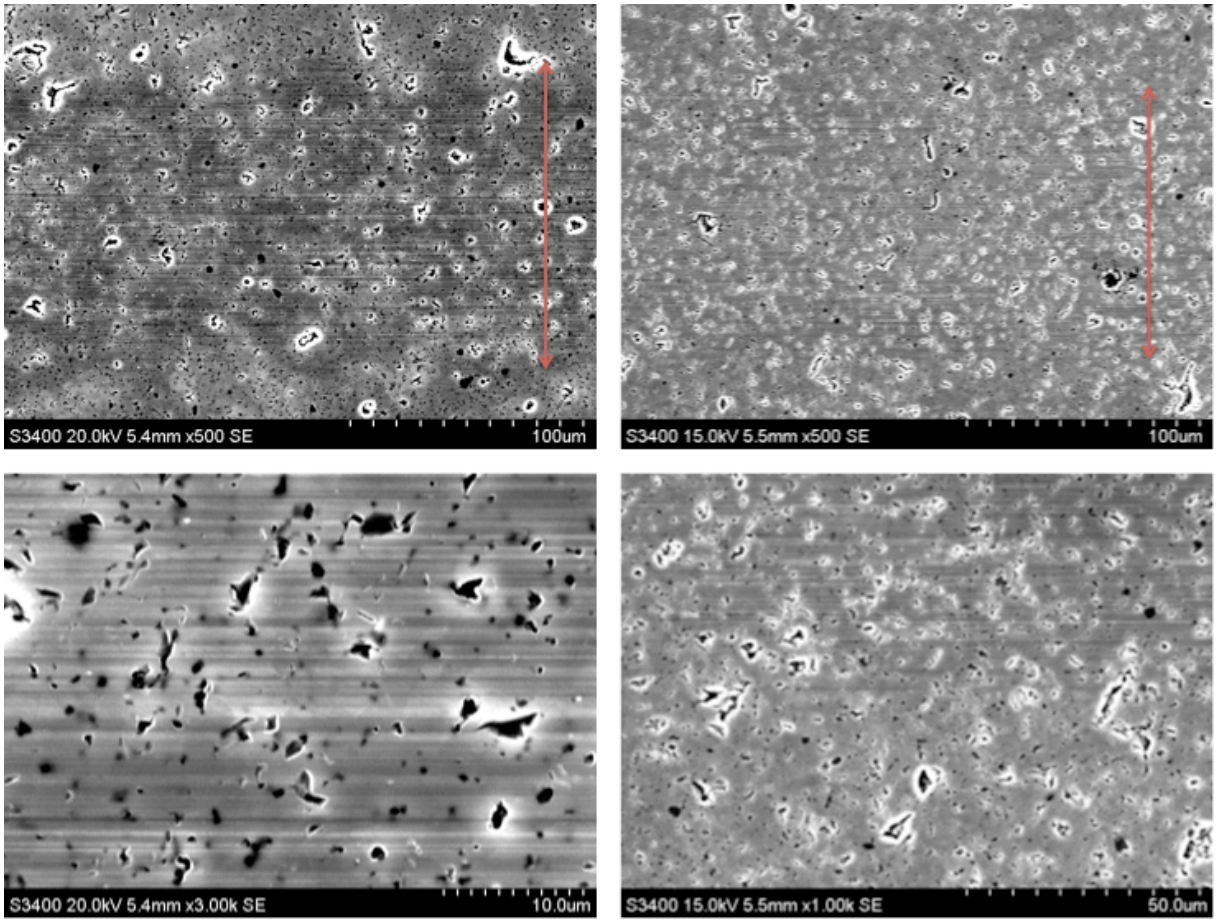

Figure B.31: SiC clean PAG. Left nr 1, right nr 2

B.18 Silicon carbide, PAG 300 ppm

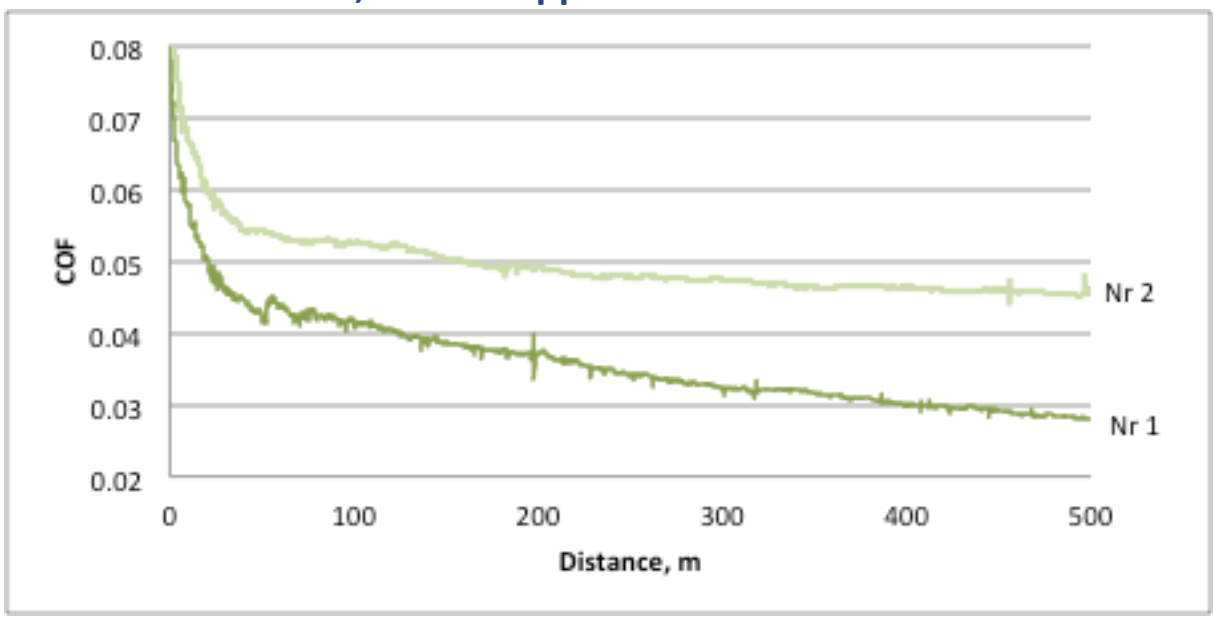

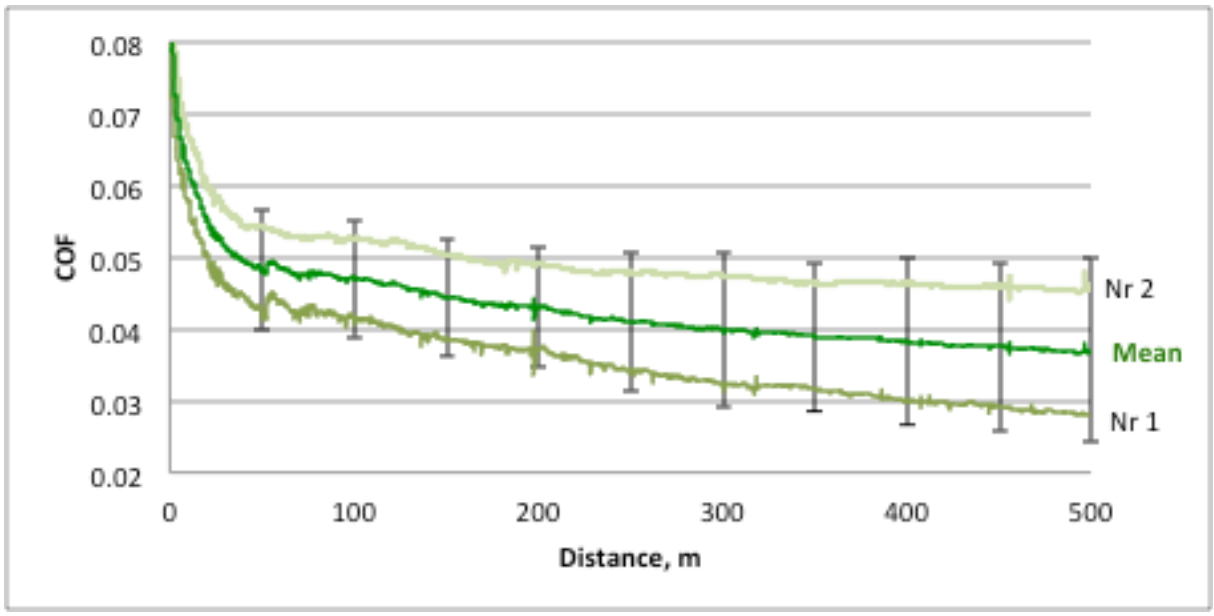

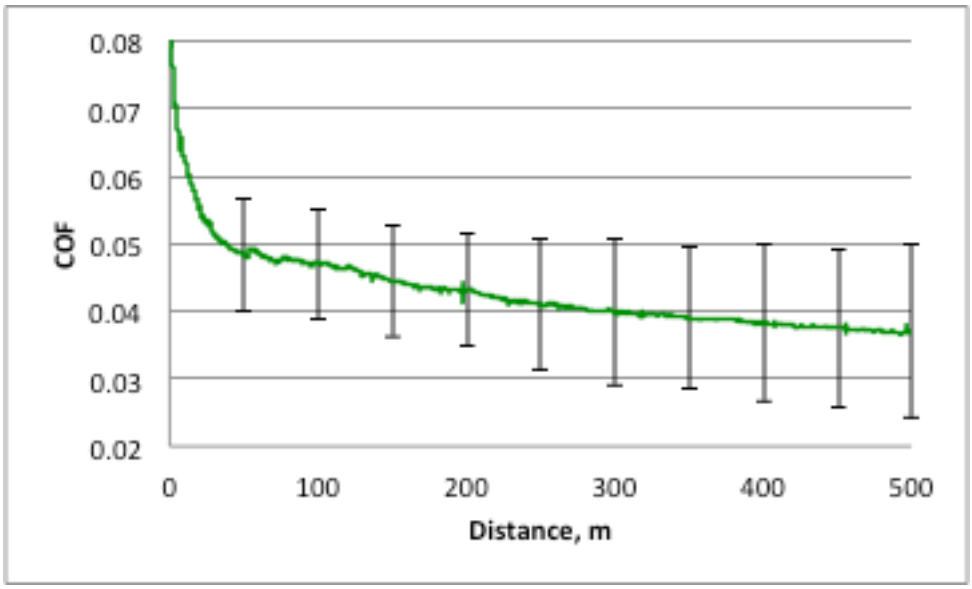

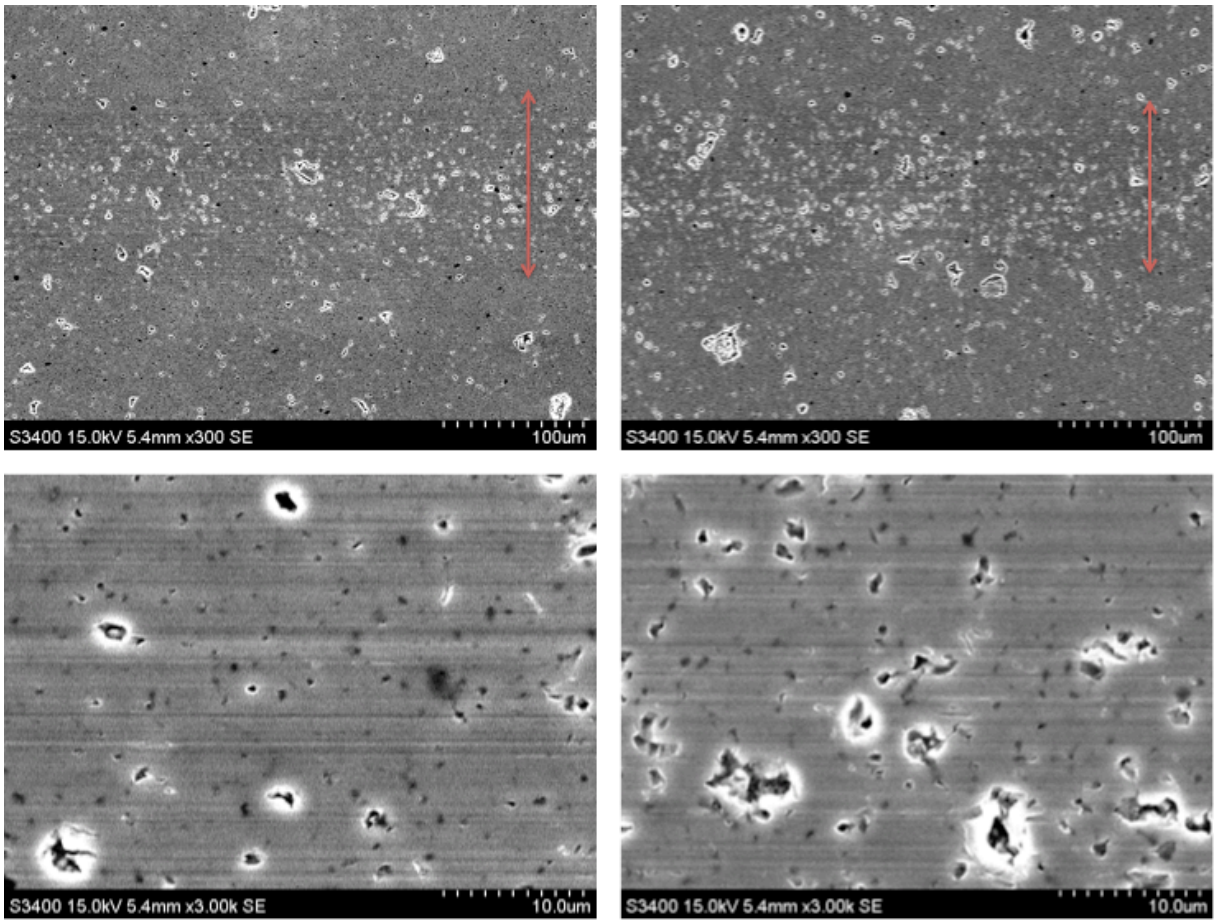

Figure B.32: SiC, PAG 300 ppm. Left nr 1, right nr 2

B.19 Silicon carbide, PAG 500 ppm

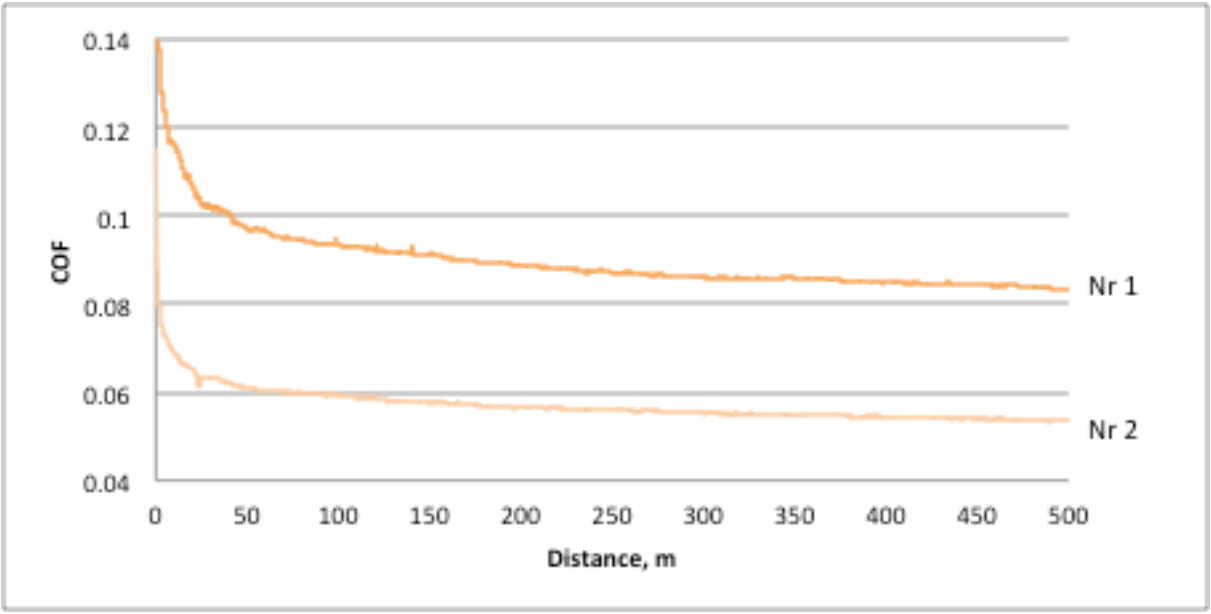

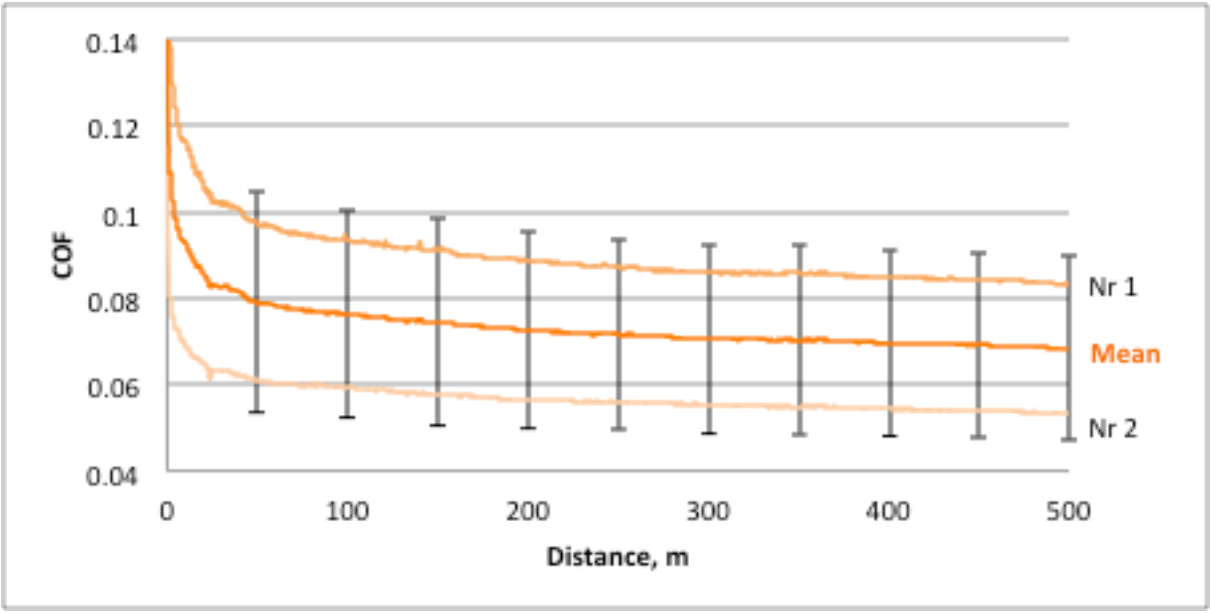

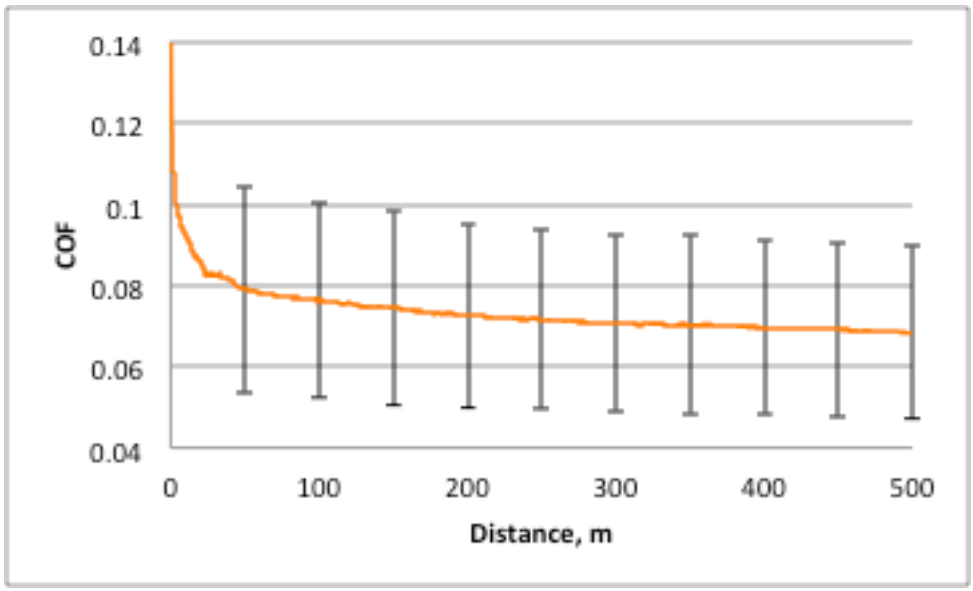

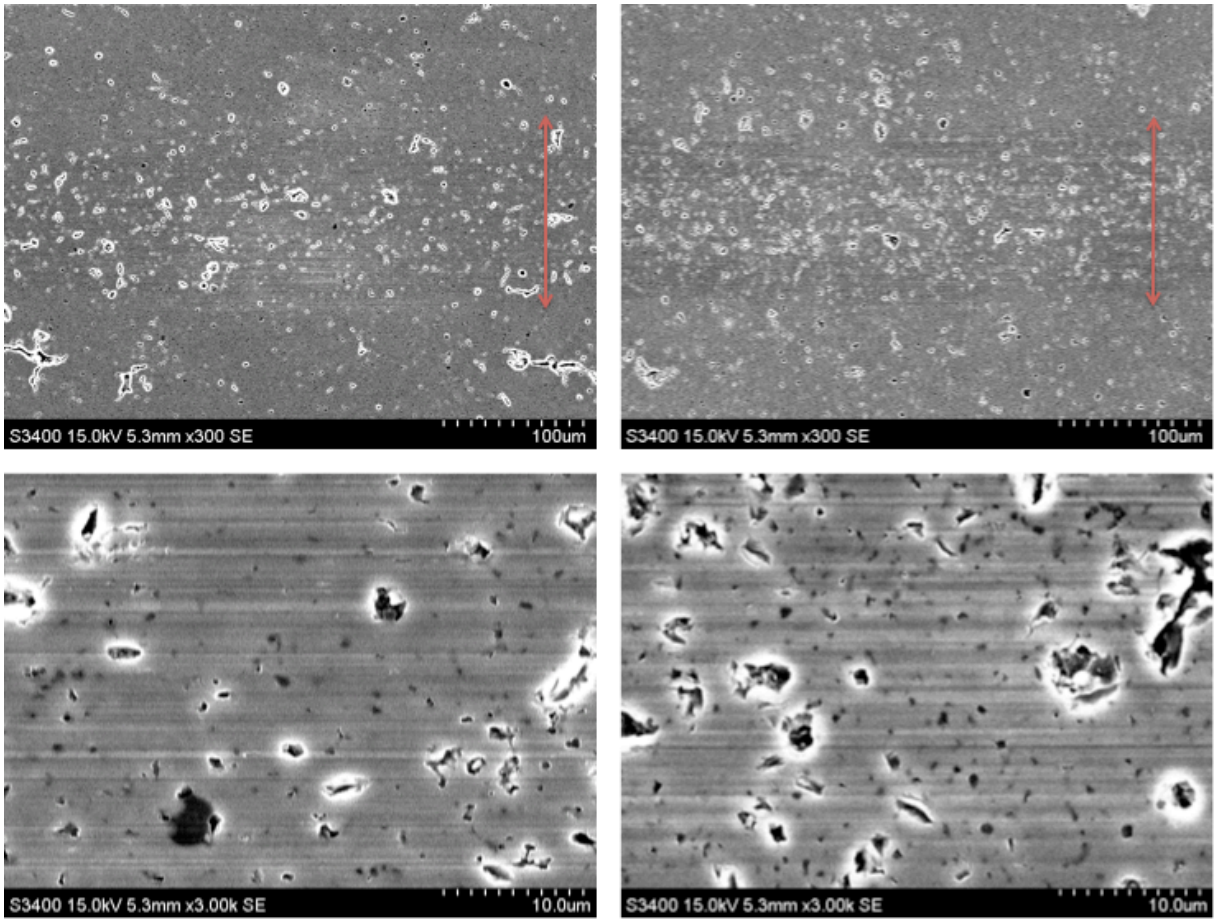

Figure B.33: SiC PAG 500 ppm. Left nr 1, right nr 2

Appendix C: Volume loss on stainless steel

Condition	Dry 1		Dry 2		Seawater nr1	
	Track width	Vol loss (mm^3)	Track width	Vol loss (mm^3)	Track width	Vol loss (mm^3)
point 1a	545.66	0.34010	545.66	0.34010		
point 1b						
point 1c	475.71	0.22535	475.71	0.22535		
point 2a	601.63	0.45586	601.63	0.45586	498.02	0.25857
point 2b	594.63	0.44013	594.63	0.44013	493.62	0.25178
point 2c	634.86	0.53564	634.86	0.53564	499.78	0.26132
point 3a	673.34	0.63906	673.34	0.63906	476.03	0.22581
point 3b	654.1	0.58583	654.1	0.58583	446.99	0.18695
point 3c	626.11	0.51380	626.11	0.51380	471.63	0.21961
point 4a	683.83	0.66940	683.83	0.66940	467.23	0.21352
point 4b	734.55	0.82966	734.55	0.82966	429.39	0.16573
point 4c	619.12	0.49678	619.12	0.49678	455.79	0.19821
average (mm^3)		0.52105		0.52105		0.22017
SD		0.16346		0.16346		0.03315

Condition	PAO clean		PAO 300ppm		PAO 500ppm		PAO 1000ppm	
	Track width	Vol loss (mm^3)	Track width	Vol loss (mm^3)	Track width	Vol loss (mm^3)	Track width	Vol loss (mm^3)
point 1a	84.0142	0.00124	94.631	0.00177			106.805	0.00255
point 1b	85.2049	0.00129	95.5313	0.00183			107.785	0.00262

point 1c	83.405	0.00121	91.2767	0.00159			107.901	0.00263
point 2a	84.771	0.00128						
point 2c					97.601	0.00195		
point 3a					96.898	0.00190		
point 3b					95.8537	0.00184		
point 3c					96.4388	0.00188		
average (mm^3)		0.00126		0.00173		0.00189		0.00260
SD		0.00004		0.00012		0.00004		0.00004

Condition	**PAG clean 2**		**PAG 300ppm nr1**		**PAG 500ppm nr2**		**PAG 1000ppm**	
	Track width	Vol loss (mm^3)	Track width	Vol loss (mm^3)	Track width	Vol loss (mm^3)	Track width	Vol loss (mm^3)
point 1a	80.0759	0.001075	83.3836	0.001214	87.4231	0.001399	106.805	0.002550
point 1b	81.4379	0.001131	80.7466	0.001102	87.3307	0.001394	107.785	0.002621
point 1c	81.5138	0.001134	82.1276	0.001160	86.567	0.001358	107.901	0.002630
point 2a	80.2539	0.001082	82.5824	0.001179	85.802	0.001322		
point 2b	79.6	0.001056	83.6793	0.001227	85.237	0.001296		
point 2c	81.3153	0.001126	82.3427	0.001169	85.7014	0.001318		
point 3a	80.1708	0.001079	84.004	0.001241	83.5927	0.001223		
point 3b	79.8502	0.001066	84.7842	0.001276				
point 3c	87.4616	0.001401	84.818	0.001277				
point 4a	79.6719	0.001059	84.2103	0.001250				
point 4b	76.5057	0.000937						
point 4c	76.014	0.000919	86.1665	0.001339				

average (mm^3)	0.001089	0.001221	0.001330	0.002600
SD	0.000119	0.000066	0.000061	0.000044

a